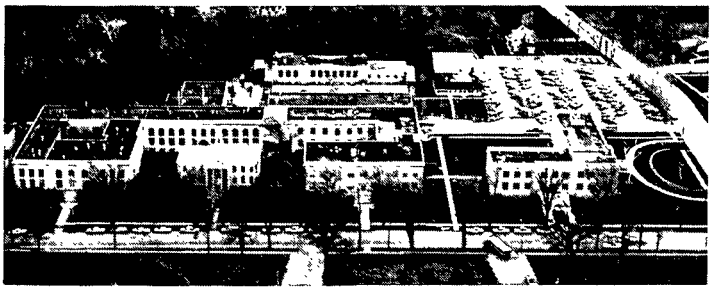

THE INSTITUTE OF PAPER CHEMISTRY, APPLETON, WISCONSIN

# STATUS REPORTS

To The

Engineering Project Advisory Committee

October 22-23, 1987
The Institute of Paper Chemistry
Continuing Education Center
Appleton, Wisconsin

NOTICE & DISCLAIMER

The Institute of Paper Chemistry (IPC) has provided a high standard of professional service and has exerted its best efforts within the time and funds available for this project. The information and conclusions are advisory and are intended only for the internal use by any company who may receive this report. Each company must decide for itself the best approach to solving any problems it may have and how, or whether, this reported information should be considered in its approach.

IPC does not recommend particular products, procedures, materials, or services. These are included only in the interest of completeness within a laboratory context and budgetary constraint. Actual products, procedures, materials, and services used may differ and are peculiar to the operations of each company.

In no event shall IPC or its employees and agents have any obligation or liability for damages, including, but not limited to, consequential damages, arising out of or in connection with any company's use of, or inability to use, the reported information. IPC provides no warranty or guaranty of results.

This information represents a review of on-going research for use by the Project Advisory Committees. The information is not intended to be a definitive progress report on any of the projects and should not be cited or referenced in any paper or correspondence external to your company.

Your advice and suggestions on any of the projects will be most welcome.

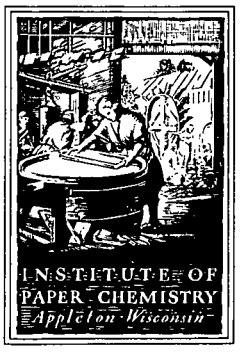


THE INSTITUTE OF PAPER CHEMISTRY
Post Office Box 1039
Appleton, Wisconsin 54912
Phone: 414/734-9251 738-3377
Telex: 469289
Lisa Sprinkle

September 29, 1987

TO: Members of the Engineering Project Advisory Committee

Enclosed is advance reading material for the October 22-23 meeting of the Engineering Project Advisory Committee. Included are status reports for active projects, an agenda, and a current committee membership list.

Rooms have been reserved in the Continuing Education Center, and meals will be provided as stated on the agenda. If you haven't already indicated your attendance, please do so at your earliest convenience by returning your registration form or calling Sandy Berghuis at 414/738-3202.

For all Project Advisory Committee meetings, the Institute invites its member companies to send one or more representatives to attend the review sessions (first day) of any or all of the meetings. These invitations were mailed September 1. PAC members from member companies are also welcome to attend the other meetings, and may stay in the CEC and attend meetings and meals of their choice, at no cost. If you wish to attend any of the other meetings, but haven't registered, please call Sandy Berghuis to do so. A meeting schedule is enclosed for your information.

We look forward to meeting with you on October 22-23.

Sincerely,

Clyde H. Sprague

Clyde H. Sprague, Director
Engineering Division

CHS/ls
Enclosures

Castelli 6263
Phillips 5430
Kyung 5956-

THE INSTITUTE OF PAPER CHEMISTRY

Project Advisory Committee Meetings
Member Dues-funded Research Reviews

October 20, 21, 22, 26, and 27

Fall, 1987

Continuing Education Center
Appleton, Wisconsin
(414) 734-9251

| Committee | Review Schedule | Research Area* |
|---|---|---|
| Pulping Processes | Tuesday, Oct. 20<br>8:00 A.M. - evening | Chemical Recovery:<br>Recovery Furnace Processes<br>Bleached Chemical Pulp:<br>Fundamental Reactions<br>Oxygen Bleaching<br>High Lignin Pulps:<br>Brightness Stability<br>Strength Development<br>Microstructure of Wood Fibers<br>Analytical |
| Paper Properties and Uses | Wednesday, Oct. 21<br>8:30 A.M. - evening | Board Properties and Performance<br>Process, Properties, Product Relationships<br>Internal Strength Enhancement<br>Strength Improvement and Failure Mechanisms<br>On-line Measurement of Paper Mechanical Properties<br>Tour of Paper Materials Division Laboratories |
| Engineering | Thursday, Oct. 22<br>10:00 A.M. - evening | Corrosion:<br>Kraft Liquor Corrosivity<br>Corrosion Control in Paper Mills<br>Recovery Boiler Corrosion<br>Corrosion in High Yield Pulping<br>Corrosion-resistant Coatings<br>Papermaking:<br>Mechanics of Refining<br>Higher Consistency Processing<br>Wet Pressing<br>Impulse Drying<br>Black Liquor Delivery Systems<br>Coating System Dynamics |

* NOT NECESSARILY IN ORDER OF AGENDA

| Committee | Review Schedule | Research Area* |
|---|---|---|
| Forest Genetics | Monday, October 26<br>1:00 P.M. - evening | Somatic Embryogenesis<br>Initiation, Spring and Summer<br>Embryo Development/Maturation<br>Conversion to Seedlings<br>Fidelity/Performance |
| Systems Analysis | Tuesday, October 27<br>1:00 P.M. - evening | MAPPS Simulator Development<br>Continuing Module Development<br>Performance Attribute Modeling<br>Optimization with MAPPS<br>User Friendly Interface |

* NOT NECESSARILY IN ORDER OF AGENDA

# TABLE OF CONTENTS

PRELIMINARY AGENDA

ENGINEERING
PROJECT ADVISORY COMMITTEE

October 22-23, 1987

Continuing Education Center (CEC)
The Institute of Paper Chemistry
Appleton, Wisconsin

Thursday, October 22, 1987

| | | |
|---|---|---|
| 10:00am -- | INTRODUCTION | Sprague/Rugowski |
| 10:15am -- | CORROSION AND MATERIALS ENGINEERING SECTION | |
| | - Fundamentals of Corrosion Control in Paper Mills | Yeske |
| | - Fundamentals of Kraft Liquor Corrosivity | Crowe |
| | - Recovery Boiler Corrosion | Crowe |
| 12:00pm -- | LUNCH | |
| 12:30pm | - Evaluation of Structural Coatings for Pulp and Paper Mill Service | Crowe |
| | - Corrosion in High Yield Pulping Processes | Crowe |
| 1:00pm -- | PAPERMAKING PROCESSES GROUP | |
| | - Impulse Drying | Lavery |
| | - Heat Transfer in Impulse Drying | Rudemiller (Student) |
| | - Demonstration of Roll Impulse Dryer | Lavery |
| 2:45pm -- | BREAK | |
| 3:00pm | - Fundamentals of Wet Pressing | |
| | • Displacement Dewatering | Lindsay |
| 3:30pm | - Applications of Flash X-Radiography | |
| | • Higher Consistency Processing | Farrington |
| | • Black Liquor Sprays | Farrington/ Spielbauer (Student) |
| | • Coating System Dynamics | Farrington/ Triantafillopoulos (Student) |
| 5:00pm | • Demonstration of X-Ray Techniques | Farrington |

Thursday, October 22, 1987 (cont'd)

5:30pm -- COCKTAILS

6:00pm -- DINNER - CEC DINING ROOM

7:00pm - Review of Strategic Research Plan – Tomorrow morning Sprague/Yeske

Friday, October 23, 1987

7:15am -- BREAKFAST -- CEC Dining Room

COMMITTEE ACTIVITIES

8:00am - Discussion of Projects and Planning ~~Eliminate~~ Committee & Staff

9:30am -- BREAK

9:45am - Continued Discussion

10:30am - Report Preparation Committee

11:30am - Adjourn

-- LUNCH - CEC Dining Room

Max – GP Leader Corrosion Press + Dry Pete Busker Son Tom ~~Bob~~ Young Percy High Constr.

NOTE: The spring Engineering PAC meeting is scheduled for March 24-25, 1988.

## ENGINEERING

### Project Advisory Committee

Mr. James Rugowski (Chairman) - 6/88
Engineering Consultant
Kimberly-Clark Corporation
2100 Winchester Road
Neenah, WI 54956
(414) 721-2000

Mr. Sven S. Arenander - 6/90*
Group Leader
Union Camp Corporation
P.O. Box 3301
Princeton, NJ 08543-3301
(609) 896-1200

Mr. William C. Bliesner - 6/90
Technical Director
Thilmany Pulp & Paper Company
P.O. Box 600
Kaukauna, WI 54130
(414) 766-4611

Mr. Percy E. Brooks - 6/90
Manager, Pulp & Paper Engineering
Georgia-Pacific Corporation
133 Peachtree Street, N.E.
P.O. Box 105605
Atlanta, GA 30348-5605
(404) 521-4618

Mr. LeRoy H. Busker - 6/88
Director, Research & Planning
Beloit Corporation
Rockton R & D Center
1165 Prairie Hill Road
Rockton, IL 61072
(608) 364-7961

Mr. Max D. Moskal - 6/88
Project Manager
Stone Container Corporation
616 Executive Drive
Willowbrook, IL 60521
(312) 655-6949

*date of retirement
8/11/87
ls

Mr. M. Thomas Neill - 6/88
Vice President R&D
Abitibi-Price Inc.
Research Centre
Sheridan Park
Mississauga, Ontario L5K 1A9
CANADA
(416) 822-4770

Dr. Robert Rounsley - 6/89
Research Fellow
Mead Corporation
8th & Hickory Street
Chillicothe, OH 45601
(614) 772-3581

Dr. W.B.A. Sharp - 6/90
Group Leader
Westvaco Corporation
Laurel Research Center
11101 Johns Hopkins Road
Laurel, MD 20707
(301) 792-9100

Dr. John Smuk - 6/89
Manager of Process Engineering
Research and Development Center
Potlatch Corporation
P.O. Box 510
Cloquet, MN 55720
(218) 879-2393

Mr. Benjamin Thorp - 6/89
Senior Vice President
Research and Engineering
James River Corporation
P.O. Box 2218
Richmond, VA 23217
(804) 644-5411

Dr. Jerry Wallace - 6/89
Mill Manager
Appleton Papers Inc.
East Main Street
Roaring Spring, PA 16673-1480
(814) 224-2131

Dr. Yung Duk Woo - 6/89
Senior Engineer
Papermaking R&D Department
Weyerhaeuser Paper Company
Tacoma, WA 98477
(206) 924-6428

# S T A T U S  R E P O R T S

To The

Engineering Project Advisory Committee

THE INSTITUTE OF PAPER CHEMISTRY

Appleton, Wisconsin

Status Report

to the

ENGINEERING PROJECT ADVISORY COMMITTEE

Project 3309

# FUNDAMENTALS OF CORROSION CONTROL IN PAPER MILLS

October 22, 1987

PROJECT SUMMARY FORM

DATE: SEPTEMBER 20, 1987

PROJECT NO.: 3309 - Fundamentals of Corrosion Control in Paper Mills

PROJECT LEADER: Ronald A. Yeske

IPC GOAL: Increase the useful life of equipment by proper selection of materials of construction and by identifying suitable process conditions.

OBJECTIVE: Improve the useful life of paper machine suction rolls by conducting corrosion and corrosion fatigue studies to establish the mechanisms of failure as the basis for developing approaches for prolonging roll life.

CURRENT FISCAL BUDGET: $150,000

SUMMARY OF RESULTS SINCE LAST REPORT: (Feb.-Sept., 1987)

Measurements of residual stresses in the vicinity of simulated cosmetic weld repairs have been completed for each of the five alloys under investigation in this program. These stresses are determined using the blind hole-drilling technique. Relaxation of residual stresses by a simulated post-weld heat treatment was also investigated. These studies are being completed to investigate the possible role of tensile residual stresses found in the vicinity of repair welds which are occasionally made on suction rolls during manufacture.

Residual stresses of similar magnitude appeared in each of the alloys upon placement of an autogenous ring weld on the surface of test coupons. These tensile residual stresses were confined to the immediate vicinity of the weld. The magnitude of the residual stress approached the tensile stresses of the alloys. Residual stress measurements on coupons subjected to a post-weld heat treatment revealed a significant reduction in the magnitude of the residual stress.

Near-threshold fatigue testing has been initiated on CA15 and 1N bronze alloys, in an effort to compare the performance of these commercially important materials with the duplex stainless steels currently under study. To date, tests have been completed in air and in two simulated paper machine whitewaters. Threshold stress intensity values for the CA15 and 1N bronze have been found to be lower than those of the duplex stainless steels, as anticipated.

High cycle fatigue testing continues in an effort to characterize crack initiation behavior in suction roll alloys. S-N curves have been completed for Alloys 63 and 75 in more aggressive simulated whitewaters. Although a significant environmental effect continues to be observed, no differences between the performance of these two alloys has been observed which would correlate with their vastly different performance in the field.

Metallographical investigation of crack path in the suction roll alloys has begun, in an effort to relate crack growth characteristics with the metallurgical structure and composition of the alloys. Cracking occurs in a transgranular mode, although microscopic deviations in crack path can be attributed to metallic phases in the path of the crack.

## INTRODUCTION

Corrosion-assisted cracking of suction roll alloys continues to be a costly problem for the paper industry. Garner(1) has documented a large number of failures of suction rolls in North America in recent years. Failure occurs when cracks begin to grow at the edge of a drilled hole in the roll, and then propagate through the shell in a longitudinal or circumferential mode. The suspected mode of failure is corrosion fatigue, wherein the fluctuating stresses imposed on the roll during rotation result in initiation and propagation of a crack. The corrosive conditions present in whitewaters promote crack initiation at pits and beneath deposits on suction rolls. Tensile residual stresses present in suction rolls as a result of manufacturing methods have also been implicated in roll failures.

The most attractive remedy for suction roll cracking is the development of suction roll alloys with improved resistance to corrosion-assisted cracking. In recent years, stainless steels with a duplex metallurgical structure have been developed and offered commercially for suction rolls. Suction rolls with low residual stresses have been made available, with a corresponding improvement in resistance to failure by corrosion-assisted cracking. However, it appears that even these alloys are susceptible to cracking, so further work is needed to optimize resistance to cracking and corrosion while minimizing alloy cost.

## LABORATORY TESTS TO PREDICT SUCTION ROLL PERFORMANCE

Corrosion fatigue resistance is usually assessed by conducting high cycle fatigue tests on smooth specimens exposed to real or simulated paper machine whitewaters. These tests involve subjecting test specimens to cyclic stresses which will initiate a fatigue crack and cause it to propagate to the point of specimen failure. As the magnitude of the cyclic stress amplitude, S, increases, the number of stress cycles that can be imposed before failure occurs, N, decreases. A plot of the data showing alternating stress versus the (logarithm of the) number of cycles to failure is the S-N curve, shown schematically in Fig. 1. Materials with greater resistance to corrosion fatigue failure exhibit S-N curves that are above (or shifted to the right compared to) curves for less resistant materials. Since a typical suction roll will experience more than $10^8$ cycles of reversed stress in a year of operation, it is necessary to examine the S-N behavior at extremely long lifetimes ( typically $10^8$ to $10^9$ cycles to failure) to quantify the resistance to cracking of any material. In this long lifetime regime, most of the cyclic lifetime is spent in initiating a crack, and relatively little in crack growth, so high cycle S-N tests characterize crack initiation behavior.

The S-N behavior of any alloy is affected by many variables, including the magnitude of steady stress superimposed on cyclic stresses, frequency of loading, corrosivity of the environment, and the metallurgical composition and structure of the test material. Accelerated failure is usually achieved by testing at a high frequency

of cyclic stressing, although this raises questions about the influence of corrosion on corrosion fatigue studies and the proper simulation of suction roll cracking conditions.

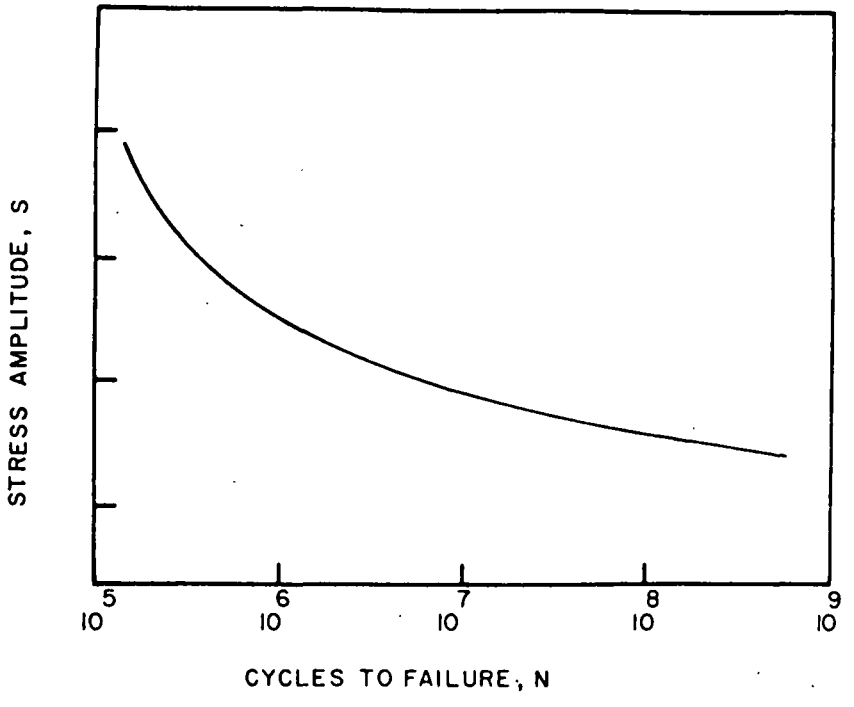


Figure 1. Schematic S-N Curve.

The resistance of a material to crack growth may also be established, by visual measurement of crack length during propagation of the crack under carefully controlled conditions of fluctuating load. In this type of test, the rate of growth of a crack is determined visually during application of a fluctuating load on a fracture mechanics specimen. The driving force for cracking is a combination of the cyclic forces applied to the specimen, the geometry of the specimen, and the instantaneous length of the crack. These factor are combined in a parameter known as the cyclic stress intensity range,

$\Delta K$, which quantifies the driving force for crack growth. Since growth rates can vary over a wide range, it is customary to plot crack growth behavior on a log-log plot of growth rate versus $\Delta K$. A schematic plot of a typical crack growth curve is shown in Figure 2.

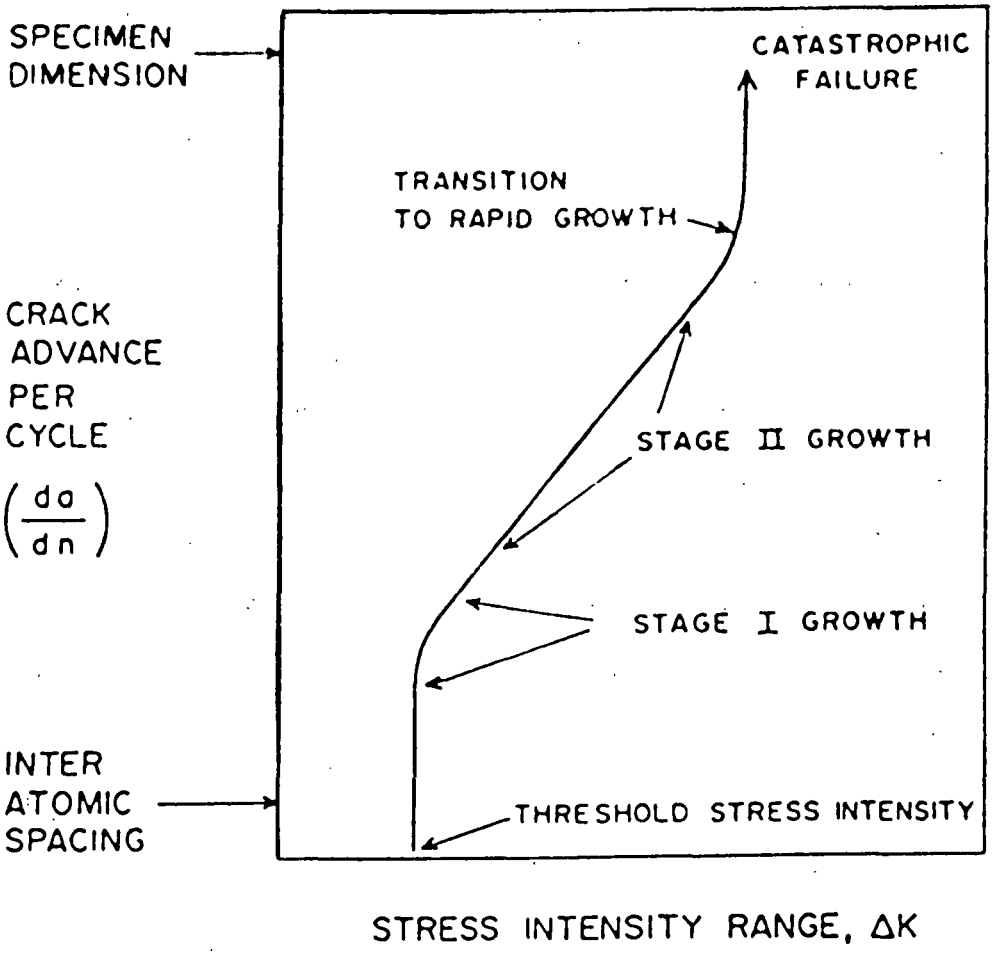


Figure 2. Schematic Plot of Crack Growth vs. Stress Intensity Range.

Typically, three stages of crack growth are observed in crack growth rate studies. At high $\Delta K$ levels, the driving force for crack growth is large and the growth rates are high and devoid of a significant environmental effect (Stage III). At somewhat lower $\Delta K$

levels, there is a regime of linear dependence of (log) growth rate versus (log)$\Delta K$, known as Stage II. At still lower $\Delta K$ levels, the rate of growth becomes very dependent on the applied stress intensity and eventually vanishes below some stress intensity range, $\Delta K_{th}$. Below this threshold value, no crack growth is apparent. Materials with superior resistance to crack propagation have high threshold stress intensities and growth curves that are shifted to the right, compared to inferior materials.

Since suction rolls accumulate large numbers of stress cycles in service, a small fraction of the lifetime can be spent in Stage II or Stage III growth. Only differences in Stage I growth near the threshold stress intensity will be relevant to crack growth behavior in actual suction rolls. For example, even at growth rates as low as $10^{-8}$ inches per cycle, a suction roll will still experience an inch of crack growth in one year of service. Consequently, crack growth behavior is relevant to suction roll performance only in the near-threshold regime where growth rates are so low that rolls will not fail by a few years of cyclic loading at these stress intensities.

Determination of the threshold stress intensity involves a complicated experimental method. If a notched or pre-cracked test specimen is simply subjected to larger and larger stress intensities until growth occurs, the apparent $\Delta K_{th}$ value would be very dependent on the details of the notch or pre-crack geometry. Furthermore, experience has shown that the threshold stress intensities determined

by increasing the stress intensity applied to a test specimen would be higher, and therefore not conservative, compared to thresholds determined by gradually reducing the stress intensity range until crack growth ceases.

The preferred method for determining the threshold stress intensity is a "load shedding" method, in which the cyclic load applied to the test specimen is gradually reduced in a controlled fashion until the rate of growth ceases. Load shedding must be done in small increments because of compressive residual stresses that appear at the crack tip immediately upon load reduction. The crack must be allowed to grow through these zones of compressive residual stress before a valid rate of growth can be measured.

Environmental effects on crack growth behavior are examined by conducting the tests in an appropriately corrosive environment. Corrosive environments generally reduce threshold stress intensities for crack growth, and increase the rate of growth at any stress intensity level above this threshold.

The resistance of suction roll alloys to crack growth under static loading conditions (i.e., stress corrosion cracking) has been examined by conducting slow strain rate tests and by exposures involving pre-stressed test coupons. In the slow strain rate test, a tensile specimen is subjected to a slow tensile test to failure while exposed to a potentially corrosive environment. If the test specimen

fails with a considerable loss in ductility, elongation, or strength, or if the mode of cracking is altered by exposure to the environment, the alloy is judged to be susceptible to SCC. Self-stressed coupons can be prepared in several ways, including mechanical pre-loading of specimens or by introducing residual stresses through controlled welding techniques. The specimens are then exposed to selected environments for prolonged periods to assess by visual inspection whether cracking will occur.

In years past, the development of improved suction rolls has proceeded at a slow pace, since there has been no good laboratory test that can be used as a predictor of service performance. The utility of new alloys is only recognized after prolonged operation in prototype roll applications.

In general, laboratory tests used to predict suction roll performance in the field have not correlated very well with this performance.. Traditionally, tests to determine mechanical strength, corrosion resistance, toughness, and corrosion fatigue resistance of smooth specimens have been used to screen candidate alloys. However, these tests have not been very useful for identification of promising new alloys. For example, Alloy 75 is vastly superior to Alloy 63 in commercial service as a suction roll alloy, yet these alloys differ little in their resistance to corrosion fatigue failure in traditional S-N fatigue testing. Furthermore, the corrosion resistance of Alloy 75 is inferior to that of Alloy 63, yet the service performance of Alloy 75 is

much better. It is clear that the test methods now available are of limited utility in identifying promising new suction roll alloys with improved resistance to corrosion-assisted cracking.

SHORT TERM OBJECTIVES.

The principal effort in this project has been devoted to identifying a laboratory test which would be a better predictor of the ultimate service performance of suction roll alloys, and which would help to characterize suction rolls with superior composition and microstruture. A variety of suction roll alloys with known service performance histories are being subjected to various laboratory tests in an attempt to identify a laboratory test that correlates with service performance. Corrosion, corrosion fatigue, and stress corrosion cracking tests have been examined in this search for a predictive laboratory test.

In the early stages of the test program, five duplex stainless steels with known service performance records were examined, including Alloys 63, 75, VK A-171 and -378, and 3RE60. Alloys 75 and 378 were resistant to cracking while alloys 171 and 63 experienced cracking in service. 3RE60 experienced early failure but has been relatively immune from cracking in recent years.

Recently, the performance of two other suction roll materials of great commercial importance have been examined, including the cast stainless steel, CA15, and 1N Bronze. CA15 is a cast martensitic stainless steel that contains 13% Cr and other minor alloying elements. The 1N bronze is a copper alloy containing 5% of each of Zn, Pb, and Sn. Both of these alloys have experienced severe cracking in service and both are perceived as being inferior to the cast duplex stainless steels in resistance to corrosion-assisted cracking in service.

PREVIOUS WORK.

A detailed report summarizing the current status of suction roll cracking has been distributed to IPC member companies (2). This report describes the results of corrosion tests of several suction roll alloys in simulated whitewaters. There is no apparent correlation between corrosion resistance and suction roll performance in service.

Near-threshold fatigue tests have been conducted in air and in simulated whitewaters to compare the threshold stress intensities for crack growth with the ranking of service performance. In these tests, little differences were found among alloys in air and in less aggressive whitewaters, but differences did appear when tests were conducted in more aggressive whitewater conditions. In particular, lowering the pH has a significant deleterious effect on threshold stress

intensity levels for most of the alloys tested, although Alloy 75 was relatively unaffected by acidification. The presence of sulfates in test environments containing chlorides increased the threshold for crack growth, as did an increase in the frequency of cyclic loading.

A large effect of superimposed tensile mean stress was observed in crack growth studies conducted in acidic simulated whitewaters, in apparent agreement with conventional wisdom that high tensile residual stresses are detrimental to cracking resistance in suction rolls. The effect of mean stress is greater in aggressive environments. Alloy 75 also appears to be more resistant to the effect of mean stress on crack growth rate.

Near threshold tests indicate that the 3RE60 alloy is consistently inferior to the other stainless steels in the test program, apparently as a result of a difference in the mode of crack growth. The 3RE60 is a wrought alloy with a fine structure, whereas the other four alloys are cast and have a relatively coarse metallurgical structure. Microbranching, which reduces the apparent stress intensity at the crack tip, occurs in cast alloys, but not in the wrought 3RE60 material.

S-N tests on Alloys 63 and 75 have failed to reveal significant differences between these alloys, even though their service performances are dramatically different, supporting the contention that S-N tests are ineffective for predicting service performance of suction roll alloys. Tests have been conducted by rotating bending on

smooth specimens and by reversed bending tests on notched specimens, using several different simulated whitewaters.

Slow strain rate tests have been conducted on five duplex stainless steel suction roll alloys in a simulated whitewater containing thiosulfate and chloride ions. Cracking has only been observed in Alloy 75, in apparent contradiction to the service performance of these alloys.

Limited tests have been conducted which show the presence of high tensile residual stresses in the vicinity of autogenous welds which simulate cosmetic weld repairs in suction rolls.

RECENT PROGRESS.

Near-Threshold Fatigue Testing. Near-threshold fatigue tests have been conducted on CA15 and 1N Bonze suction roll materials, to compare the resistance of these alloys to that of the duplex stainless steels which were tested previously. Tests were conducted in air and in simulated whitewater environments. Crack growth rate data for CA15 and 1N Bronze tested in air are shown in Fig. 3. For comparison, previously reported crack growth rate data for the duplex stainless steels are also shown in Fig. 3. From these data, it is apparent that the threshold stress intensities for both CA15 and 1N Bronze are well below those of all of the duplex stainless steels. Furthermore, at any given stress intensity range, the extrapolated rate of crack growth in

the bronze and the CA15 is higher than that of the duplex stainless alloys by several orders of magnitude.

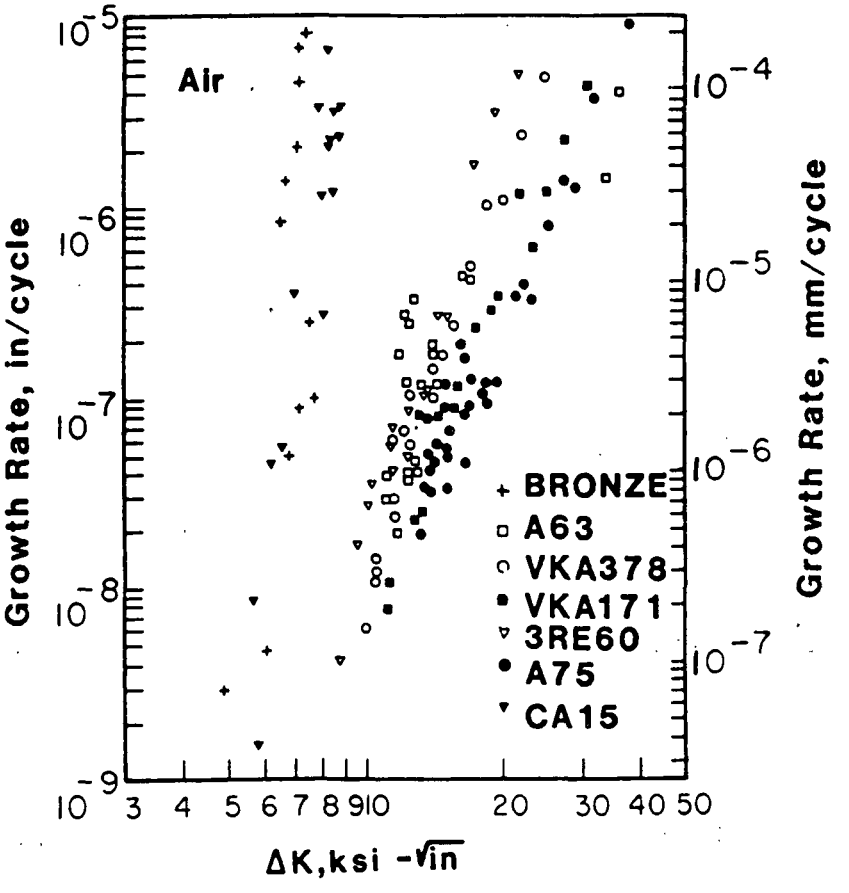


Figure 3. Crack Growth Rate Data for 1N Bronze and CA15 Tested in Air.

In an acidic chloride environment selected to simulate an aggressive environment developed beneath deposits, the resistance to crack growth of the CA15 alloy is inferior to that of the duplex stainless steels tested previously. Figure 4 compares the crack growth data for these alloys in Environment E, containing 1000 ppm $Cl^-$

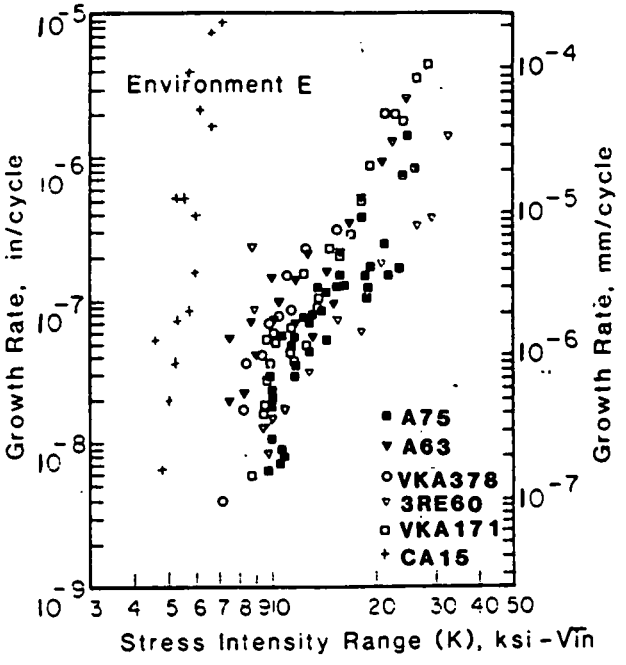


Figure 4. Crack Growth Rates in Environment E Containing 1000 ppm $Cl^-$ and and pH of 3.5.

and a pH of 3.5. For the CA15 alloy, exposure to the simulated whitewater environment reduces the threshold stress intensity slightly, relative to the value obtained in air tests. Since the duplex alloys experience a similar reduction in threshold stress intensity with this exposure, the CA15 remains inferior to the duplex alloys in this environment, as was the case for air tests. The threshold stress intensity for CA15 is approximately 5 MPa-$m^{-3/2}$, whereas the duplex stainless steels all have threshold stress intensities greater than 7 MPa-$m^{-3/2}$.

The rate of crack growth of the CA15 alloy in a more acidic chloride environment (Environment G, pH 1, 3000 ppm $Cl^-$) is shown in

Fig. 5, together with the data for the duplex stainless steels tested in the same environment. The CA15 threshold stress intensity is only slightly decreased by the exposure to the more acidic environment, whereas the duplex stainless steels experience a significant reduction in threshold stress intensity values by this exposure. Thus, the performance of the cast duplex stainless steels is, at best, only slightly superior to, the martensitic CA15 stainless steel in this highly aggressive environment. The threshold stress intensity for the wrought duplex stainless steel, 3RE60, is actually inferior to that of the CA15 material in this environment. All four of the alloys tested thus far experience a significant reduction in threshold stress intensity from exposure to this highly acidic chloride-containing environment.

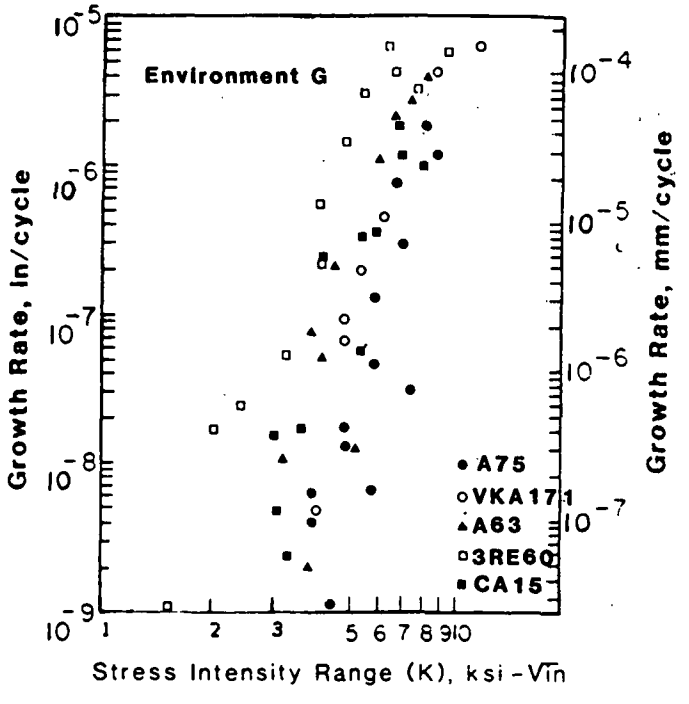


Figure 5. Crack Growth Rates in Environment G containing 3000 ppm $Cl^-$ and a pH of 1.0

Crack Path Studies. Metallography is being used to investigate the path of the fatigue crack through the two phase microstructure of the duplex stainless steels, in an attempt to understand the origins of differences in resistance to cracking exhibited by the different alloys. Generally speaking, the crack path is found to be transgranular through the two-phase structure, as shown by the crack microbranches seen in Figs. 6-7. Although the crack path is transgranular through both phases, the crack growth direction does appear to deviate upon passage through a phase boundary, as shown by the arrow in Figure 7. As reported previously, the path of cracking through the wrought material (3RE60) is less affected by the fine structure than the path through the coarse cast structures, and there is virtually no evidence of any significant

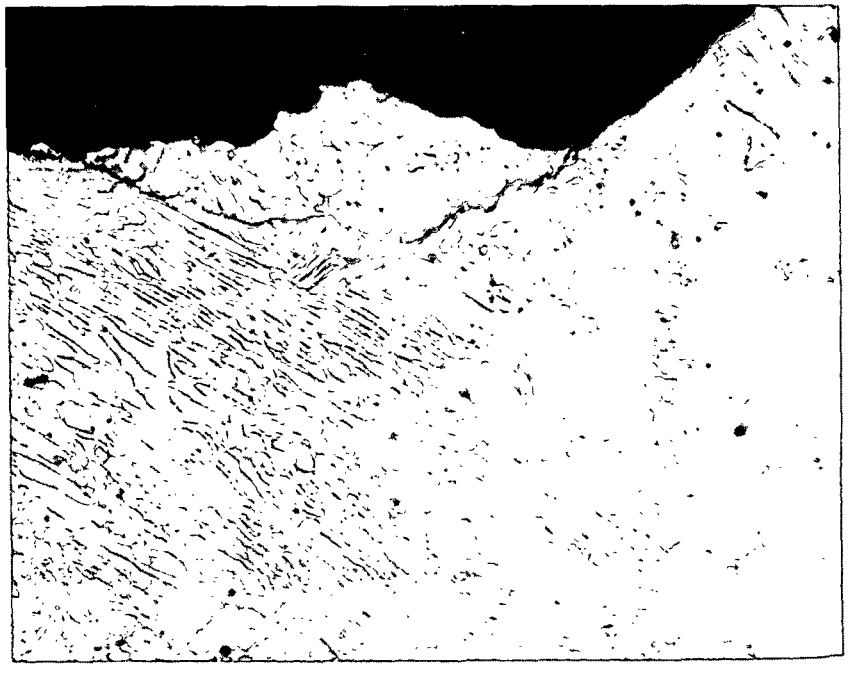

Figure 6. Crack Path Through Alloy 63, showing Transgranular Microbranching.

Figure 7. Crack Path Through Alloy 75 Showing Transgranular Microbranching.

crack branching seen in the 3RE60 alloy, whereas the cast alloys frequently exhibit microbranching of the crack. Additional microscopy is underway to investigate the influence of exposures to corrosive environments and to elucidate the effect of crack growth rate on crack paths.

Crack Initiation Studies using S-N Tests. To date, S-N tests in several different environments with pH levels above 3 have not differentiated between Alloys 63 and 75, as might be expected from differences in their service performance. Testing continues in order to determine if the test environment has an effect on the relative performance of these two suction roll alloys. Figure 8 shows the results of recent tests completed in Environment E (1000 ppm $Cl^-$, pH 3.5) and Environment G (3000 ppm $Cl^-$, pH 1). The acidifcation and increased levels of chloride

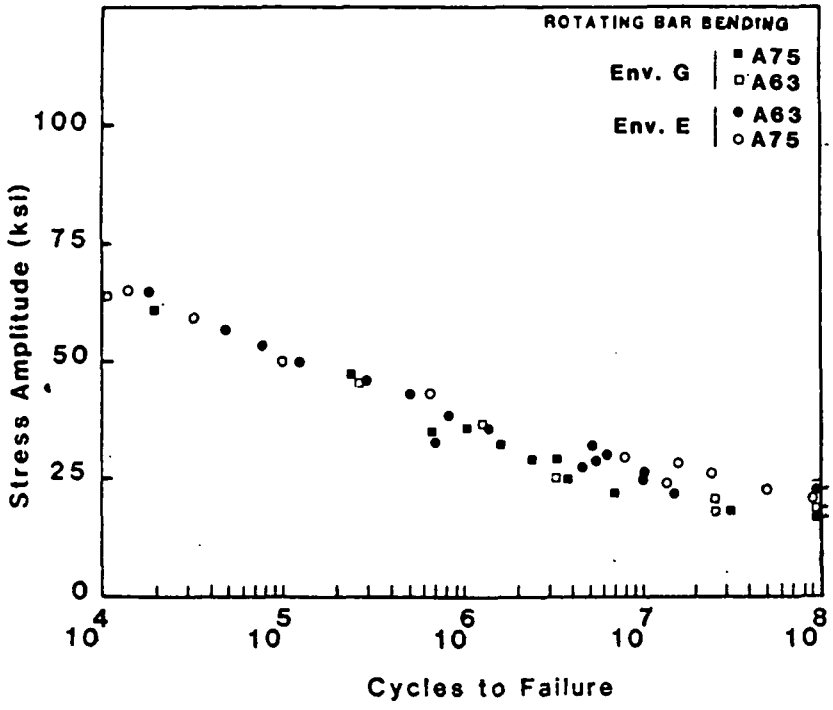


Figure 8. S-N Data for Alloys 63 and 75 in Acid Chloride Environments.

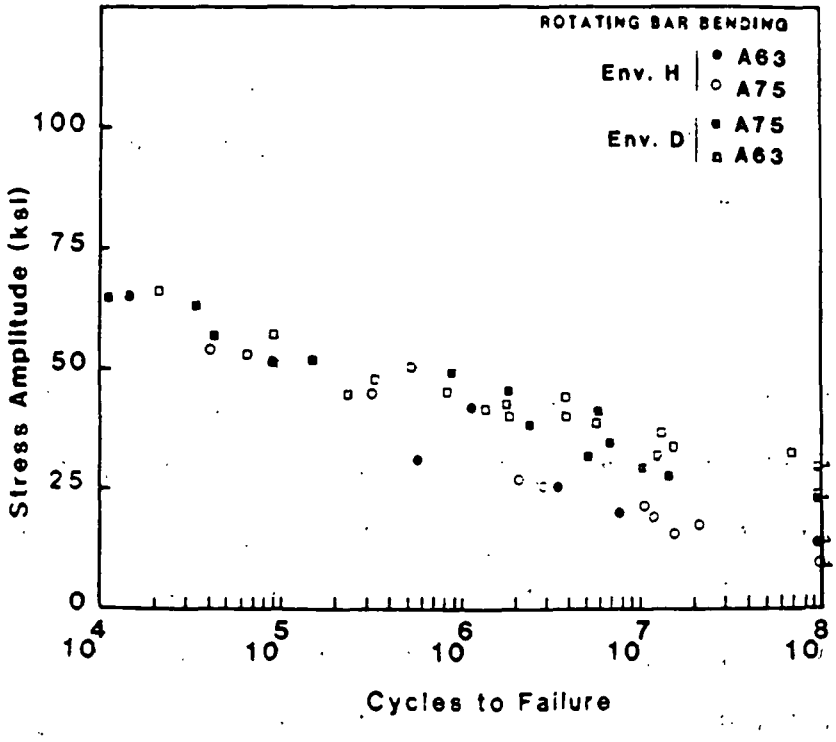


Figure 9. S-N Data for Alloys 63 and 75 in Acid Chloride Environments Containing Thiosulfate.

ion result in a slight reduction in the $10^8$ cycle fatigue strength for both alloys, but no difference in fatigue resistance of these two suction roll alloys is evident. Figure 9 shows the results of S-N tests in Environment D (220 ppm $Cl^-$, 500 ppm $SO_4^=$, 50 ppm $S_2O_3^=$, and a pH of 4) and Environment H ( 3000 ppm $Cl^-$, 500 ppm $SO_4^=$, 50 ppm $S_2O_3^=$, and a pH of 1.0). Although the S-N curves are not complete, it is clear that there is a deleterious effect on the fatigue strength of increasing the acidity and chloride concentration, but the increased severity of the environment still fails to discriminate between alloys with vastly different service performance. No test environment yet identified would have predicted the different service performance of these two suction roll alloys.

Weld Residual Stress Effects. Tests have been conducted to determine the magnitude and sign of the biaxial stress distribution in the vicinity of autogenous welds which simulate cosmetic welds on duplex stainless steel suction roll alloys. Cosmetic welds may be made to repair small machining defects and porosity revealed by the machining process. High tensile residual stresses may be detrimental to resistance to stress corrosion crack initiation or corrosion fatigue cracking.

Residual stresses are measured by the hole-drilling technique, in which a hole of controlled dimensions is drilled in a block of the metal, while the strains introduced by relaxation of the stresses

in the excavated metal are measured via strain gages mounted on the surface of the metal in the vicinity of the hole. The apparatus to measure the residual stresses is shown in Fig. 10.

Residual stresses were measured in alloys processed in three different ways: 1) as-received, 2) ring-welded, and 3) ring-welded and stress-relieved. The ring weld coupons, with and without stress relief, are currently being exposed to Environment E (1000 ppm $Cl^-$, pH of 3) to determine if stress corrosion cracking will occur as a result of the high tensile residual stress and the aggressive environment.

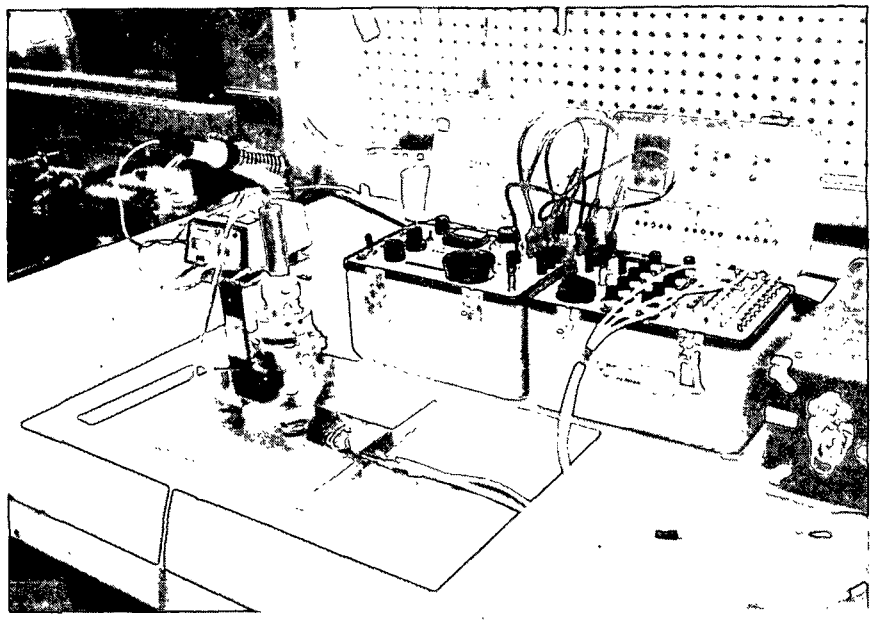

Figure 10. Hole Drilling Apparatus used to Determine Residual Stresses.

The stress relief treatment involved a two hour anneal at a temperature of 550 °C, followed by a slow cool to 425 °C, followed by air cooling to room temperature.

The distributions of the residual stresses for the five duplex stainless steels are shown in Figs. 11-15. The as-received materials exhibited little residual stress, apparently because of relaxation of any stresses in the process of machining coupons from roll stock material. On the other hand, all of the alloys exhibited large tensile residual stresses in the vicinity of welds on the as-welded specimens. Stresses as high as 90,000 psi were measured. However, the stress relief treatment completely relaxed these stresses.

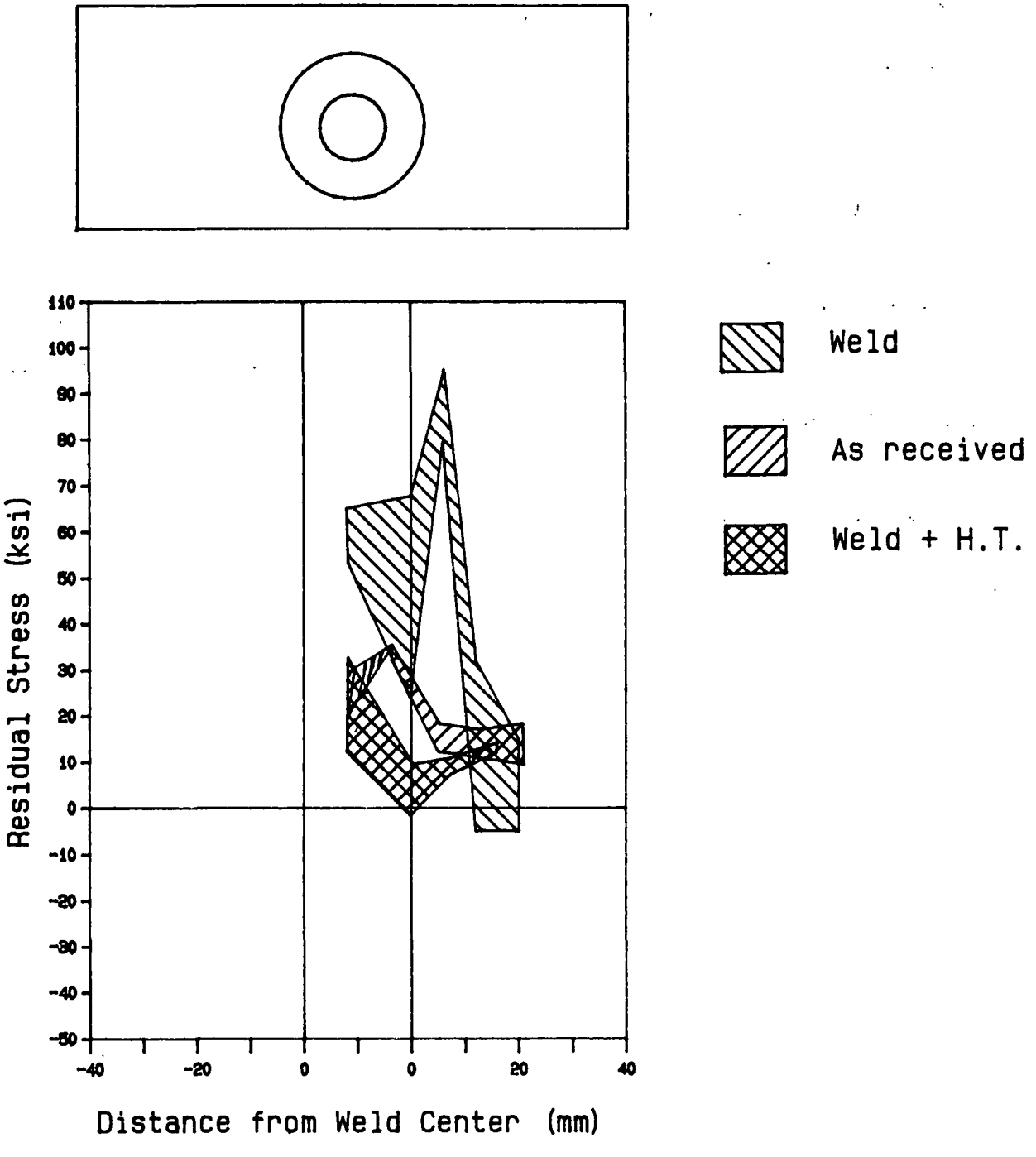


Figure 11. Residual Stress Distributions in Ring Welded Alloy 63.

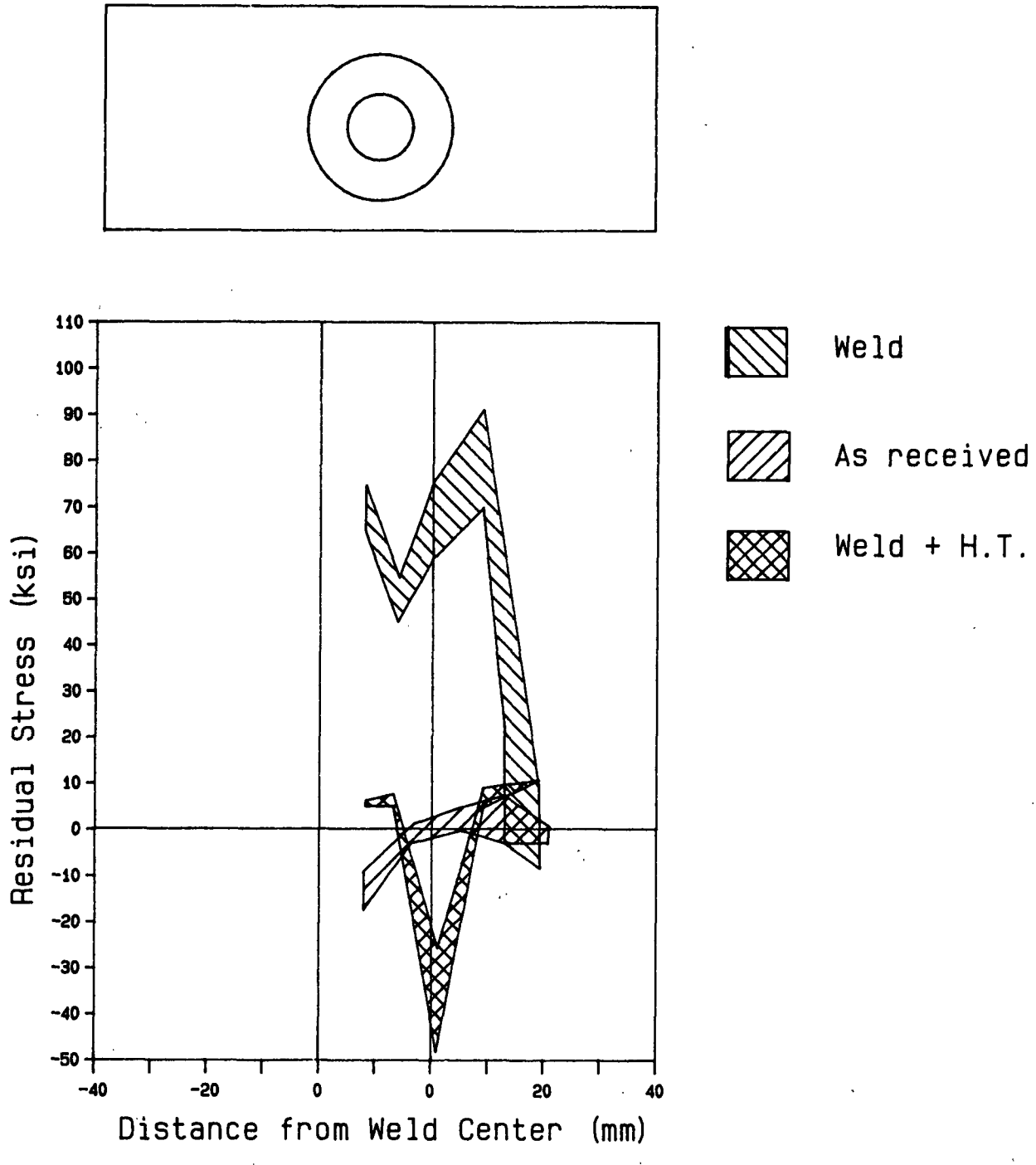


Figure 12. Residual Stress Distributions in Ring Welded Alloy 75

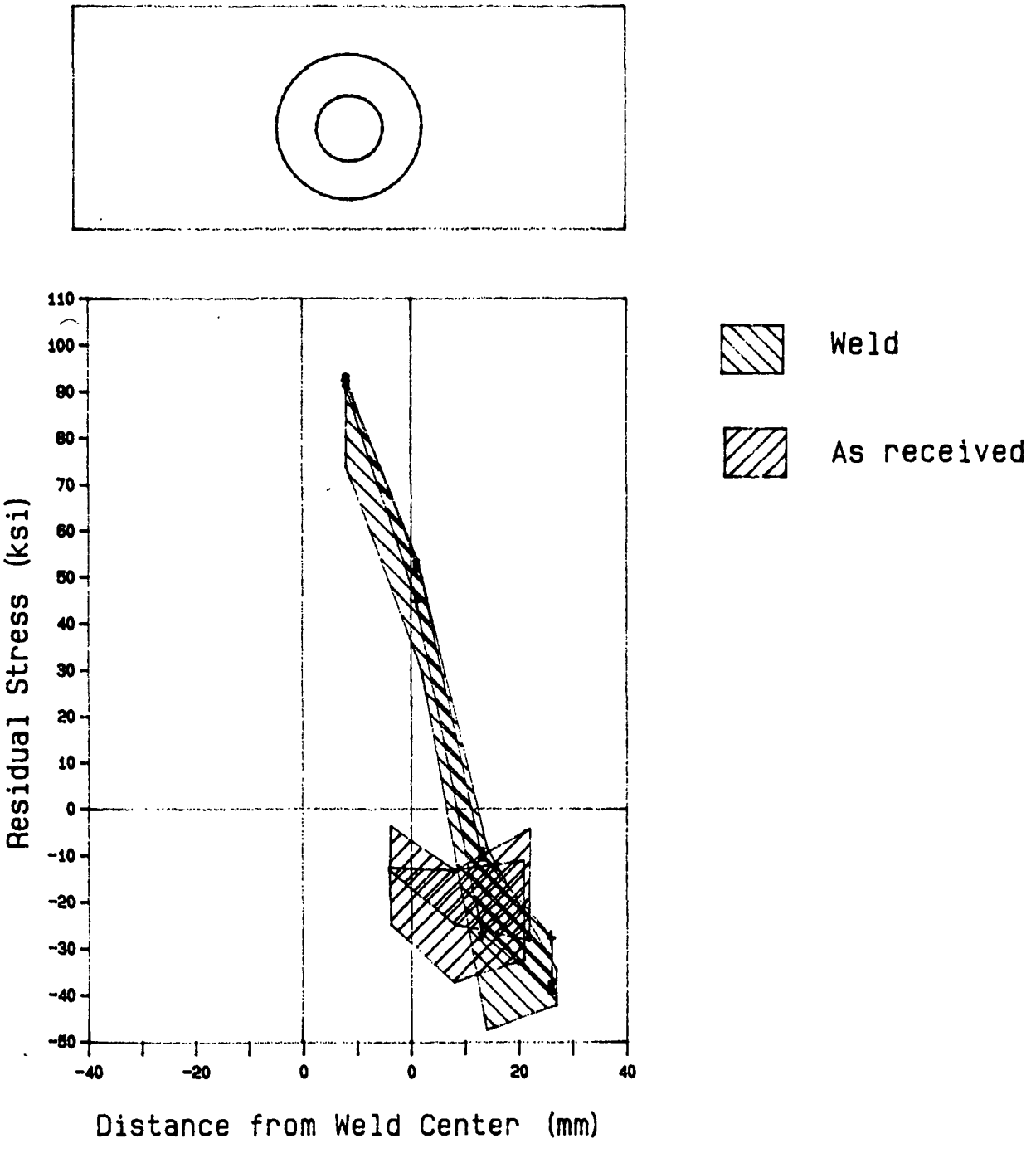


Figure 13. Residual Stress Distributions in Ring Welded Alloy VKA-171.

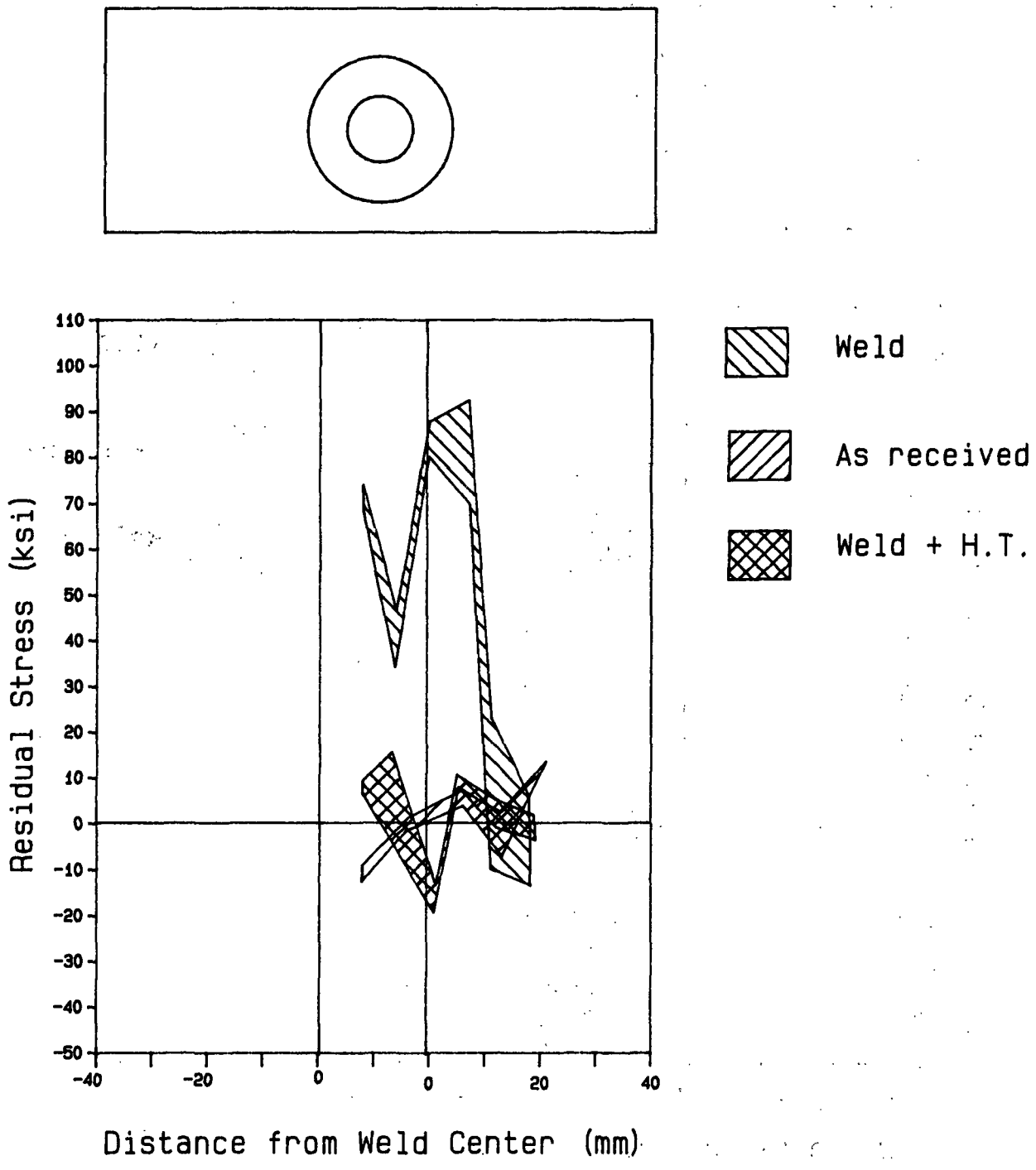


Figure 14. Residual Stress Distributions in Ring Welded Alloy VKA 378.

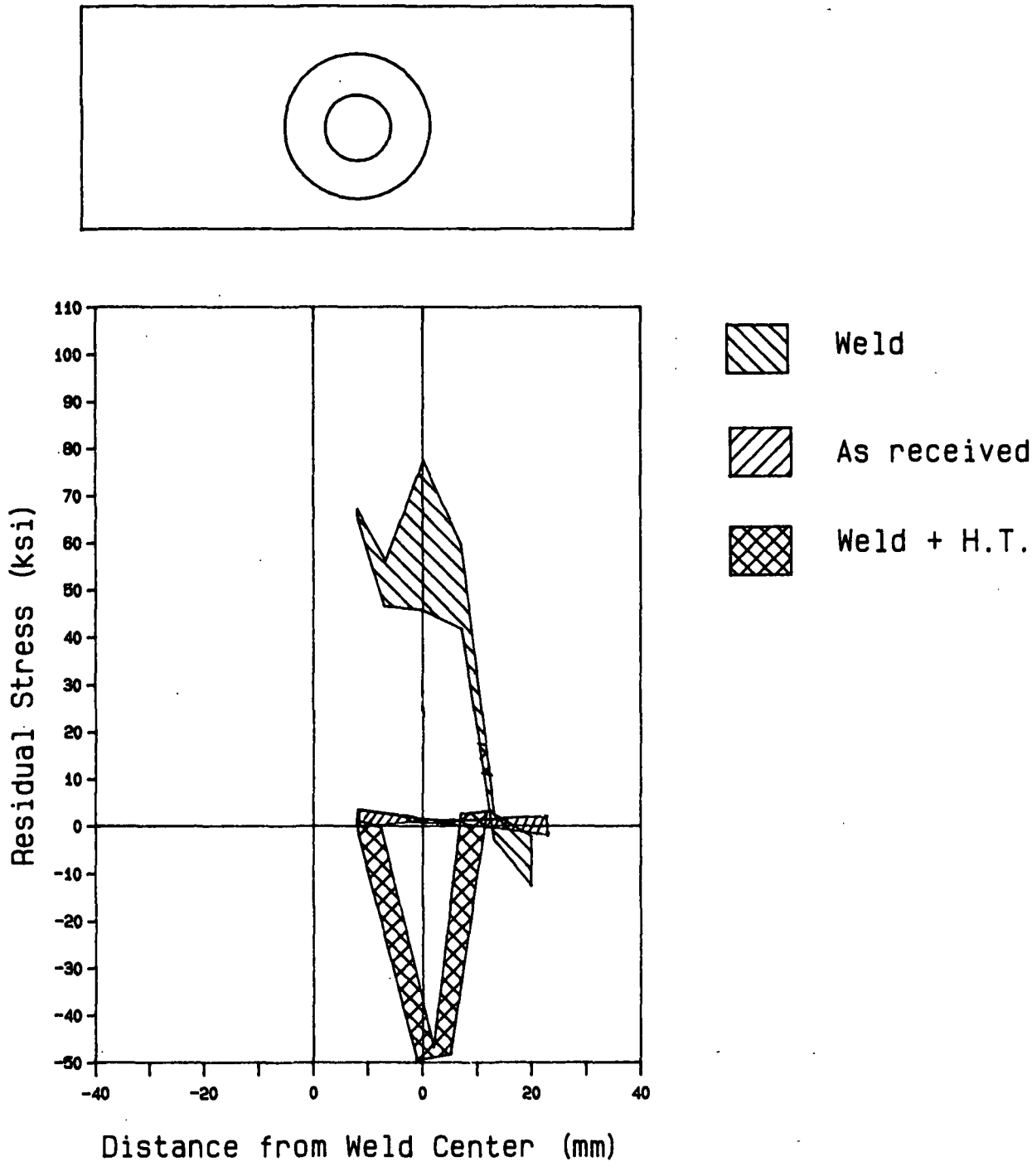


Figure 15. Residual Stress Distributions in Ring Welded Alloy 3RE60.

PLANS FOR THE NEXT PERIOD.

In the next period, the effect of imposed electrochemical potential on near-threshold fatigue crack growth will be examined to enhance the understanding of the origins of differences in crack growth among the various alloys now under test. Metallographic studies of crack path, relative to metallographic structure, will be pursued to assist in the assessment of the origins of differences in resistance to near-threshold crack growth. Exposures of ring weld coupons will continue in the current test environment, as well as the thiosulfate environment known to induce stress corrosion cracking in slow strain rate tests. Reversed bending tests to establish S-N behavior of Alloys 63 and 75 in other simulated whitewaters will be pursued. S-N tests on these alloys under a superimposed tensile mean stress will be conducted if fatigue machines suitable for such tests can be obtained.

SIGNIFICANCE TO THE INDUSTRY.

The near-threshold crack growth behavior of two additional classes of suction roll alloys is consistent with their service performance records, lending additional credence to this test method as a predictor of service performance of suction rolls.

The crack initiation behavior of suction rolls, as determined by fully reversed loading S-N tests, continues to be of little value in differentiating between suction roll alloys.

Measurements have documented the high tensile residual stresses thought to be present in the vicinity of non-stress-relieved welds placed on suction rolls. The deleterious effect of high tensile residual stress on resistance to near-threshold fatigue cracking has already been documented. The relevance to SCC behavior is being examined.

REFERENCES.

1. A. Garner, "Suction Roll Failures in Canada", Proc. 70th Annual Meeting of the CPPA, Paper A209, (1984).

2. D. Bowers, "Corrosion and Corrosion Fatigue of Paper Machine Suction Rolls", Report No. 2, Project 3309, (1984).

THE INSTITUTE OF PAPER CHEMISTRY

Appleton, Wisconsin

Status Report

to the

ENGINEERING PROJECT ADVISORY COMMITTEE

Project 3556

# FUNDAMENTALS OF KRAFT LIQUOR CORROSIVITY

October 22, 1987

PROJECT SUMMARY

DATE: September 25, 1987

PROJECT NO.: 3556 - Fundamentals of Kraft Liquor Corrosivity

PROJECT LEADER: D. C. Crowe

IPC GOAL:

Increase the useful life of equipment by paper selection of materials of construction and by identifying suitable process conditions.

OBJECTIVE:

To understand the causes of corrosion and corrosion-assisted cracking of carbon steels exposed to kraft liquor, as a basis for developing methods for reducing corrosion damage in kraft process streams.

CURRENT FISCAL BUDGET: $75,000

SUMMARY OF RESULTS SINCE LAST REPORT: (February 1987 - September 1987)

Modifications of the programming of the microprocessor-based corrosion monitoring system have been completed and it is being tested in the laboratory. Slow strain rate tests to determine stress corrosion susceptibility of carbon steel in liquor from continuous digesters have been completed. The effects of additions of combinations of sulfite and thiosulfate on corrosion in white liquor have been studied. Work to determine the effects of velocity on corrosion in white liquor has been reactivated.

INTRODUCTION:

Corrosion in kraft white liquor has been studied intensively in this project. A better understanding of the influence of liquor constituents has been garnered and the behavior of liquors in mills has been elucidated. A significant part of our effort has been devoted to development of improved corrosion monitoring methods.

A microprocessor-based corrosion monitoring system has been built to collect corrosion rate data from a commercial measuring instrument. The measured corrosion values were obtained by that instrument via the linear polarization resistance method. This method was demonstrated to be reliable, and was used in on-line continuous corrosion measurements in mills. The microprocessor-based system was very successful; it improved data collection and made the data accessible by telephone from the Institute. Currently, improvements are being made to the microprocessor system to make it capable of replacing the commercial measuring instrument. The resultant system will be more compact and reliable.

Another area of effort has been the investigation of stress corrosion cracking of continuous digesters. Some digesters suffer extensive cracking, while others appear to be immune. The reasons for these differences are unknown. It is clear that cracking susceptibility is greatest within a range of corrosion potentials; if the digester steel has a potential in this range it will crack. This raises the question whether the size of this range varies from digester to digester. The present study is aimed at answering this question.

The corrosivity of kraft liquor is a function of its composition. Previous work has explored the influence of sulfide, hydroxide, thiosulfate, polysulfide and sulfite, and combinations of thiosulfate and polysulfide. As a final phase of this laboratory work, the effects of additions of combinations of thiosulfate and sulfite to an NaOH and $Na_2S$ solution have been investigated, and are described below.

Laboratory studies are underway, also, to determine the effects of liquor velocity on corrosion rate. One objective is to relate corrosion rates to some hydrodynamic factor such as shear so that corrosion rate may be factored into piping design. A rotating electrode and a flow loop are being utilized in this work.

PROGRESS:

Corrosion Monitoring System

The microprocessor-based corrosion monitoring system described previously was built to collect and store data from an instrument which measured corrosion rate. It was designed with the idea that, with the addition of further cards, it could also make the corrosion measurements and replace the old corrosion measuring instrument.

The system will measure corrosion rates by the linear polarization resistance technique. The programming of this measurement technique has been a nontrivial pursuit. Preliminary testing indicates that the present program is successful. Laboratory tests will continue to qualify the system prior to use in a mill. This system will be compact, reliable and convenient. When installed in a mill, it will require minimal attention from mill personnel, and may be monitored remotely by telephone.

Slow Strain Rate Testing in Digester Liquors

Liquor samples were obtained from top separator/top circulation lines of four Kamyr continuous digesters. Tests have also been conducted in simulated white liquor of the same composition as mill E9. Liquor analyses were performed and are summarized in Table 1.

Table 1

DIGESTER LIQUOR COMPOSITION

| | MILL M5 | MILL P7 | MILL E9 | MILL H10 |
|---|---|---|---|---|
| NaOH | 14.1 | 39.5 | 50.7 | 25.4 |
| $Na_2S$ | 11.1 | 18.9 | 21.6 | 14.5 |
| $Na_2CO_3$ | 30.7 | 16.6 | 26.6 | 17.3 |
| $Na_2S_2O_3$ | 2.54 | 2.48 | 6.8 | 2.8 |
| $Na_2SO_3$ | 1.32 | 2.6 | 4.8 | 1.5 |
| $Na_2SO_4$ | 3.42 | 2.24 | 7.7 | 3.3 |
| NaCl | 1.17 | 1.46 | 0.53 | 0.4 |
| $Na_2S_x$ | 0.67 | 0.18 | -- | 0.64 |

Data from slow strain rate tests in mill liquors are plotted in Fig. 1-3, and for a simulated liquor in Fig. 4. The mills have been identified as M5, P6 and E9. The simulated liquor was to have the composition of mill E9 except for the organics and trace inorganics. The objective of testing with

this simulated liquor was to determine whether the major inorganic species control stress corrosion susceptibility, or whether organics play a role.

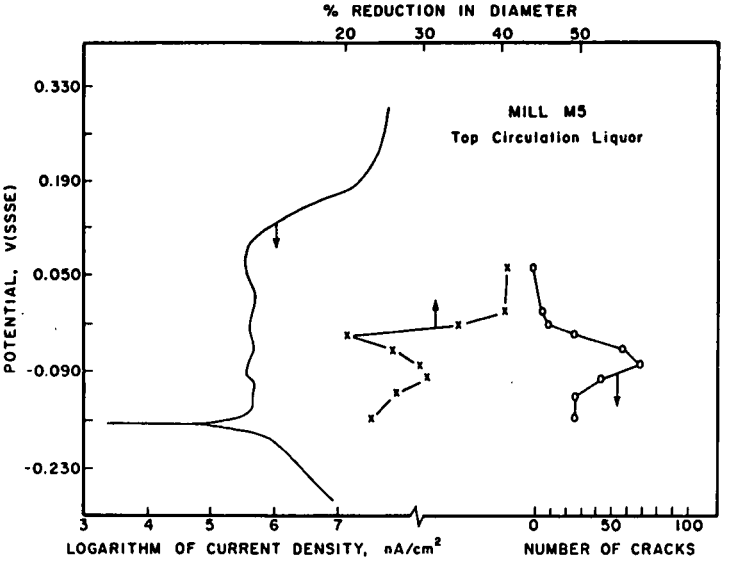


Figure 1. Polarization curve, and percent reduction in diameter and number of stress cracks in test samples as a function of potential for mild steel in mill M5 liquor, illustrating the susceptibility to stress corrosion in the active/passive range.

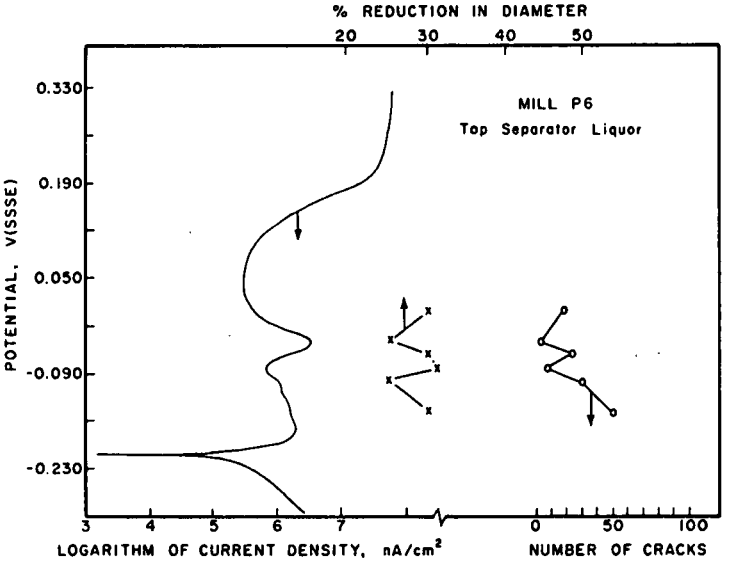


Figure 2. Polarization curve, and percent reduction in diameter and number of cracks in test samples as a function of potential for mild steel in mill P6 liquor.

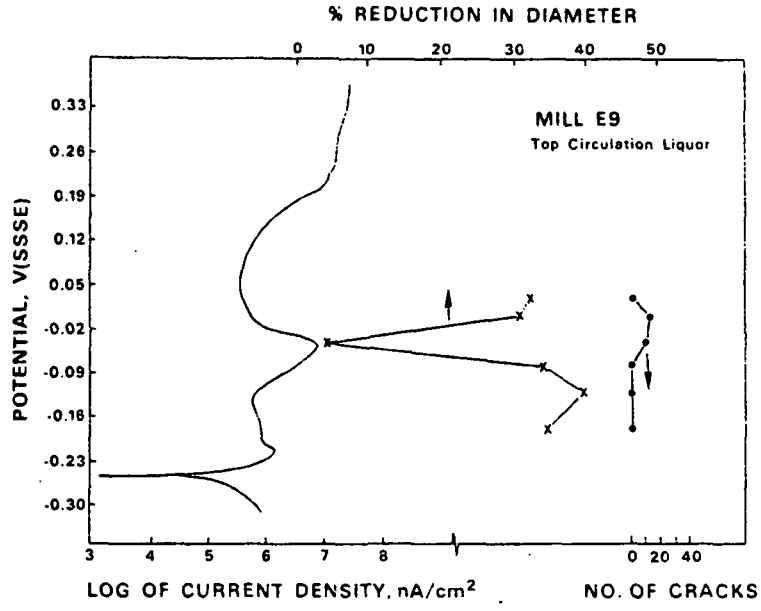


Figure 3. Polarization curve, and percent reduction in diameter and number of cracks in test samples as a function of potential for mild steel in mill E9 liquor.

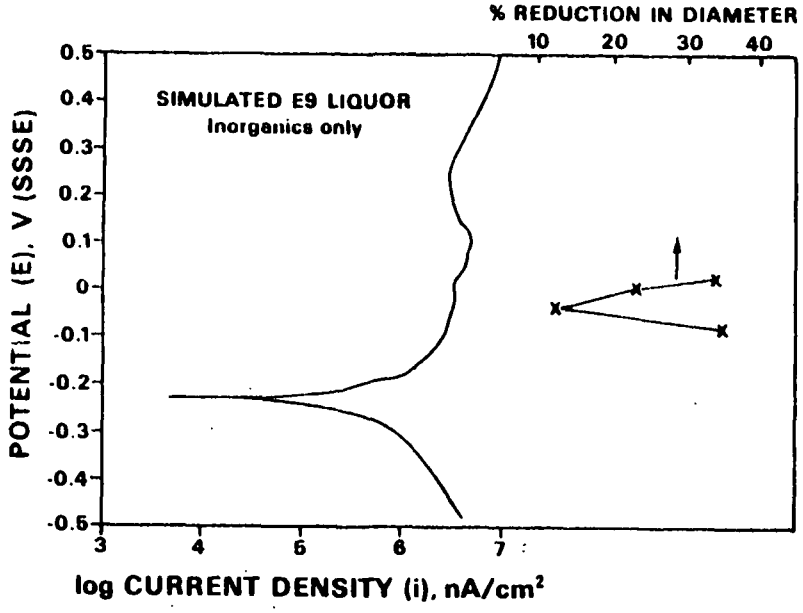


Figure 4. Polarization curve and percent reduction in diameter of test samples as a function of potential for mild steel in simulated E9 liquor, containing the major inorganic species of the E9 liquor.

The polarization curves were different in shape in the different mill liquors. The curve obtained for mild steel in mill M5 liquor had low current peaks; this would be expected for a relatively weak liquor. Curves for steel in liquor from mills P6 and E9 had significant active/passive peaks typically found in stronger liquors. The peak was less pronounced in the simulated E9 liquor.

Cracking susceptibility is measured by the percent reduction in diameter of the test specimen. If a specimen does not experience stress corrosion cracking (SCC), it will fail in a ductile fashion after considerable elongation and necking. On the other hand, if cracking occurs during the test, the specimen will fail early in the test, from a crack in its surface. The fracture surface will be rough and many other cracks will be present. The specimen will not have 'necked down', so its diameter will be closer to the original. Thus the percent reduction in diameter will provide a measure of susceptibility to SCC. Results for the test liquors are plotted in Fig. 1-4.

In Mill M5, a large number of cracks were associated with the SCC range of potential, as measured by % reduction in diameter (Fig. 1). Correlation between number of cracks and % reduction was less clear for Mill P6, but a good correlation was seen for mill E9. The number of cracks was not plotted for the simulated E9 liquor because the numbers of cracks in the cracked specimens was very large. There were many mere cracks than in the actual E9 liquor, suggesting that organics in the real liquor may have inhibited crack formation.

The range for cracking varied from mill to mill. For mill M5 liquor, the most severe cracking was in the range from +10 to -100 mV(SSSE). For

mill P6 liquor, cracking was not severe, as judged by relatively high percent reduction in diameter measurements; cracking was most severe between -40 and -80 mV(SSSE) and cracking at potentials below 20 mV(SSSE). In mill E9 liquor, the cracking range spanned +20 to -40 mV(SSSE). A similar range was observed with the simulated E9 liquor. The lack of organics in the simulated E9 liquor did not appear to have a strong influence on the range for stress corrosion. The reasons for differences between mills have not been determined yet, but may be related to different concentrations of inorganic species.

Testing is underway in liquor from mill H10.

Effects of Thiosulfate and Sulfite Combinations on Corrosion in White Liquor

In the liquors tested previously with thiosulfate additions alone, the corrosion potential tended to be in the active-passive region. Sulfite, on the other hand, kept the potential in the active region. These results pointed to the possibility that a tension could exist between these two species which would result in corrosion potential in the active-passive range, very slow passivation and sustained high corrosion rates as a result. Thus, combinations of thiosulfate and sulfite were tested.

Corrosion rates were investigated by exposing 1018 carbon steel weight loss coupons to liquors at 90 C for 2, 4, 6 and 8 weeks. The base solution was 100g/L NaOH + 40 g/L $Na_2S$ with additions of 2, 5, and 25 g/L $Na_2S_2O_3$ and 2, 5 and 25 g/L $Na_2SO_3$. Solutions were changed at two week intervals in a glove bag under nitrogen atmosphere to prevent oxidation by air. Polarization curves were obtained in each liquor composition at 90 C. All

measured potentials have been quoted with respect to the silver/silver sulfide reference electrode, (SSSE).

Representative polarization curves are illustrated in Figure 5. The large number of current peaks and the variability in their heights was typical of behavior in these solutions at higher thiosulfate concentrations.

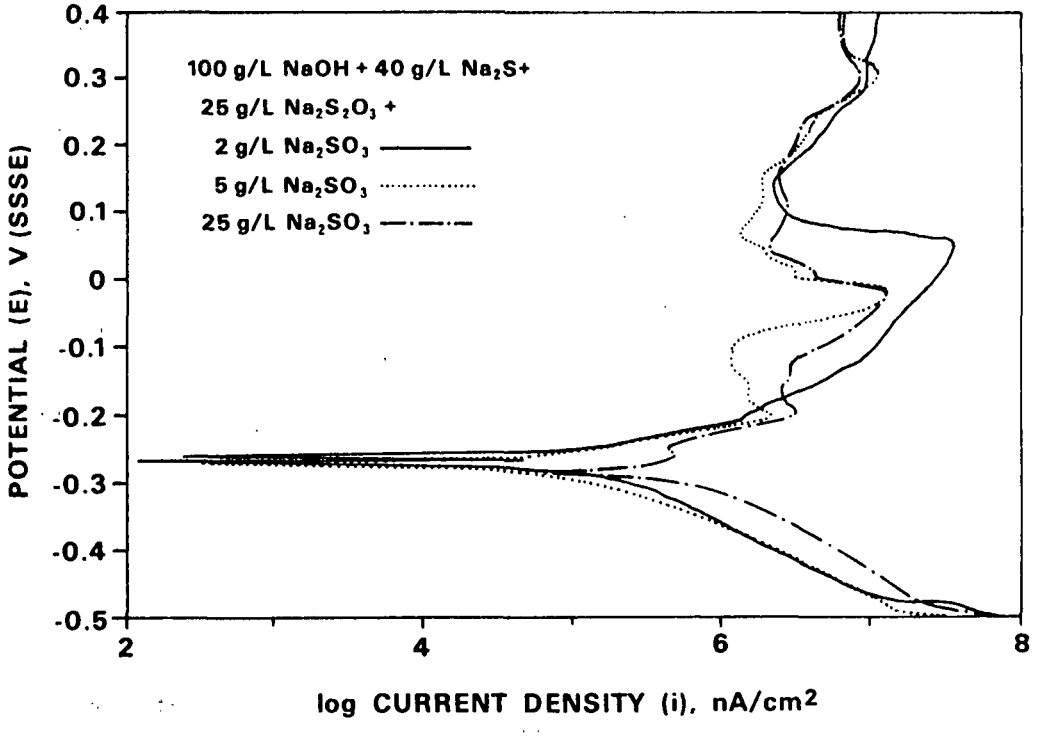


Figure 5. Polarization curves in solutions containing thiosulfate and sulfite. The curves had many current peaks and considerable variability in the heights of peaks.

Corrosion rates have been tabulated in Table 2.

Table 2

Effect of combinations of thiosulfate and sulfite.

| NaOH, g/L | $Na_2S$, g/L | $Na_2S_2O_3$, g/L | $Na_2SO_3$, g/L 2 | 5 | 25 |
|---|---|---|---|---|---|
| | | | After 2 weeks | | |
| 100 | 40 | 2 | 25 | 19 | 13 |
| | | 5 | 17 | 21 | 19 |
| | | 25 | 51 | 39 | 40 |
| | | | After 4 weeks | | |
| 100 | 40 | 2 | 23 | 22 | 14 |
| | | 5 | 15 | 20 | 17 |
| | | 25 | 48 | 35 | 42 |
| | | | After 6 weeks | | |
| 100 | 40 | 2 | 19 | 23 | 15 |
| | | 5 | 13 | 17 | 19 |
| | | 25 | 41 | 33 | 40 |
| | | | After 8 weeks | | |
| 100 | 40 | 2 | 19d | 19d | 17d |
| | | 5 | 13d | 20d | 17d |
| | | 25 | 34c | 37d | 28d |

a Immediate passivation
b Passivation in < 200 h
c Passivation in > 200 h
d No passivation

In weight loss tests, sulfite increased the corrosion rate below 5 g/L but had less effect above 5 g/L as can be seen in Fig. 6. Both sulfite and thiosulfate would have inhibited passivation, thereby maintaining the corrosion rate at a high level throughout the 8 week exposure. Only the test with 25 g/L $Na_2S_2O_3$ + 2 g/L $Na_2SO_3$ passivated and then only after 7 weeks, resulting in a lower corrosion rate. Higher corrosion rates were observed as

thiosulfate concentration was increased, Figure 7, consistent with higher dissolution currents in the active/passive region with increasing thiosulfate and with control of potential at higher values. These values persisted throughout the test. Thus, sulfite may sustain the high corrosion rates due to the thiosulfate. Corrosion rates were in the range normally experienced in mills and behavior was complex like in mill liquor, suggesting that thiosulfate and sulfite must be present to properly simulate a mill liquor. No regression equations were calculated due to the small number of data collected.

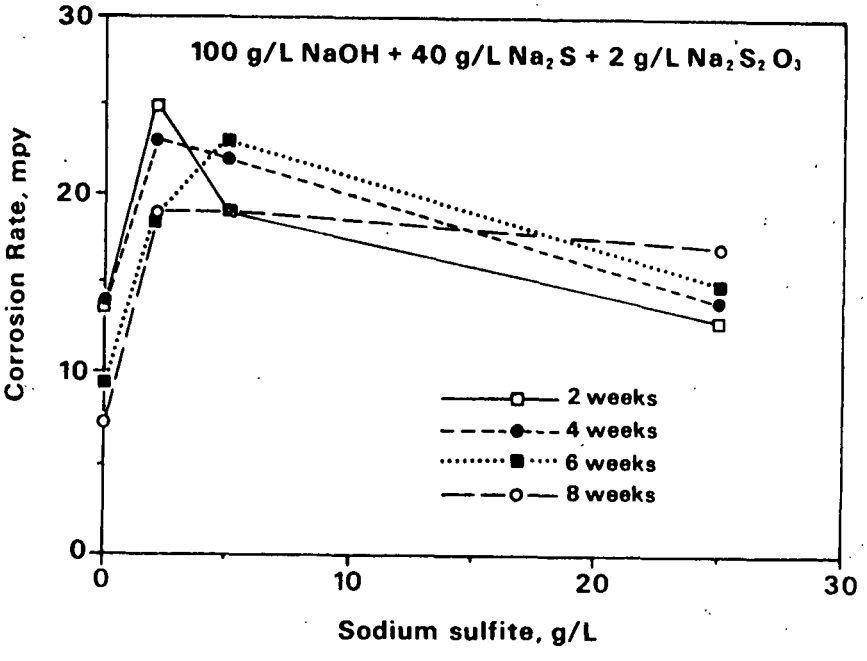


Figure 6. The effect of sulfite concentration and exposure time on corrosion rates in 100g/L NaOH + 40 g/L, $Na_2S$ + 2g/L $Na_2S_2O_3$, illustrating the influence of sulfite concentration below 5 g/L and the lack of variation with exposure time.

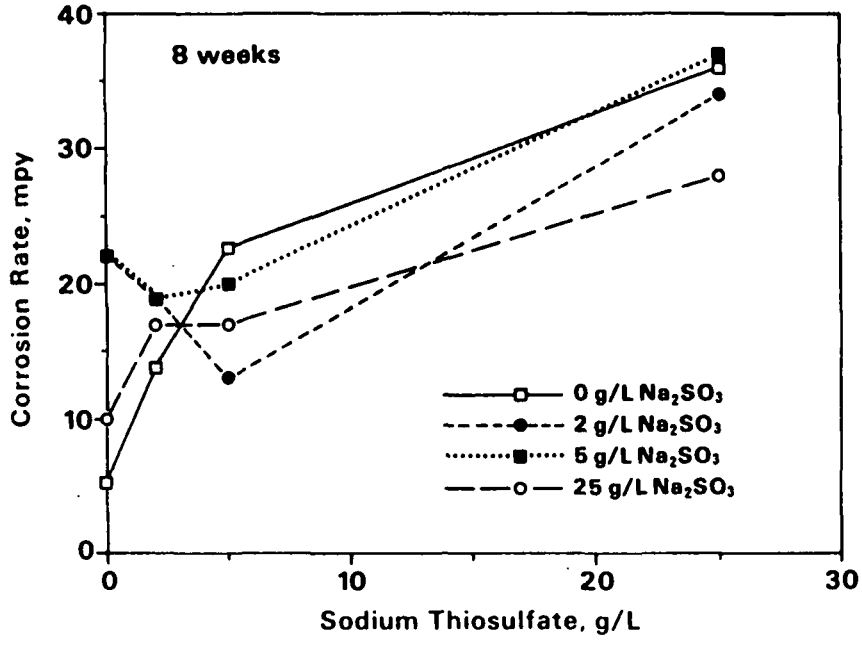


Figure 7. Corrosion rates with additions of sulfite and thiosulfate after 8 weeks, illustrating the substantial effect of thiosulfate in these solutions.

Potential was monitored and found to be in the active region throughout the tests. This indicates that sulfite played an important role in controlling the potential.

These results conclude the study of the effects of various white liquor constituents.

Velocity Effects in White Liquor

Previously, the effect of liquor velocity on corrosion rates has been shown. Increases in corrosion rate by an order of magnitude or more have been observed in flowing white liquor.

A student research project to study velocity effects using a rotating

electrode was completed by Rob Kalishek last spring. Due to his efforts, the experimental apparatus was improved and effects of temperature, rotation rate and exposure time were investigated. The results indicated that mass transfer to the electrode surface was rate controlling.

The rotating cylindrical electrode provides reproducible hydrodynamic conditions which may be varied from laminar to turbulent. Conditions can be characterized by parameters such as shear or Reynolds number, etc. The objective of the present work is to relate the corrosion rate to hydrodynamic conditions.

In parallel with this study using the rotating cylindrical electrode, work is commencing in a study of corrosion rates versus flow in a pipe loop. Corrosion rates will be measured at various flows, for which parameters such as Reynolds number and shear will be calculated. A comparison of corrosion rates at given values of these parameters in the flow loop and the rotating electrode apparatus will be used to determine whether the rotating cylindrical electrode can be used instead of the flow loop to study velocity effects. The rotating electrode method is cheaper and experimentally simpler than the flow loop (maybe more accurate), and so may prove to be superior for generating data on velocity effects.

Ultimately, data will be available on the effects of velocity on corrosion rates. This will be in a form which will be useful to pipe and equipment designers, who can estimate the hydrodynamic values.

During this period, some improvements have been made to the rotating electrode to improve its alignment (to reduce whip) and to control ingress

of nitrogen purge gas and temperature. Tests at various rotation rates are in progress.

A flow loop is under construction. This will comprise a heated liquor storage tank, a pump, flow detector, piping and associated probes. Air tightness is especially important for long-term tests to prevent liquor oxidation. Tests of corrosion rate at various velocities will commence when the equipment is ready.

THE INSTITUTE OF PAPER CHEMISTRY

Appleton, Wisconsin

Status Report

to the

ENGINEERING PROJECT ADVISORY COMMITTEE

Project 3628

# RECOVERY BOILER CORROSION

October 22, 1987

PROJECT SUMMARY FORM

DATE: September 22, 1987

PROJECT NO.: 3628 - Recovery Boiler Corrosion

PROJECT LEADER: D. C. Crowe

IPC GOAL:

Increase the useful life of equipment by proper selection of materials of construction and by identifying suitable process conditions.

OBJECTIVE:

To understand the causes of corrosion in the kraft recovery boiler, as a basis for devising methods of reducing corrosion damage.

CURRENT FISCAL BUDGET: $75,000

SUMMARY OF RESULTS SINCE LAST REPORT: (July 1987 - September 1987)

The technical literature concerned with recovery boiler corrosion has been reviewed. Experimental apparatus for study of corrosion in smelt at high temperature has been designed and ordered. Construction and start-up have begun on some of the equipment.

INTRODUCTION:

Corrosion and cracking of tubes and smelt spouts in the lower furnace region of the kraft recovery boiler are chronic, costly problems which can lead to catastrophic smelt/water explosions. Remedial measures involving composite tubes, thermal sprayed coatings or pin-studding are either expensive or ineffective. Effective remedies for existing carbon steel tubes and smelt spouts are needed. The planned studies will focus on problems in the lower furnace.

LITERATURE REVIEW:

Studies of Corrosion in the Recovery Boiler

Extensive efforts were made in the 1960's to understand recovery boiler corrosion. Concerned with rising tube temperatures due to increasing steam pressure, Plumley, Lewis and Tallent (1) conducted some of the first investigations of recovery furnace corrosion. Tests in recovery boilers, using horizontal probes, indicated that the effect of temperature on corrosion rate was slight up to 580°F, but increased with temperatures above 580°F. Using air-cooled probes installed vertically in the plane of the waterwall of recovery boilers, they found wastage of carbon steel tubes to increase dramatically with temperature above about 650°F. Heat transfer rate was considered to have a great influence on tube temperature. Panels of tubes protected by various means were installed for testing; protective coatings were found to be effective in preventing wastage. Deposit analysis showed that FeS scale was associated with wastage.

Laboratory studies (1) involved corrosion of steel (cooled to 500-700°F) in molten smelt (1500°F) and in powdered smelt constituents (700°F). Smelt constituents were varied and controlled mixtures of gases or actual recovery boiler flue gases were used in the latter experiments on a number of metals. The laboratory tests showed that higher temperature and oxygen content in the gas increased corrosion rates. Results in molten smelt showed discrepancy between field and lab results (especially with respect to the effect of sulfide). They found that oxygen could not be added conveniently to simulate furnace conditions. Furthermore, the atmospheric composition could not be varied independently of the smelt composition. The tests in powdered smelt showed that sulfide in air was very corrosive. Thiosulfate produced the highest

corrosion rates. The effects of gas composition were investigated, also. They concluded that wastage of carbon steel observed near air ports may be due to a gas-solid reaction, perhaps involving the localized concentration of oxygen, carbon dioxide and sulfur containing gases.

In subsequent work, Tallent and Plumley (2) noted difficulty in duplicating conditions of kraft furnace corrosion in the lab. Controlled mixtures of gases were passed across coupons embedded in powdered smelt constituents. Their experiments did not incorporate effects of smelt thickness, molten smelt effects or heat transfer. They concluded that elemental sulfur was formed by reaction of $CO_2$ and $SO_2$ with $Na_2S$, and that this sulfur reacts with the steel. These conclusions were based on indirect evidence including 1) production of FeS, 2) similarities with corrosion by sulfur and 3) lab tests in which free sulfur was produced. They were unable to detect more than a trace of free sulfur in field material.

In 1964, committees were established in Sweden and Finland to study recovery boiler corrosion. The Swedish work was summarized by Stelling and Vegeby (3). They obtained smelt and gas samples from recovery boilers to determine variations with operating conditions. Using these data, they also carried out laboratory tests of: 1) bar steel in gas, 2) steel in molten simulated smelts, 3) steel covered with frozen smelt in contact with flue gas and 4) steel covered with frozen smelt in contact with flue gas with periodic renewal of the smelt. In their experiments in various gases, they found that the maximum corrosion rate occurred at a ratio of $H_2S/O_2$ of about one. This corresponded to the ratio for maximum formation of sulfur. At lower ratios, FeS would be formed and at higher ratios, $Fe_3O_4$ would form. High corrosion rate correlated with FeS

formation which would provide poor protection. Smelt composition may have changed during tests although renewal should have minimized this effect. Corrosion from smelt itself was negligible at the tube temperature normally expected. They related corrosion rates to the type of corrosion product formed (i.e. FeS, $FeS_2$, $Fe_3O_4$) under various conditions.

Clement (4) (1970) published results of corrosion investigations in Babcock boilers, which mostly concerned corrosion on the windbox side of the flat stud boilers. He attributed corrosion to the reaction of condensed NaOH with $Fe_2O_3$ to form nonprotective $NaFeO_2$. Oxygen was considered necessary to form $Fe_2O_3$. This study would have benefitted from laboratory or field tests to confirm the proposed mechanism.

In 1970, a cooperative investigation was started in Finland and Sweden. Moberg (5) summarized this research. The Finnish group studied corrosion in the gas phase. Conditions described by Stelling and Vegeby (3) were used to look at various steels at a range of temperatures and gas composition. The Swedish group focussed on corrosion of steel in smelt exposed to gas. Tests involving repeated dipping of steel specimens into smelt were also conducted. The apparatus used for this more closely simulated furnace conditions by incorporating cooling in the tube specimens to provide a temperature gradient at least while the smelt was cooling. Smelt composition was observed to change during the tests. Corrosion rate was lower if the samples were coated with a layer of frozen smelt. They concluded that chromium steels possessed superior resistance to corrosion. Additional tests in synthetic smelt with various gas combinations were performed. A hollow sample with cooling to provide a temperature gradient was used also.

Ahlers (6), in a study of effects of chloride, metal composition, liquor and gas composition and temperature, dipped steel specimens into smelt and then exposed them to simulated flue gas. He observed that corrosion rate was slow during the first couple of hours, then increased, suggesting that some interaction between smelt and gas may have generated corrosive species, or that some time was required before the film broke down.

Bruno (7) described corrosion of recovery boilers in the region of the primary air ports, behind tubes, as due to NaOH condensation. Moderately high NaOH content was found in deposits. The melting point of this NaOH may be lowered by various smelt constituents.

More recently, wastage of stainless steel from composite tubes was reported at a meeting of the National Association of Corrosion Engineers (8). Corrosion and cracking was described further by Wensley (9).

Barna and Rogan (10) have reported on the appearance and occurrence of corrosion of composite port opening tubes. They considered that the corrosion process depends on formation of crevices that have the capability of accumulating deposits and that form a non gas-tight seal between the furnace and casing side of the tubing. They suggested that hydroxide vapors condense at deposits and form a molten phase at the deposit/substrate interface.

Wensley (11) reported that there was a "strong correlation between tube cladding wastage and the preferential corrosion of the stainless cladding from flat studs. Further, that those openings which evidently experienced higher temperature conditions in service, resulting in both flat stud burn-back and flat stud notch cracking, were less likely to exhibit pronounced stainless

cladding wastage." Conversely, areas of cladding wastage experienced less flat stud burn-back and notch cracking. These results suggest that stainless steel removal is a low temperature phenomenon.

In a failure analysis of a cracked composite recovery boiler tube, Odelstam (12) determined that the tube temperature had reached 500-550°C. In explaining preferential corrosion of stainless steel, he referenced work by Rahmel which indicated that carbon steel is more resistant to molten hydroxide than are Cr and CrNi steels. The corrosion rate depends on $Na_2O_2$ content which depends on oxygen and steam partial pressure in the gas above the melt. The chromium is especially reactive to form $Na_2CrO_4$.

Poturaj (13) has studied the corrosion rates of carbon steel, austenitic stainless steel and ferritic-austenitic steel in stagnant and flowing kraft smelts at 757°C. Corrosion rates were higher in the flowing smelts, except for 304L which was not much affected. Sodium hydroxide decreased the corrosion attack on all steels except the carbon steel in flowing smelt and probably the 304L in stagnant smelt. Scales formed on the carbon steel consisted of a single layer composed of Fe and S; the other alloys formed two oxide layers without sulfur.

Corrosion Mechanisms

Corrosion is generally considered to be worse when FeS is formed because it provides poor protection (1,3). Magnetite ($Fe_3O_4$) is more protective, its formation is assisted by oxygen and water vapor (3). The FeS may form by reaction of Fe with elemental sulfur (7). Tallent and Plumley (2) have suggested reactions for FeS formation:

1) $Fe + H_2S \rightarrow FeS + H_2$

2) $Fe + \frac{1}{2} O_2 \rightarrow FeO$

$FeO + Na_2S \rightarrow FeS + Na_2O$

3) $Fe + S \rightarrow FeS$

Reaction 1 was considered to be unlikely due to fast reaction of $H_2S$ with the alkaline smelt. Reaction 2 was also considered unlikely because FeO was not observed in deposits. Reaction 3 was thought to be the most likely reaction.

Sulfur dioxide ($SO_2$) may cause $H_2S$ to be released from smelt (3). Alternatively, $SO_2$ may form S by reaction with $Na_2S$ (2) via:

$2 Na_2S + 3 SO_2 \rightarrow 2 Na_2SO_3 + 3 S$

Plumley et al. (1) found that $SO_2$ cause a sixfold increase in corrosion rate of steel in $Na_2S$. Stelling and Vegeby (2) thought that $SO_2$ might react with $H_2S$ via:

$SO_2 + H_2S \rightarrow 2 H_2O + 3/2 S_2$

However, in contrast to the results of Plumley et al., they found $SO_2$ to have a negligible effect on corrosion rates.

Stelling and Vegeby (3) found that $CO_2$ also caused $H_2S$ to be released. They found that $CO_2$ had only a small influence when no $H_2O$ was present, and no effect in 3.5% $H_2O$. In contrast, Plumley et al. (1) found that $CO_2$ accelerated corrosion of steel in $Na_2S$. They suggested that $CO_2$ combines with $Na_2S$ via:

$Na_2S + 2 CO_2 \rightarrow Na_2CO_3 + S + CO$

to produce corrosive elemental sulfur. Ahlers (6) found that $CO_2$ increased corrosion rate but above a certain level it reduced corrosion rate.

Oxygen also plays an important part. The importance of the ratio between $H_2S$ and $O_2$ has been noted above. It may form $Na_2S_2O_3$ which decomposes to

form $Na_2SO_3$ + S. Alternatively, it may react with $H_2S$ via:

4. $H_2S + \frac{1}{2} O_2 \rightarrow H_2O + S$

with the elemental sulfur causing severe corrosion (Ref. 2) or

5. $H_2S + 3/2\ O_2 \rightarrow H_2O + SO_2$ (Ref. 3).

Sodium sulfide ($Na_2S$) plays a major role in corrosion, perhaps via reaction with gases to form elemental sulfur as suggested by Tallent and Plumley (2). Plumley, et al. (1) found that powdered $Na_2S$ in air produced high corrosion rates on steel. Oxidation of sulfide to form corrosive $Na_2S_2O_3$ and other species may have been responsible in these cases.

Clement (4) attributed corrosion on the windbox side of flat stud boilers to reaction of condensed NaOH with $Fe_2O_3$ to form nonprotective $NaFeO_2$, with oxygen considered necessary to form the $Fe_2O_3$. Apparently, the hydroxide condenses at lower temperatures, and with oxygen, it oxidizes iron to $NaFeO_2$. Hydroxide condensation was further implicated by Bruno (7). The hydroxide condensation is questionable due to the difficulty of producing NaOH fume in the recovery boiler, as described by Cameron (14). Furthermore, there is good reason to believe that the NaOH would react quickly with the carbonate in the smelt and would be consumed.

Deposits

Plumley, Lewis and Tallent (1) noted that tube surfaces may be exposed due to fluctuating operating conditions. The smelt layer appeared to be separated from the tube surface by porous material, possibly dried black liquor, thereby affording access of gas to the surface.

There is uncertainty about the conditions under smelt deposits. Bruno

(7) had perhaps the most to report regarding deposits (formed on carbon steel in lower pressure boilers). Sulfur content of these deposits was very low. Potassium was said to lower the melting point. He reported that deposits from Iggesund recovery boiler began to melt at 250°C. Deposits containing 12% NaOH were encountered in a B&W boiler (280°C, 64 bar) near the primary and secondary air ports. Sodium sulfide (2.1%) and sodium sulfate (2.8%) were very low, although he presented other analyses from around air ports which showed higher sulfate concentrations. Clement (4) described chemical accumulations at air ports, with a black and red deposit ($NaFeO_2$) next to the tube, yellow and green layers outside that, and extending into a gray layer of unreacted "Hydrochrome" refractory material. The pH was about 12 and sulfur (as $SO_3$) was less than 2%. The temperature in the area was about 315°C (600°F). Odelstam (12) has estimated that the tube temperature can get as high as 500-550°C.

## Conclusions

At high temperatures, in the presence of hot gases, oxidation and sulfidation can seriously jeopardize materials. These are the conditions in a recovery boiler where corrosion has been a constant problem. Corrosion of recovery boilers is not well understood, to the extent that problems are unpredictable. The importance of variables including smelt composition and flow, gas composition and distribution, metal composition and microstructure, temperature, temperature fluctuations and temperature gradients due to heat transfer are unknown. Furthermore, the influence of boiler pressure, water treatment, sulfidity, firing practice and other operational variables are poorly understood. One thing is certain: corrosion in recovery boilers is a complex phenomenon.

References

1. A.L. Plumley, E.C. Lewis and R.G. Tallent, Tappi 49(1):72A-81A (1966).

2. K.G. Tallent and A.L. Plumley, Tappi 52(10): 1955-1959 (1969).

3. O. Stelling and A. Vegeby, PulpPap.Mag.Can., 70(15):51-77 (1969).

4. J.L. Clement, Tappi 53(2):269 (1970).

5. O. Moberg, PulpPap.Ind.Corr.Prob. 1:125-136 (1974).

6. P.E. Ahlers, PulpPap.Ind.Corr.Prob. 2:133 (1977).

7. F. Bruno, PulpPap.Ind.Corr.Prob. 4:68 (1983), Swedish Corrosion Institute, Stockholm (1983).

8. NACE T-5H-1 Task Group on Recovery Boiler Fireside Corrosion, Minutes of Meeting, Atlanta, September 19, 1985.

9. D.A. Wensley, Corrosion and Cracking of Composite Boiler Tubes, p.231-245 in 1986 Kraft Recovery Operations Seminar, TAPPI, Atlanta (1986).

10. J.L. Barna and J.B. Rogan, Proc. TAPPI 1986 Engineering Conf. pp.377-385 (1986).

11. D.A. Wensley, "Corrosion of Recovery Boiler Waterwall Composite Tubes", Paper 205, Corrosion 87 (San Francisco), NACE, 1987.

12. T. Odelstam, pp.277-288 in Proc. 1987 Kraft Recovery Operations (Orlando) TAPPI Press, Atlanta (1987).

13. S. Poturaj, Tappi 70(1):55-58 (1987).

14. J.H. Cameron, "Vaporization from Alkali Carbonate Melts", The Institute of Paper Chemistry Technical Paper Series No. 237 (April 1987).

PROGRESS:

1. A literature review has been completed.

2. An old tube furnace has been refurbished and fitted with a variable transformer and temperature controller. Construction of a gas supply system and fume hood, and calibration of the temperature controller are underway.

3. A second (larger) tube furnace has been ordered. Delivery is anticipated in late November.

4. A crucible furnace and auxiliary equipment have been selected for use in studies of corrosion and electrochemistry of materials in molten carbonate/sulfide salts.

PLANS FOR NEXT PERIOD:

1. Testing of carbon steel in simulated smelts of various composition in gases at 300-600°C is planned. Coupons of steels will be placed in ceramic boats, covered with simulated smelts, and placed in the tube furnace for these studies. The objective will be to determine the effect of relevant smelt species at various temperatures. The stability of the smelts in the test gases will be investigated as a necessary part of this work.

2. The second tube furnace will be placed in operation when it arrives.

3. Investigation of the effect of gas composition on hot corrosion of carbon steel will be performed to a limited extent.

SIGNIFICANCE TO THE INDUSTRY:

An improved knowledge of corrosion mechanisms in recovery boilers will aid in design of remedial measures.

THE INSTITUTE OF PAPER CHEMISTRY

Appleton, Wisconsin

Status Report

to the

ENGINEERING PROJECT ADVISORY COMMITTEE

Project 3607

# EVALUATION OF STRUCTURAL COATINGS FOR PULP AND PAPER MILL SERVICE

October 22, 1987

PROJECT SUMMARY FORM

DATE: September 22, 1987

PROJECT NO.: 3607 - Evaluation of Structural Coatings for Pulp and Paper Mill Service

PROJECT LEADER: D. C. Crowe

IPC GOAL:

Increase the useful life of equipment by proper selection of materials of construction and by identifying suitable process conditions.

OBJECTIVE:

To rank commercially available paint systems based on their ability to protect structural steel in the aggressive environments found in the pulp and paper mill, especially if applied under less than optimum conditions.

CURRENT FISCAL BUDGET: None

SUMMARY OF RESULTS SINCE LAST REPORT: (February 1987 - September 1987)

Racks of test coupons have been removed from mills following a period of exposure for pre-rusting. The coupons have been coated with candidate systems each over a range of surface preparation treatments. The racks are ready to be returned to the mills for long term exposure.

INTRODUCTION:

Structural coating selection and application is crucial to good performance. Successful coatings must be resistant to the environments found in various parts of the pulp and paper mill; actual exposure to these environments

of a collection of panels will aid in coating comparison. The quality of surface preparation prior to application is critical for many coatings. Most mills experience difficulties in obtaining 100% compliance with surface preparation recommendations made by vendors. The sensitivity of the coatings to inadequate surface preparation may be a significant factor in coating selection; it is being explored here.

Standardized carbon steel test panels have been obtained from KTA-Tator Co. These panels have a piece of channel welded to their face, and various defects which will challenge the coatings applied. These test panels have been exposed for approximately three months at various test locations in mills. Test location included the recovery boiler superstructure, paper machine wet end, bleach plant, evaporator and chemical preparation areas. After the exposure time, the panels were badly rusted in many cases. In this way, the surface of a rusted mill structure was simulated. The surface attack will be similar to that on actual structures, and impurities incorporated in the surface (chlorides, etc.) will be the same.

PROGRESS:

Since the last PAC report, the test panels have been exposed in the mills for pre-rusting and then returned to the Institute to be sent for coating. Surface preparation and coating was performed by KTA-Tator Co. under the direction of Institute personnel. The coatings have been returned and made ready for re-installation in the mills.

Five different surface preparation methods were used. The first was a water wash with a hose to remove loose rust and contamination. The second surface preparation method comprised water washing and power tool cleaning. The

power tool cleaning was performed according to SSPC-SP3. This standard calls for the removal of loose rust by mechanical means such as power sanders, wire brushes, chipping hammers, grinding wheels or needle guns. This method is considered to be inadequate for most high performance coating systems. The third surface preparation technique involved commercial blast cleaning according to SSPC-SP6. In commercial blast cleaning, two-thirds of all visible rust, scale, paint or foreign matter must be removed from each square inch of surface. This cleaning is done with compressed air nozzle blasting, centrifugal wheels or other specified method. The fourth surface preparation technique was a white metal blast as described by SSPC-SP5. This surface is free of all rust, dirt, scale, grease, paint or foreign material and is roughened to form a suitable anchor pattern for coating. The fifth, and last surface condition is a new surface, not pre-rusted and not contaminated. All surface preparation techniques will not be tested with each coating system. A range of preparation techniques better and worse than that recommended by the coating vendor will be tested.

Ten coating systems have been selected for the test program. These are compatible with a range of surface preparation techniques. The coatings are listed in Table 1. They include epoxies applied over various primers, some with organic and some with inorganic zinc. Chlorinated rubber vinyl and vinyl ester coatings have been selected. A conversion coating will be tested also. The coatings which will be tested in each area are listed in Tables 2, 3 and 4.

As already noted, the test panels have surface flaws which will challenge the coating. Additionally, a cross will be scribed on each to determine the effects of surface damage.

PLANS FOR THE NEXT PERIOD:

Return the coated test panels to the mills in which they were prerusted. Leave them there until they fail, or the test program is terminated.

SIGNIFICANCE TO THE INDUSTRY:

This project will provide mills with an independent assessment of the long-term reliability of structural coatings for pulp and paper mill applications.

Table 1. Coating Systems

1. Epoxy Amide Primer Plasite 7103
   Epoxy Phenolic Topcoat Plasite 7122

2. Inorganic Zinc Rich Epoxy Primer Porter ZincLock 351
   Chlorinated Rubber Porter CR1131

3. Organic Zinc Rich Primer Porter ZincLock 308
   High Build Epoxy Porter 4361 MCR 43
   Gloss Epoxy Porter 4310 MCR 43

4. Epoxy Mastic Plasite C720
   Epoxy Phenolic Topcoat Plasite 7122

5. Rust Inhibitive Alkyd Primer Porter U-Prime
   High Build Epoxy Porter 4361 MCR 43
   Gloss Epoxy Porter 4310 MCR 43

6. NeutraRust 661

7. Inorganic Zinc Rich Epoxy Porter ZincLock 351
   High Build Epoxy Porter 4361 MCR 43
   Vinyl Porter 1710 VC 17
8. Vinyl Ester Plasite 4100
9. Inorganic Zinc Rich Epoxy Porter ZincLock 351
   High Build Epoxy Porter 4361 MCR 43
   Gloss Epoxy Porter 4310 MCR 43
10. Gloss Epoxy Porter 4310 MCR 43

Surface Finishes

1. Water Wash
2. Wash + SSPC-SP3
3. SSPC-SP6
4. SSPC-SP5
5. New

Table 2

BLEACH PLANT > Bleach Plant Chemical Prep.

NUMBER OF PANELS EXPOSED

| COATING* TYPE | SURFACE FINISH* 1 | 2 | 3 | 4 | 5 |
|---|---|---|---|---|---|
| 1 | | | 6 | 6 | 6 |
| 2 | | | | | |
| 3 | | | | | |
| 4 | | 6 | | | |
| 5 | | 6 | | | |
| 6 | 6 | | | | |
| 7 | | | 6 | 6 | 6 |
| 8 | | | 6 | 6 | 6 |
| 9 | | | 6 | 6 | 6 |
| 10 | 6 | | | | |
| | | | | | |

*For coating types and surface finishes, use Table 1 as a key.

Table 3

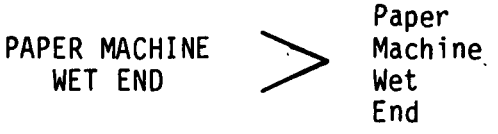


| COATING* TYPE | NUMBER OF PANELS EXPOSED<br>SURFACE FINISH* | | | | |
|---|---|---|---|---|---|
| | 1 | 2 | 3 | 4 | 5 |
| 1 | | | 9 | 8 | 8 |
| 2 | | 9 | 9 | 8 | 8 |
| 3 | | | 9 | 8 | 8 |
| 4 | | 9 | | | |
| 5 | | 9 | | | |
| 6 | 9 | | | | |
| 7 | | | | | |
| 8 | | | | | |
| 9 | | | 8 | 8 | 8 |
| 10 | 9 | | | | |
| | | | | | |

*For coating types and surface finishes, use Table 1 as a key.

Table 4

RECOVERY > Recovery
Outside structure
Batch digesters
Recausticizing
Evaporators

NUMBER OF PANELS EXPOSED

| COATING* TYPE | SURFACE FINISH* 1 | 2 | 3 | 4 | 5 |
|---|---|---|---|---|---|
| 1 | | | 24 | 20 | 24 |
| 2 | | | | | |
| 3 | | | | | |
| 4 | | 26 | | | |
| 5 | | 26 | | | |
| 6 | 26 | | | | |
| 7 | | | | | |
| 8 | | | | | |
| 9 | | | 24 | 20 | 24 |
| 10 | 26 | | | | |
| | | | | | |

*For coating types and surface finishes, use Table 1 as a key.

THE INSTITUTE OF PAPER CHEMISTRY

Appleton, Wisconsin

Status Report

to the

ENGINEERING PROJECT ADVISORY COMMITTEE

Project 3606

# CORROSION IN HIGH YIELD PULPING PROCESSES

October 22, 1987

PROJECT SUMMARY FORM

DATE: September 22, 1987

PROJECT NO.: 3606 - Corrosion in High Yield Pulping Processes

PROJECT LEADER: D. C. Crowe

IPC GOAL:

Increase the useful life of equipment by proper selection of materials of construction and by identifying suitable process conditions.

OBJECTIVE:

Use electrochemical methods to understand corrosion and corrosion-assisted cracking processes occurring in high yield pulping to identify potential problems and solutions.

CURRENT FISCAL BUDGET: None

SUMMARY OF RESULTS SINCE LAST REPORT: (February 1987 - September 1987)

Experimental work has been completed on this exploratory project. This has included polarization studies, weight loss tests and measurements of corrosion potential at 90 and 150°C. Effects of chloride and thiosulfate were investigated. Slow strain rate tests to determine susceptibility of 316 stainless steel to stress corrosion cracking have been completed.

INTRODUCTION:

Mechanical pulping processes (CMP, TMP, CTMP) are gaining wider use. Some corrosion problems in these processes have been reported. These include chloride cracking of steaming vessels, sulfuric acid condensation and organic

acid formation. Very little is known about the conditions which can cause corrosion in these processes.

PROGRESS:

In the previous report, results in alkaline sulfite, bisulfite and acid sulfite solutions at 90°C were described. In some cases, the solution pH decreased during the test and corrosion in the vapor phase was observed. However, these results were not reproducible. Although no significant problems were identified, these tests formed the basis for investigation of the effects of additives and higher temperatures.

In this reporting period, polarization and weight loss tests were performed at 90°C with additives of NaCl and $Na_2S_2O_3$. These species did not increase the corrosion rates substantially.

Weight loss tests were performed at 90°C in the alkaline sulfite, bisulfite and acid sulfite solutions letting air into the cell in the hope that the oxygen in the air would assist the formation of corrosive species such as $H_2SO_4$. The air did not cause high corrosion rates to result.

Weight loss tests and potential monitoring of 304 and 316 stainless steels were completed at 150°C in the liquid and vapor phases. These tests were performed in a Hastelloy test cell. No dramatic effect of temperature was observed.

Slow strain rate tests at 150°C for 316 stainless steel were performed to determine susceptibility to stress corrosion cracking. Tests were run at open circuit potential in a range of environments, but no stress corrosion cracking was observed.

The testing completed thus far has failed to duplicate the corrosion observed in some systems. This has provided useful information on what is not the problem, but further funded research cannot be justified. The project leader hopes to pursue some more possibilities in future via student research.

PLANS FOR THE NEXT PERIOD:

A report is in preparation to summarize the results of this project. Directions for further work will be identified in the report.

SIGNIFICANCE TO THE INDUSTRY:

These studies will provide a basis for decisions regarding materials selection for TMP and CTMP equipment.

THE INSTITUTE OF PAPER CHEMISTRY

Appleton, Wisconsin

Status Report

to the

ENGINEERING PROJECT ADVISORY COMMITTEE

Project 3470

# FUNDAMENTALS OF DRYING

October 22, 1987

# PROJECT SUMMARY FORM

DATE: October 22, 1987

PROJECT NO. 3470 - Fundamentals of Drying

PROJECT LEADER: Hugh P. Lavery

IPC GOAL:

Reduction of the "necessary minimum" complexity (number and/or sophistication) of process steps.

OBJECTIVE:

To develop an understanding and a database sufficient for the commercialization of advanced water removal systems, based on high-intensity drying principles. This new technology will reduce capital costs, increase machine productivity, reduce the amount of energy used, and improve paper properties.

CURRENT FISCAL BUDGET:

$150,000 from Institute funds, plus $350,000 from a Department of Energy grant (as Project 3595). This grant is for a total amount of $1.5 million over four years; 1987 is the second grant year for the project. The Fourdrinier Kraft Board Group has funded a parallel study of linerboard and medium conversion issues in impulse drying with a grant for $30,000.

SUMMARY OF RESULTS SINCE LAST REPORT
(February 1987-October 1987)

Impulse drying received its initial tests at the pilot scale during this period. The pilot roll impulse dryer and the bench-scale platen press used in earlier work were compared for water removal and density development effectiveness on linerboard. The roll versus platen press comparison shows no significant differences between the two geometries, thus the bench-scale database is probably a valid prediction of roll geometry performance. Early results from a study of the effects of impulse drying on linerboard conversion show that glueability of impulse dried linerboard to conventional medium is equal or superior to conventional liner. Work is now in progress to evaluate further conversion issues, including printing quality, of linerboard, medium, newsprint, writing papers, and lightweight coating rawstock. A second nip for the pilot roll press is being designed to learn how to produce a non-two-sided sheet for newsprint and fine papers applications.

## INTRODUCTION

The Institute of Paper Chemistry research program on impulse drying has been in progress for the past five years, with a concentrated effort underway for the past two years. The early work on impulse drying, documented in the first Progress Report for the Department of Energy (1), identified the potential of the process during a study of several possible new drying and pressing processes. The second year's work, which is summarized in Progress Report Two (2), included an extensive study on the response of several commercially important grades to impulse drying. The excellent performance of the process in terms of water removal, energy use and properties development was demonstrated during these studies. A third DOE Progress Report is currently in preparation, covering work between October, 1986 and September, 1987. This report to the Project Advisory Committee is a shortened version of the DOE Report, which will be completed by early November, 1988.

The principal project activity during this period was the design, construction, and preliminary testing of a pilot-scale roll impulse dryer. In addition to this significant equipment development task, experiments were performed to evaluate the effects of impulse drying on very wet sheets and to further develop mechanistic understanding of the process. The major conclusions from these efforts are:

1. Impulse drying continues to perform well when implemented in a pilot-scale roll geometry. Water removal and properties development are similar on the roll press and on the platen press used in earlier experiments. Initial work on the roll press has produced 42 pound per thousand square foot southern pine linerboard with strength properties similar to 69 pound board. as measured by ?

2. The energy use and water removal performance of impulse drying improves rapidly as sheet moisture content is increased. Impulse drying may be able to replace portions of the press section of conventional paper machines, as well as part of the dryer section. Water removal rates can be twice those which would be found in an unheated press operating at the same pressure and nip residence time. The overall drying system energy consumption, combining impulse dryers and conventional dryers to complete the dewatering process, can be less than half the requirement of conventional papermaking if impulse drying is implemented in a third press position.

3. Linerboard sheet surface properties important in the production of combined board are improved by impulse drying. Glueability of board, as measured on the Institute of Paper Chemistry Double-Backer Bonding Simulator equipment, is enhanced by impulse drying.

Work is continuing on characterization of sheet surface quality after impulse drying in terms of its effects on conversion processes such as gluing, printing and coating. Corrugating medium, newsprint, writing papers, and lightweight coating rawstock are now being evaluated for their conversion response to impulse drying, in addition to he linerboard studies which will be reported at the October meeting. Work is also underway to improve understanding of sheet delamination, which can occur if excess vapor pressure develops in the web during impulse drying; preliminary results will be reported at the meeting.

## IMPULSE DRYING

Significant progress has been made over the past two years in developing a promising new technology called Impulse Drying. The characteristic features of impulse drying are the use of pressures and temperatures at much higher levels than normally used in paper drying, but with a very short exposure of the sheet to these intense conditions. The process concept in its present form was suggested by Wahren (3). A related high-intensity drying method has been described mechanistically by Williams, Halsey and Gottwald (4). The conditions required to perform impulse drying are all attainable by combinations of existing pressing and heat transfer technologies.

Impulse drying works by bringing the wet paper into contact with a very hot metal roll, typically at 400°F to 700°F, while maintaining pressure on the sheet at 400 to 700 pounds per square inch for between 15 and 100 milliseconds. The lower limit on temperature is set by the tendency of wet sheets to stick to hot rolls at temperatures below 380°F, the upper temperature limit is determined by damage to the sheet through scorching or delamination. Nip residence time is limited by current practices in wide nip press design. Pressure is applied in impulse drying principally to maintain good thermal contact between the hot surface and the sheet as steam pressures develop in the web. High pressure levels offer limited improvements in process performance.

The equipment needed to provide the pressure and time conditions is already available from several manufacturers. Impulse drying involves adding a source of heat to these "wide nip presses" to raise the temperature of the process. A conceptual sketch for a roll impulse dryer is illustrated in Figure 1.

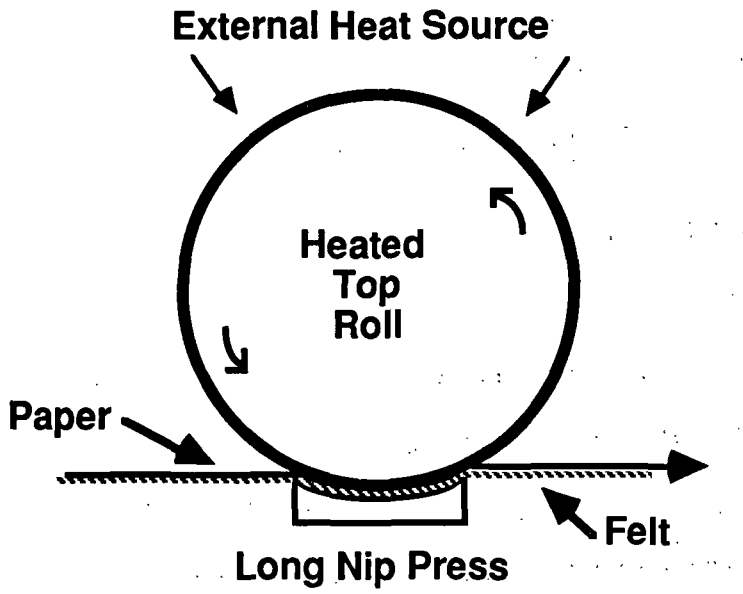


*Figure 1. The impulse drying concept: wide-nip press technology modified to include a very hot press roll.*

## IMPULSE DRYING

Once sufficient temperature, pressure, and time are provided, water is removed from the sheet by mechanisms which are fundamentally different from those which govern conventional paper drying. Student research at the IPC (5), (6) has shown that under impulse drying conditions high pressure steam is generated rapidly in the surface of the sheet next to the hot roll. Growth of the steam layer displaces liquid water from the sheet into the water receiver, typically a press felt. The rates of water removal achieved by this vapor displacement mechanism are 100 to 1000 times greater than in conventional drying. Large amounts of water are removed from the sheet in the liquid phase, saving the energy which would otherwise be used to evaporate the water from the sheet. This report includes a summary of additional work which has extended this mechanistic understanding to sheets as wet as 35% solids.

Impulse drying also influences sheet properties. Web temperatures near the hot surface increase to levels which promote fiber conformability and interfiber bonding, particularly if the sheets are formed from high-yield, high lignin content furnishes. Impulse drying is interrupted before the sheet is completely dry, and the vapor flashing in the sheet

interrupts the densification process. The sheet is left with a distinctive density profile, a combination of surface density and mid-sheet bulk which is advantageous in the development of many important physical properties.

The steam generation and flashing processes can have harmful effects on sheet quality at the upper limits of impulse drying intensity. The grades studied during the past two years of project work have all had a wide range of useful temperature, pressure and nip residence time conditions which could be applied without delamination. We can not be certain that all grades of interest in the future will respond equally well. Work has begun to improve our understanding of the delamination process and to learn how to control heat release into the sheet to avoid generating excess steam. Preliminary results will be available by the October meeting.

The work performed during the current project year has been of two types. First, a pilot roll impulse dryer was designed, built, and used in a series of preliminary experiments. The purposes of this pilot device include a demonstrating that the process works in a realistic roll geometry and providing large paper samples for conversion testing. The second major type of project work has been an extension of previous experiments on water removal and energy use during impulse drying to much wetter sheets than were studied earlier. These tests were performed to determine whether impulse drying can be effective as a substitute for at least part of the conventional wet pressing process, as well as providing an alternative to cylinder drying. This report will present data from these project activities.

## PROJECT PLAN

The principal objective of this project is to provide the data necessary to support and encourage commercial implementation of the impulse drying process. Figure 2 presents the project flowchart which has guided research in this area for the past three years. The program began with exploratory and feasibility work, which was completed in 1985 and documented in Progress Report One (1). Work on step two, the investigation of water removal mechanisms, has progressed with the assistance of student theses, notably those

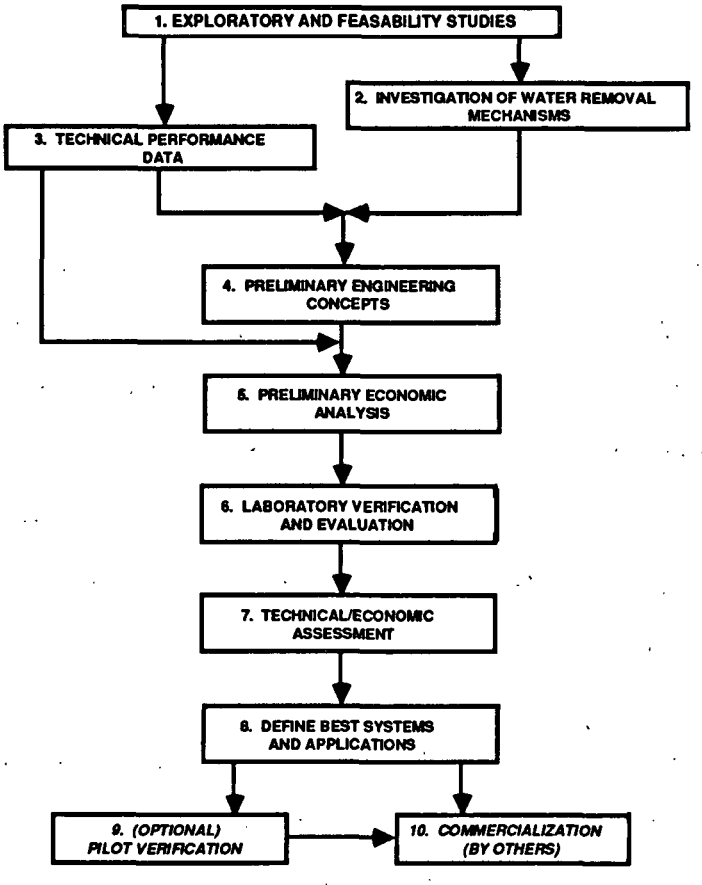


*Figure 2. Project plan flowsheet*

of Burton (5) and Devlin(6). A major portion of step three, obtaining technical performance data on a number of commercially important grades, was performed in 1986 and documented in Progress Report Two (2), although work in this area will continue throughout the life of the project. The preliminary engineering concepts of step four which were needed to build the pilot roll impulse dryer were developed during 1986, and have been further refined during this year's construction process.

Recent work on the project has concentrated on Step 6, the laboratory verification and evaluation of the process using pilot scale equipment, with further work on mechanisms and technical performance data, Steps 2 and 3. Work is continuing on laboratory pilot scale evaluation, and on technical and economic assessment of the process (Steps 5 and 7).

**Review of key data from past work**

The new data which is presented in this report may be better understood in the context of the overall performance of impulse drying as defined in previous work (2). Recent experimentation has concentrated on one grade, kraft linerboard. This choice reflects both the ease of working with that grade and its commercial importance. Wide nip press technology is found principally on linerboard machines, and the conversion of such a press to an impulse dryer is the most straightforward, and so most likely, means of bringing impulse drying to commercialization.

Recent emphasis on linerboard could obscure the excellent effects impulse drying has on a wide variety of important paper and board grades. A review of the most significant results of the earlier multiple grade studies may help keep current results in perspective.

Past impulse drying studies have evaluated grades which comprise the majority of total United States paper and board production. Grades evaluated to date have included linerboard, corrugating medium, newsprint, uncoated freesheet writing paper, and coated paper rawstock. Together, these grades account for two-thirds of total production (Figure 3). All responded well to impulse drying. The composition of these furnishes is presented in Table 1.

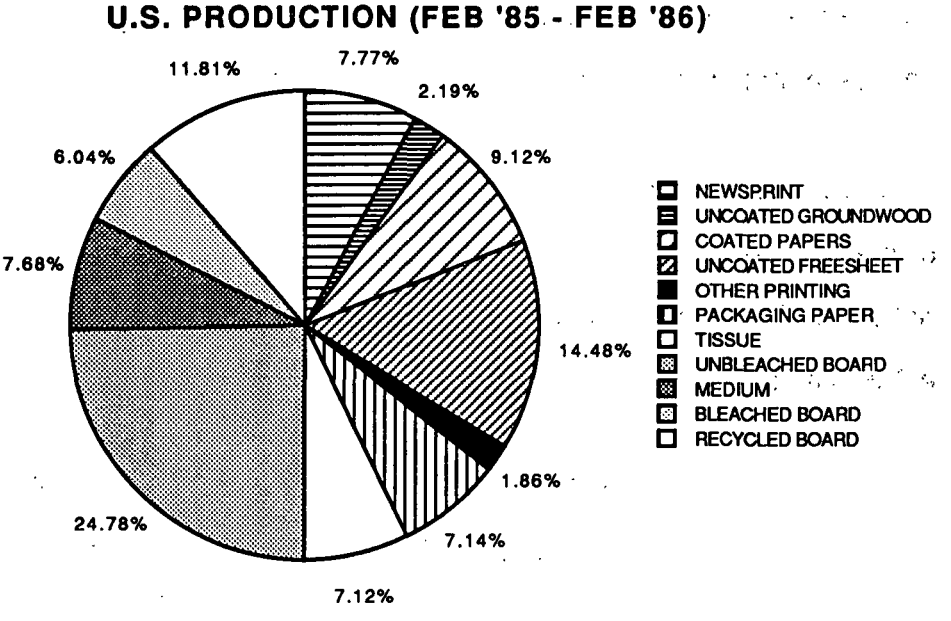


*Figure 3. Production figures by grade for the United States paper and board industry*

| FURNISH | FIBER MAKEUP | | |
|---|---|---|---|
| Linerboard | 100% UBSWK | | |
| OCC Recycled Liner | 100% OCC | | |
| Corrugating Medium | 91% NSSC | 1.5% UBHWK | 7.3% UBSWK |
| Writing Paper | 73% BHWK | 27% BSWK | |
| Newsprint | 22% BSWK | 78% Groundwood | |
| Lightweight Coating | 47% BSWK | 53% TMP | |

*Table 1. Composition of furnishes used in the technical performance evaluation of impulse drying*

The first major effect of impulse drying is its ability to remove large amounts of water from sheets in very short periods of time. Figure 4 illustrates the sheet final percent solids content achievable with impulse drying. A lightweight grade, such as coating rawstock at 50 grams per square meter, can be dried from 35% to 76% solids in a single, 25 millisecond nip. This performance could eliminate most of the conventional cylinder drying section of a machine producing a similar grade. Heavier weight materials, such as 125 gram per square meter linerboard, are also effectively dewatered by impulse drying, although the final percent solids after a single nip is not as high.

For both grades, the final solids content of the sheet is nearly constant for a wide range of solids entering the impulse dryer. For a lightweight grade, initial solids levels between 35% and 58% can be increased to approximately 78% solids in a single nip. This effect may improve the moisture profile in the cross-machine direction.

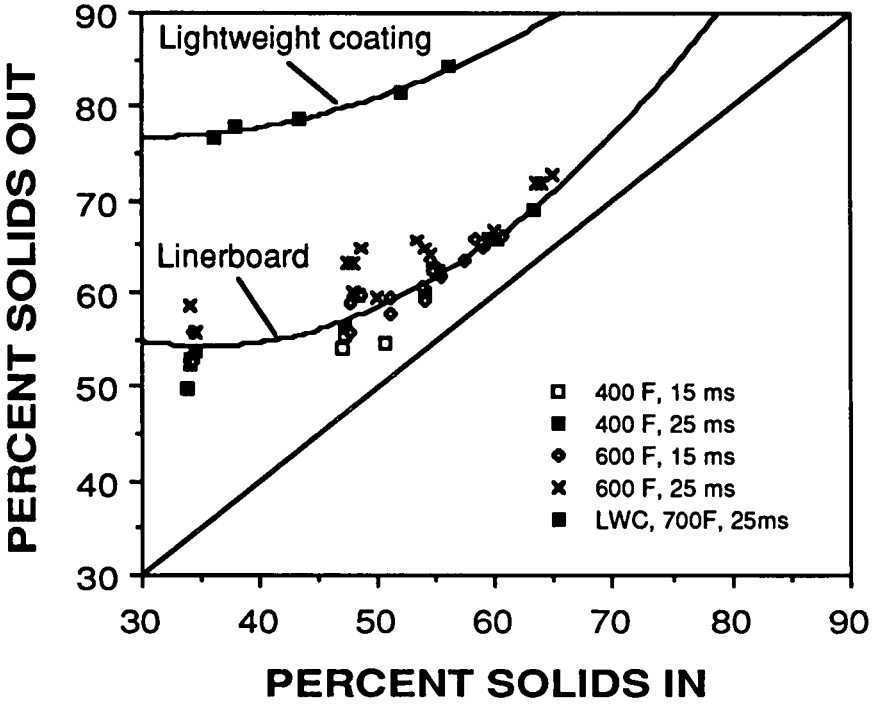


*Figure 4. Linerboard and lightweight coating rawstock final solids plotted against initial solids content. Linerboard at 125 grams per square meter and LWC at 50 grams per square meter, both preheated to 180°F. Linerboard data includes a range of pressures from 400 to 700 psi; pressure did not significantly impact water removal rates for these grades.*

Higher impulse drying temperatures and longer nip residence times favor the production of dryer sheets, but the pressure applied in the nip is of minor importance above about 300 psi peak. Operating at 700°F rather than 400°F increases the final percent solids of the sheet by five percentage points at 35% solids for linerboard. However, the process will be much simpler to implement at lower temperatures. Preheating the sheet from room temperature to 180°F improves water removal rates by 30 to 50 percent, with most of the additional water removal occurring in the liquid phase (2).

A further major effect of impulse drying is a significant increase in sheet density. The combination of temperature, pressure and nip residence time set up conditions which promote fiber conformability and bond development (5). In general, the apparent density produced by impulse drying is a straight-line function of the percent solids after impulse drying. (Figure 5). The temperature, pressure, and time used to attain the final percent solids do not influence the final density appreciably. For all the grades shown in Figure 5, the point furthest to the left represents a conventionally processed sheet which has received no impulse drying; the remaining points were obtained by impulse drying at a variety of conditions.

Impulse drying increased the density of all grades tested. However, the density increases were particularly large for high-yield chemi-mechanical pulp. Such high-yield grades are difficult to consolidate using conventional technology, and so tend to produce weak sheets. The highest yield material, at 88% yield, densified slowly under mild impulse drying conditions, but resumed a linear relationship between density and final solids above 55% final solids. The density of both high yield pulps was more than doubled at the most intense impulse drying conditions tested.

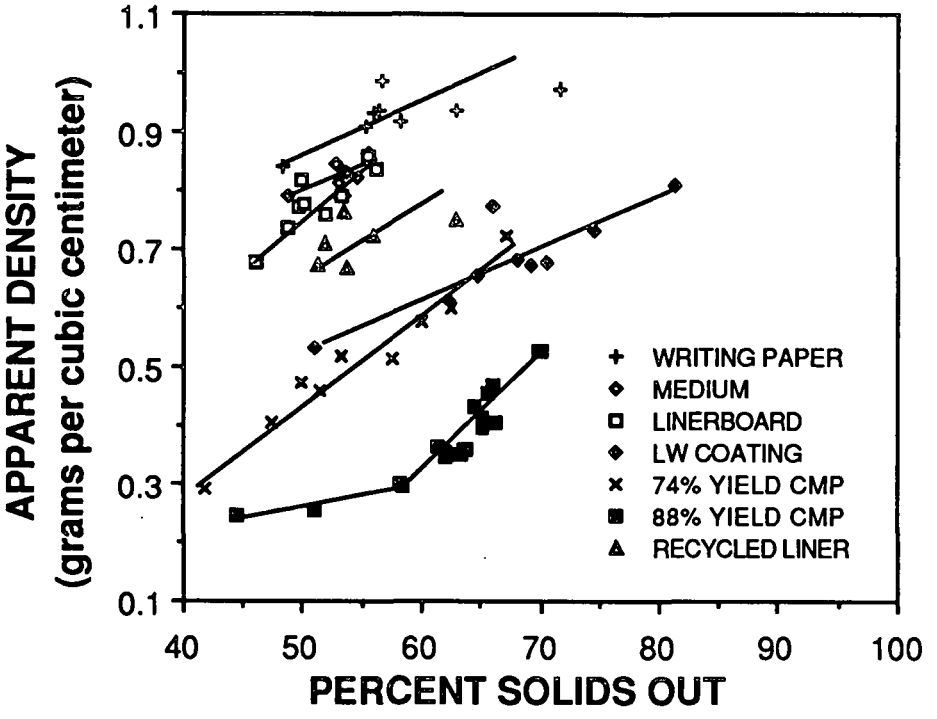


*Figure 5. IPC apparent density development for several commercially important grades. Medium, Linerboard, recycled liner and CMP grades all at 125 grams per square meter, newsprint and lightweight coating rawstock at 50 grams per square meter and writing paper at 80 grams per square meter. Data include peak pressures at 400 and 700 psi, temperatures from 400 to 700°F, and nip residence times between 15 and 30 milliseconds. All sheets initially at 50% solids and 70°F.*

The density increases presented in Figure 5 correspond to improved bonding between fibers in the sheet, leading to improved physical properties. Strength properties tend to be straight-line functions of the apparent density, with little dependence on the temperature, pressure, or nip residence time used to produce the densification. For example, the tensile strength of all grades was improved by impulse drying (Figure 6). The tensile strength of high-yield chemi-mechanical pulp sheets is very low after conventional processing, about 2 kilometers of breaking length. Impulse drying can bring the tensile strength of this material to the 4.3 kilometer level measured for conventional 50% yield kraft pulp at the same 125 gram per square meter basis weight.

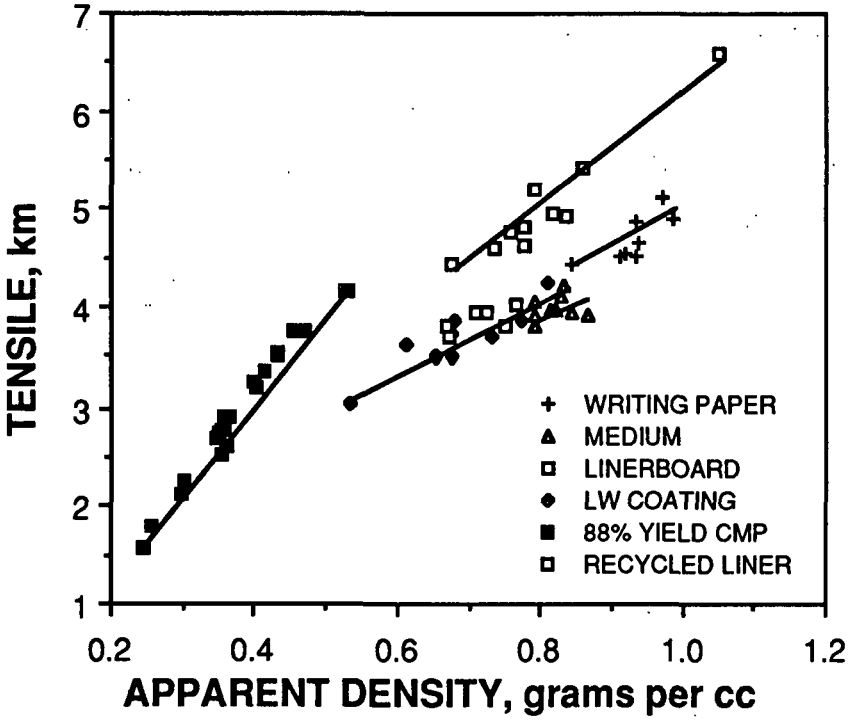


*Figure 6. Tensile strength development with densification for several commercially important grades. Medium, Linerboard, recycled liner and CMP grades all at 125 grams per square meter, newsprint and lightweight coating rawstock at 50 grams per square meter and writing paper at 80 grams per square meter. Data include peak pressures at 400 and 700 psi, temperatures from 400 to 700°F, and nip residence times between 15 and 30 milliseconds. All and nip residence times between 15 and 30 milliseconds. All sheets initially at 50% solids and 70°F.*

The amount that sheets can be stretched before failure occurs also increases with higher density from impulse drying (Figure 7), although the increases are small for some grades. Embrittlement of the sheet due to excessively high sheet temperatures would reduce stretch. This effect is not observed for the grades and conditions tested. Improvements in stretch is particularly important in the case of corrugating medium, where the ability of the sheet to stretch during the flute forming process is a major factor in runability on the corrugating machinery.

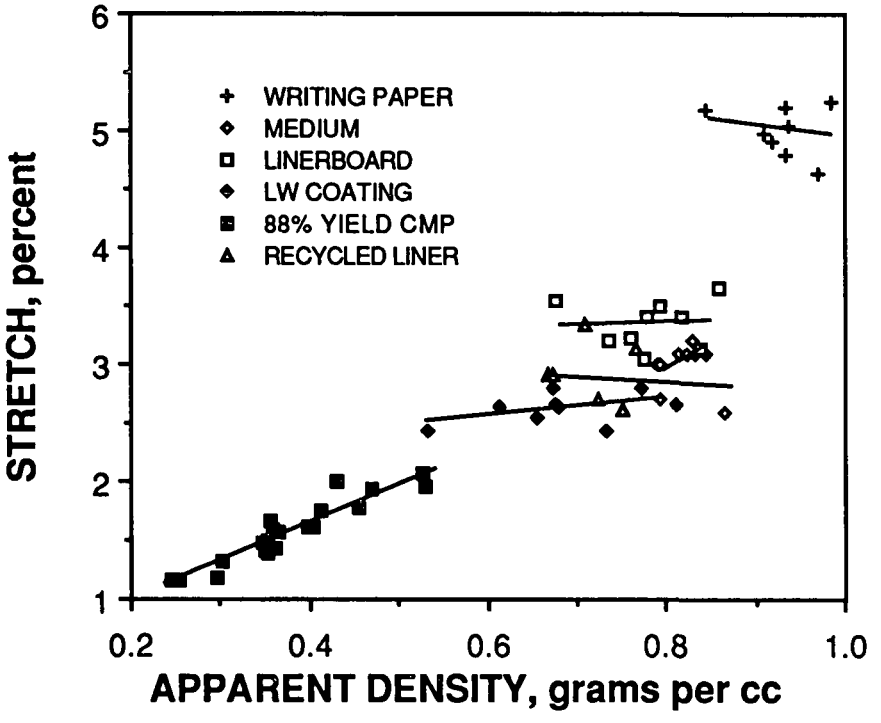


*Figure 7. Percent sheet stretch at failure for several commercially important grades. Medium, Linerboard, recycled liner and CMP grades all at 125 grams per square meter, newsprint and lightweight coating rawstock at 50 grams per square meter and writing paper at 80 grams per square meter. Data include peak pressures at 400 and 700 psi, temperatures from 400 to 700°F, and nip residence times between 15 and 30 milliseconds. All sheets initially at 50% solids and 70°F.*

Compressive strength properties are also enhanced by impulse drying. Figure 8 summarizes the STFI compression test performance of linerboard, medium and alternative linerboard furnishes. Conventionally processed chemi-mechanical pulp furnishes have one-third the compressive strength of typical kraft linerboard. After impulse drying, the STFI performance of these grades can actually exceed that of kraft pulp at a constant density. This suggests that the bond strength of the high yield materials is higher than the kraft sheet, possibly due to softening and flow of the lignin content of the chemi-mechanical pulp.

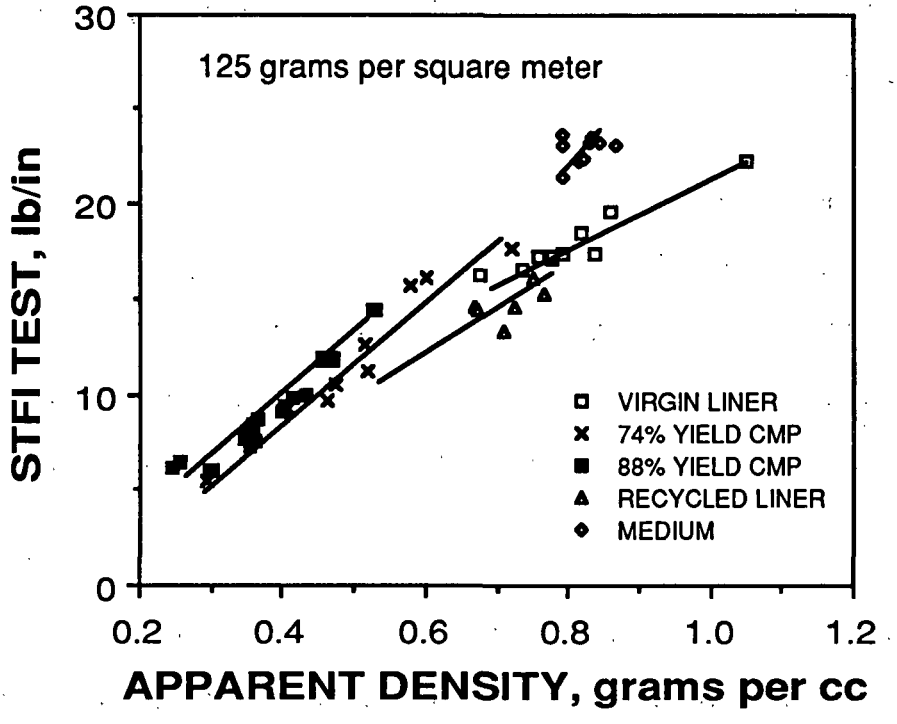


*Figure 8. STFI compression test for medium and several alternative linerboard furnishes. Medium, Linerboard, recycled liner and CMP grades all at 125 grams per square meter. Data include peak pressures at 400 and 700 psi, temperatures from 400 to 700°F, and nip residence times between 15 and 30 milliseconds. All sheets initially at 50% solids and 70°F.*

Under many impulse drying conditions, the density profile produced in the sheet will be non-uniform. The region in the sheet near the hot surface tends to densify under the influence of local high temperatures which promote softening and conformability of the fiber constituents. The middle of the sheet is not exposed to high temperatures during most impulse drying conditions and so densifies differently. In addition, the middle of the sheet tends to expand at the end of the nip as hot water flashes to vapor. Additional data to define these phenomena was obtained during the past year, and will be summarized later in this report.

Photomicrographic evidence for a non-uniform density profile is shown in Figure 9, taken from Burton' thesis (5). Room temperature wet pressing produces a density profile through the sheet which indicates that the apparent density is the consequence of a random variation of local density at various points through the sheet thickness. Increasing the hot surface temperature to 700°F and impulse drying under the same pressure and nip residence time conditions produces a notable increase in density in the 25% of the sheet thickness closest to the hot surface. The middle of the sheet is relatively bulky, with many open fiber lumens and an overall appearance which is not significantly different from the results of wet pressing.

This non-uniform density profile causes some sheet properties to behave differently than they would if the entire sheet were uniformly densified to the observed average density. This presents an opportunity to develop paper and board products with unusual combinations of properties. For example, lightweight coating rawstock (Figure 10) experiences only a four percentage point loss in opacity when its density is increased by 1.5 times. The optical properties of the sheet are retained because most of the light scattering surfaces inside the sheet are relatively unaffected by impulse drying.

PRESSED SHEET:

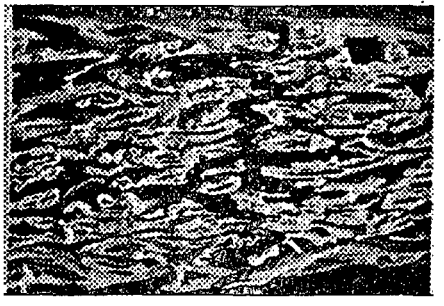

IMPULSE DRIED SHEET:

*Figure 9. Scanning electron microscope cross sections with density profile mapping of a sheet wet pressed at 68°F and a impulse dried sheet (600°F surface temperature). Both tests were performed on a bleached softwood sheet, 100 grams per square meter basis weight, 735 CSF freeness, with a peak pressure 780 pounds per square inch and nip residence time of 4.5 milliseconds.*

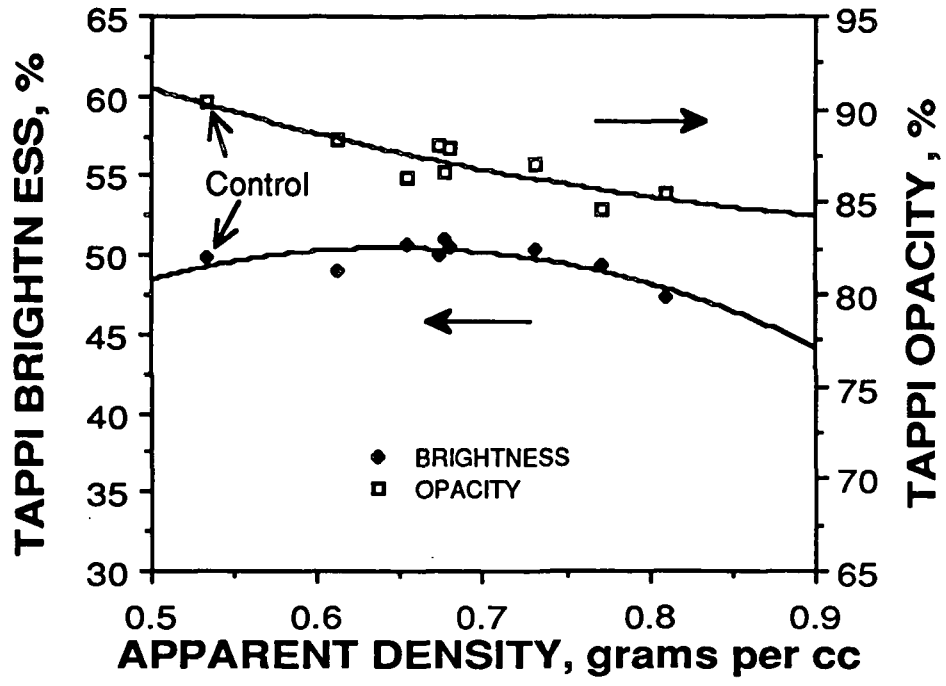


*Figure 10. TAPPI brightness and opacity for a 50 grams per square meter coating rawstock sheet. Data include peak pressures at 400 and 700 psi, temperatures from 400 to 700°F, and nip residence times between 15 and 30 milliseconds. All sheets initially at 50% solids and 70°F.*

Finally, the amount of energy required to produce these dewatering and densification effects is small, due to the displacement of liquid phase water from the sheet. Further evidence for this displacement mechanism and its effects on energy use has been obtained over the past year, and will be reviewed later in this report. The initial data on specific energy use in BTUs per pound of water removed from the sheet is shown in Figure 11 for linerboard and in Figure 12 for newsprint. Impulse drying either of these grades requires less than one-half the 1600 to 1800 BTUs per pound typical of cylinder drying. The specific energy requirement for both grades decreases rapidly as initial sheet solids content decreases. This observation indicated a need to extend the energy use database to much wetter sheets, to evaluate whether impulse drying could be effectively implemented as a substitute for part of the conventional wet pressing process, in addition to replacing portions of the cylinder dryers. This effort became a major portion of the recent year's work

*Figure 11. Specific energy use for linerboard. Specific energy as BTUs per pound of total water removed during impulse drying, as calculated using the lithium chloride tracer method. All data at 127 grams per square meter, with sheets preheated to 180°F before impulse drying. Data include a pressure range of 400 to 700 psi peak pressure and 400 to 600°F, at 15 and 25 milliseconds. Data at for sheets drier than 58% solids were taken on the reverse side of a previously impulse dried sheet.*

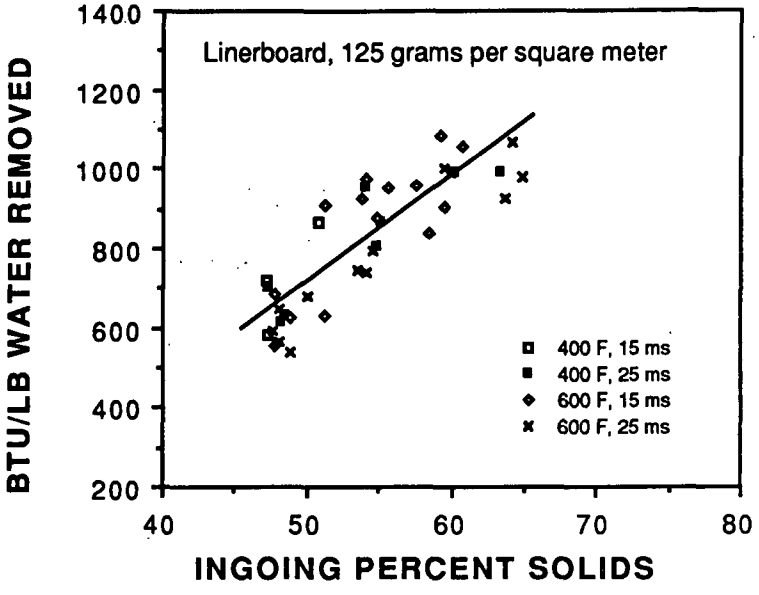


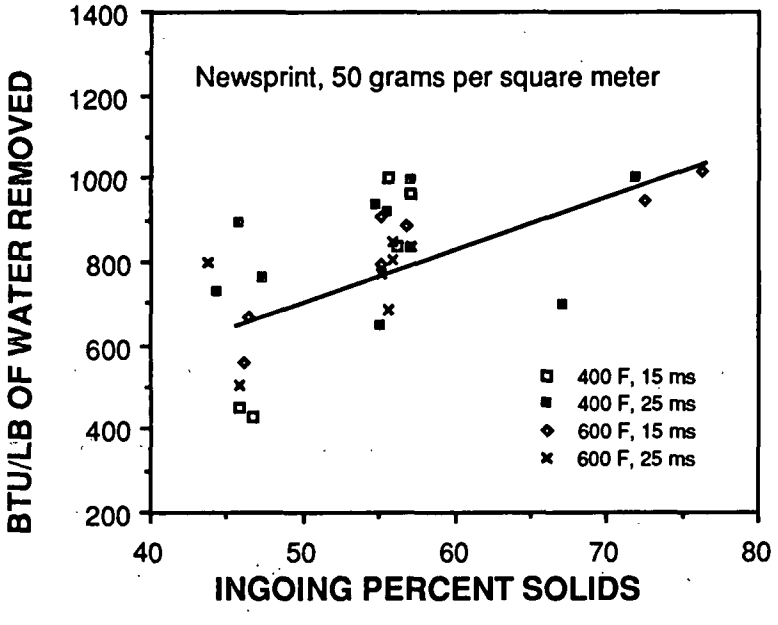


*Figure 12. Specific energy use for newsprint. Specific energy as BTUs per pound of total water removed during impulse drying, as calculated using the lithium chloride tracer method. All data at 50 grams per square meter, with sheets preheated to 180°F before impulse drying. Data include a pressure range of 400 to 700 psi peak pressure and 400 to 600°F, at 15 and 25 milliseconds. Data at for sheets drier than 58% solids were taken on the reverse side of a previously impulse dried sheet.*

## PROGRESS IN IMPULSE DRYING RESEARCH

Significant progress was made over the past year in developing further evidence for the mechanisms governing impulse drying, performing pilot-scale verification of the process, and producing large samples suitable for small scale conversion testing. This section will review each of these areas in turn.

### MECHANISTIC STUDIES

The mechanisms of impulse drying have been studied extensively at The Institute of Paper Chemistry over the past three years. Most of this work was done in the course of student theses (5) (6), and involved relatively dry sheets. The objective of the recent study which is reported below as to collect mechanistic data from wetter sheets than previously studied to evaluate impulse drying as a substitute for wet pressing. One commercially significant furnish, never-dried southern pine kraft linerboard at 125 grams per square meter basis weight, was selected for use in these experiments. The response of this furnish has been otherwise well characterized, as summarized in the previous Progress Report for this project (2).

#### Experimental methods

A variety of experimental techniques was used in this study to simulate impulse drying on the bench scale and to measure heat transfer, water removal, and web compression. All work was done on handsheets using the bench-scale impulse drying simulator illustrated in Figure 13. This device consists of a heated platen and a Materials Testing Systems (MTS) electrohydraulic system to provide the pressure pulse which simulates pressure and time conditions in a press nip. This bench-scale press can simulate any likely

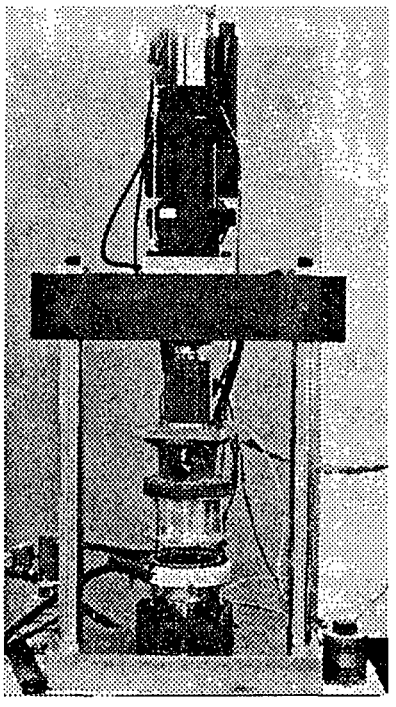

*Figure 13. The Institute of Paper Chemistry bench-scale impulse hydraulic press. The ring surrounding the lower platen is used for pre-steaming sheets to increase their temperature before impulse drying.*

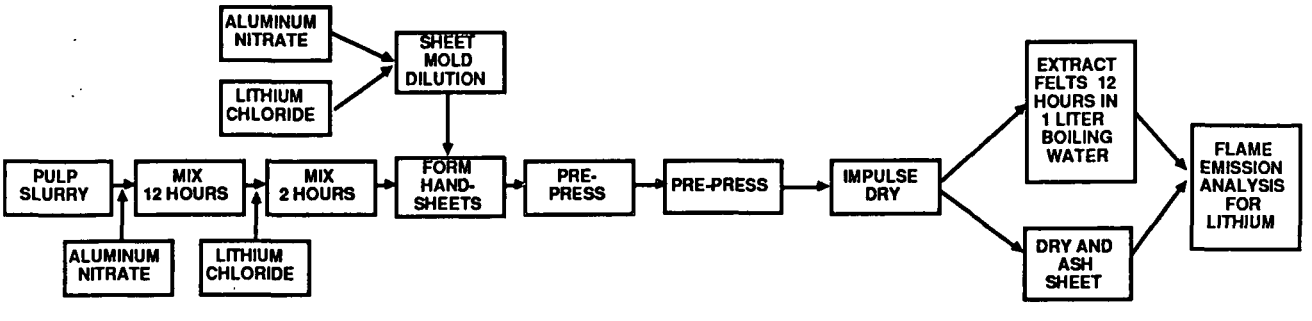


*Figure 14. The salt tracer method of measuring liquid water from impulse dried sheets (6).*

impulse drying condition, as its actuator capacity is 22,000 lb-force maximum with simple adjustment of nip residence times from ten milliseconds on up. The electronic control system allows a wide range of pressure-time profiles to be generated reproducibly. A load cell above the upper platen is used to measure and control the total load and the pressure profile.

The platens are five inches in diameter, which allows paper samples to be tested which are large enough for most standard physical test methods. A pre-steaming ring surrounding the lower platen can be used to raise sheet temperatures to near 180°F before impulse drying.

The total amount of water removed from a sheet and its final percent solids is measured gravimetrically, using the weight of the sheet before and after impulse drying and its oven dried weight. Measurement of the separate amounts of liquid phase and vapor phase water removed from the sheet and the energy consumed in the process is more complex.

The principal method used for measuring liquid phase water removal is a lithium chloride tracer technique which was developed in its present form in C. Devlin's Ph.D. thesis (6). The flowsheet for the method is presented in Figure 14. The pulp slurry is first treated with aluminum nitrate and its pH adjusted to 4.1 with nitric acid, if necessary. The purpose of this step is to saturate the negatively charged sites on the fibers with aluminum ions. After allowing 12 hours for this reaction to occur at all possible sites, a lithium chloride solution is added to the slurry. Handsheets are then formed, using dilution water made up to the same concentration of aluminum nitrate and lithium chloride as in the slurry. The handsheets are pre-pressed to the desired initial percent solids and impulse dried using the equipment which was described above. After impulse drying, the felt is removed and extracted in one liter of boiling water for twelve hours. The weak salt extract is then analyzed for its lithium content using flame emission analysis. Any lithium in the felt was car-

ried there by liquid water only. The amount of water needed to transport the lithium into the felt is readily calculated from the initial lithium concentration in the handsheet liquid phase. It is also possible to analyze the sheet for its remaining lithium content, but the process of ashing the sheet and re-dissolving the ash make this approach much less reproducible.

Once the amount of liquid water removed is known, the amount of water vapor formed can be calculated from the difference between the total water removal, measured gravimetrically, and the liquid phase water removal. The heat required to bring the sheet to its final state may then be calculated from a simple energy balance shown in Table 2. The energy balance requires assumptions about the average pressure at which the water vapor forms and about the average temperature to which the water and fiber in the sheet are heated during impulse drying. The balances in this report have been constructed assuming all evaporation occurs at one atmosphere pressure and that all water in the sheet is heated to 212°F. Both of these assumptions are conservative, as the heat of vaporization of water decreases with increasing pressure over the range of conditions of interest in impulse drying, and internal sheet temperature measurements, which will be discussed below, indicate that much of the sheet remains below 212°F.

*Table 2. Energy balance calculations based on lithium chloride tracer ion results.*

$$e_{min} = \frac{E_{min}}{(RMR)\, m_{w_0}} = \left[\frac{c_f}{m_{r_0}} + \frac{c_w}{RMR}\right]\left[T_b - T_0\right] + \left[1 - \alpha_L\right]\Delta h_b + \frac{c_f\left[T_h - T_b\right]}{2\, m_{r_0}}$$

$c_f$ = heat of fiber, BTU/lb/°F
$c_w$ = specific heat of water, BTU/lb/°F
$e_{min}$ = specific energy use, BTU/lb of water removed
$E_{min}$ = heat transferred per pound of fiber, BTU/lb fiber
$Dh_b$ = latent heat of vaporization, BTU/lb
RMR = Relative moisture removal (dimensionless)
$T_b$ = boiling temperature, °F
$T_h$ = final hot sheet temperature, °F
$T_0$ = initial sheet temperature, °F
$a_L$ = fraction of water removed as liquid
$m_{wo}$ = initial moisture ratio (lb water / lb fiber)
$m_{ro}$ = lbs water removed per lb fiber = $m_{wo}$ * RMR

The probable errors in the lithium chloride technique include adsorption of the lithium by the sheet and felt fibers, lithium losses in handling the samples, and transport of lithium to the evaporation front by the capillary movement of water in the sheet. All of these processes, if they actually occur, will reduce the amount of lithium in the final analysis. If the concentration of lithium in the sheet is reduced by adsorption and losses, the material and energy balance calculations will underestimate the amount of liquid water removed and overestimate the amount of energy required to produce the steam. The technique is, therefore, conservative.

The lithium chloride displacement technique measures only the total amount of liquid water removed and the total quantity of energy needed to account for the final state of the sheet. To obtain more detailed information on when heat is released from the hot surface into the sheet during impulse drying, a surface junction thermocouple technique is used. The instantaneous heat flux measurement technique was originally developed for ballistics applications (7). A surface junction thermocouple is made up of concentric cylinders of standard thermocouple metals separated by a fine layer of high temperature insulation. The junction between the metals is made by a layer of plating which bridges the insulation, forming the junction. The active area of the probe is very small, about 0.0005 inch in width and thickness, and so has microsecond response to changes in temperature.

To measure heat flux during impulse drying, the thermocouple tip is mounted flush with the hot surface as shown in Figure 15. During the impulse drying event, changes in temperature with time are measured by the thermocouple and recorded using TransEra high speed data acquisition equipment. The heat flux from the metal surface required to produce the observed temperature history is then deduced from the temperature measure-

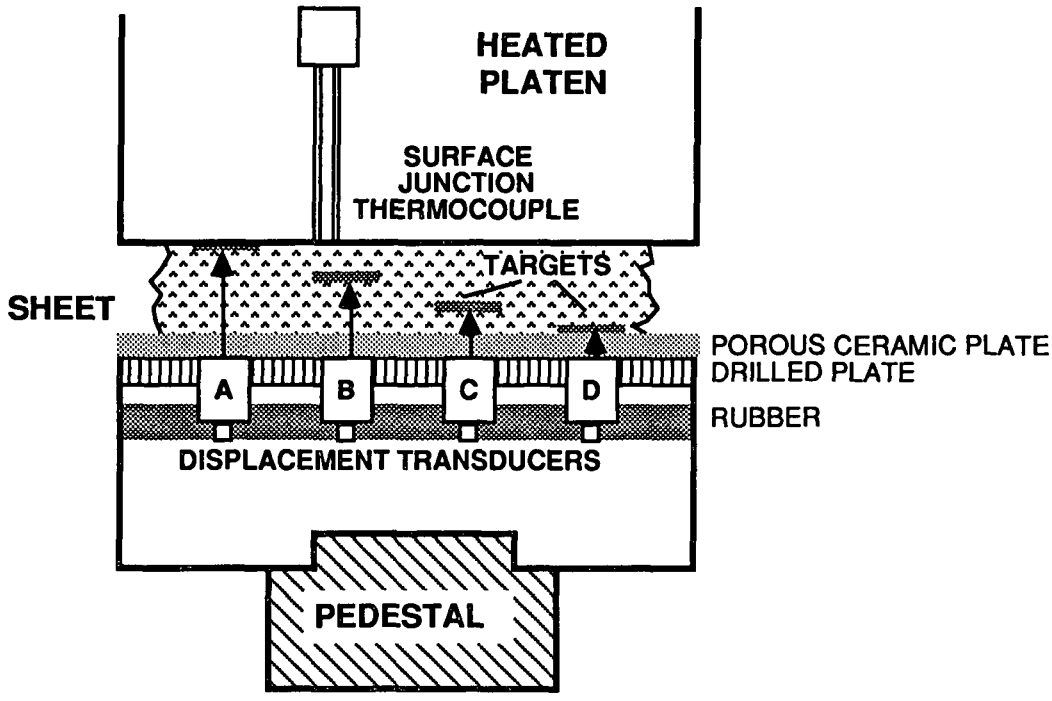


*Figure 15. General arrangement of the apparatus for measuring sheet internal caliper changes and surface heat fluxes, as built by Burton (5).*

ments by assuming that the metal mass acts as a semi-infinite slab initially at constant temperature. The numerical integration which is required is performed using a FORTRAN computer program on a Burroughs B6900 mainframe.

The instantaneous heat flux may be integrated over time to give a measurement of the total heat flux to the sheet. However, the lithium chloride technique is preferred because the known errors are all conservative and so will not overstate the energy effectiveness of the process. The surface junction thermocouple technique is influenced by non-uniformities in the temperature of the heated platen. Extreme care is required in insulating the hot surface before each test to establish a near-uniform temperature profile.

The natural tendency of the system to lose heat from the exposed surface leads to temperature gradients in the hot metal plate. Excessive temperature gradients appear in the calculated flux profile as false negative readings at the end of the nip. These negative heat fluxes occur because heat flows in the hot platen are induced by the original non-uniform temperature profile. The numerical method interprets these heat flows as proceeding from the sheet into the platen surface rather than from the depth of the platen to its surface, which is what is actually occurring. These problems can be minimized by careful experimental technique, but the precautions are time consuming and much data must be rejected because of false negative readings. The small size of the thermocouple junction also introduces the possibility of measuring local heat transfer phenomena which may not reflect the average experience of the sheet. However, the technique provides valuable data on how heat is released into the sheet if it is carefully implemented and cautiously interpreted.

Heat flows within the sheet itself have not been measured directly, but can be interpreted from measurements of sheet internal temperature histories. Sheet internal temperature is measured by placing fine-gage thermocouples (0.025 mm diameter) between the layers of handsheets built up of multiple plies. The thermocouples are spaced one-eighth, one-third, two-thirds, and seven-eighths of the way through the sheet thickness. The composite sheet is then pressed to the target moisture content and impulse dried. The signals from the thermocouples were recorded by a high-speed TransEra data acquisition system.

The final measurement used in recent mechanistic studies is the change in sheet thickness during impulse drying. Information on the internal deformations of the sheet have been useful in considering where displacement phenomena may be occurring during the impulse drying event. The dynamic change of sheet thickness in response to applied pressure was measured using a method developed in its present form by Burton (5). Eddy

current displacement transducers mounted in the bottom pedestal of the bench impulse drying simulator (Figure 15) were used to follow the motion of small copper mesh targets embedded in handsheets. The targets were dynamically formed in to the handsheets, using a special sheet mold originally described by Cowan (8).

The small dimensions (0.0254 mm in thickness) and 65% open area of the copper mesh help secure good integration of the targets into the sheet structure. Targets were positioned at the top and bottom surfaces of the sheet, and inside the sheet at levels corresponding to one-quarter and three-quarters of the total sheet basis weight. The general arrangements of the targets and transducers is shown in Figure 15. The apparent void fraction of the region of the sheet between any two targets can be calculated from the caliper information as follows:

Void fraction=(total caliper-fiber caliper)/(Total caliper)

Fiber caliper=(Basis weight/density)/(Fraction of sheet thickness between targets).

A fiber solids density of 1.5 grams per cubic centimeter was assumed in the void fraction calculation. An initially uniform distribution of fiber through the sheet was also assumed in these calculations.

**Results of recent mechanistic work**

The very low energy requirements of impulse drying wet sheets suggested by the data in Figures 11 and 12 indicate an opportunity to implement impulse drying in what is now a wet pressing position. Recent mechanistic work has concentrated on extending previous observations to much wetter sheets. A virgin kraft, never-dried unbleached softwood pulp obtained from a southern U.S. linerboard mill was used in these experiments.

The pulp was lightly refined to 730 ml CSF, and formed to a 125 grams per square meter basis weight. Five-inch diameter handsheets were formed, couched and stored in sealed plastic bags until needed. Non-standard handsheets containing salt tracer or copper mesh targets or thermocouples were made following the methods outlined in the previous section. The target moisture content before impulse drying was reached by pressing the sheets in a laboratory roll press using press impulse levels typical of commercial equipment. Most of the experiments which will be described below were performed on 35% solids sheets.

Impulse drying represents the addition of a new variable, hot roll surface temperature, to the familiar papermaking process of wet pressing in a wide-nip press. Wet pressing acts to remove water principally through a volume reduction mechanism (9). Water flows from the sheet into a water receiving felt in response to a hydraulic pressure gradient which develops as the sheet is compressed. Although the process of compressing a web to drive out water appears simple, DeCrosta (10) has compiled a list of almost forty process variables which have been found to be significant in the commercial application of wet pressing. Wide nip press technology was developed to enhance the range of one of the principal variables, press impulse, by extending the time available for water to flow from the sheet.

Water removal in a press nip is strongly influenced by the temperature in the web. Raising the web temperature will improve wet pressing performance both by reducing the viscosity of water and by softening the fibers to promote web compressibility. Similar effects are observed as the roll surface temperature is increased toward 212°F. Figure 16 illustrates the effect of increasing the hot surface temperature on the final percent solids achieved in a 25 millisecond nip at 700 psi peak pressure starting from a sheet solids content of 35%. As hot surface temperatures approach 212°F, the final percent solids achieved will climb gradually into the 38% to 42% solids range.

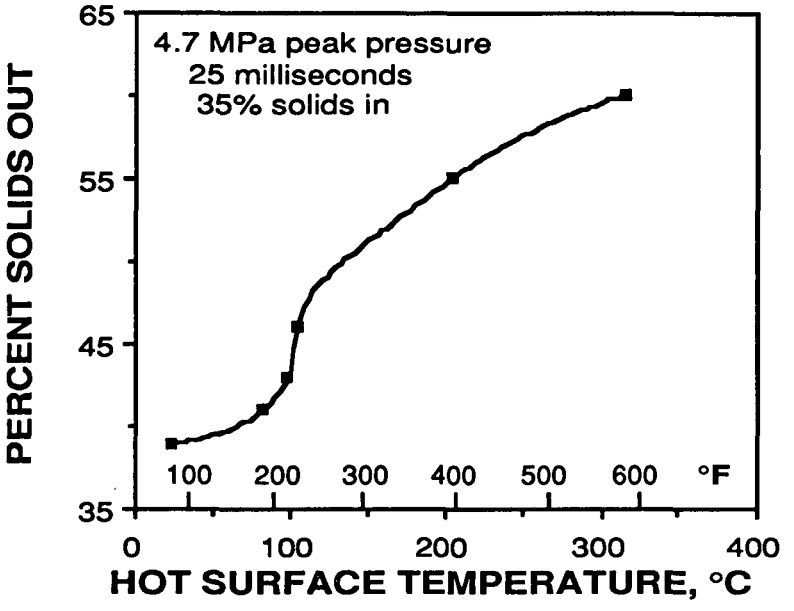


*Figure 16. Water removal performance as one pressing surface is heated from room temperature to 600°F. Nip conditions were 25 milliseconds nip residence time at 700 psi peak pressure applied to a kraft linerboard sheet at 125 grams per square meter.*

Above 212°F, the percent solids out of the nip increases rapidly with further increases in hot surface temperature. At 600°F, impulse dried linerboard sheets can reach 60% solids. However, a portion of this temperature range is not practically useful, as sheet adhesion to the hot surface is a problem between 220° and 380°F. Impulse drying has only been studied in the surface temperature range above 400°F, where sticking is no longer a severe problem.

Increasing the hot surface temperature into the impulse drying regime does more than simply enhance the action of wet pressing. The water removal performance of impulse drying and wet pressing differ in several important respects, as shown in Figure 17. Impulse drying is much less dependent on sheet moisture content than wet pressing. Figure 17 presents a comparison between the sheet dryness after the nip achieved by wet

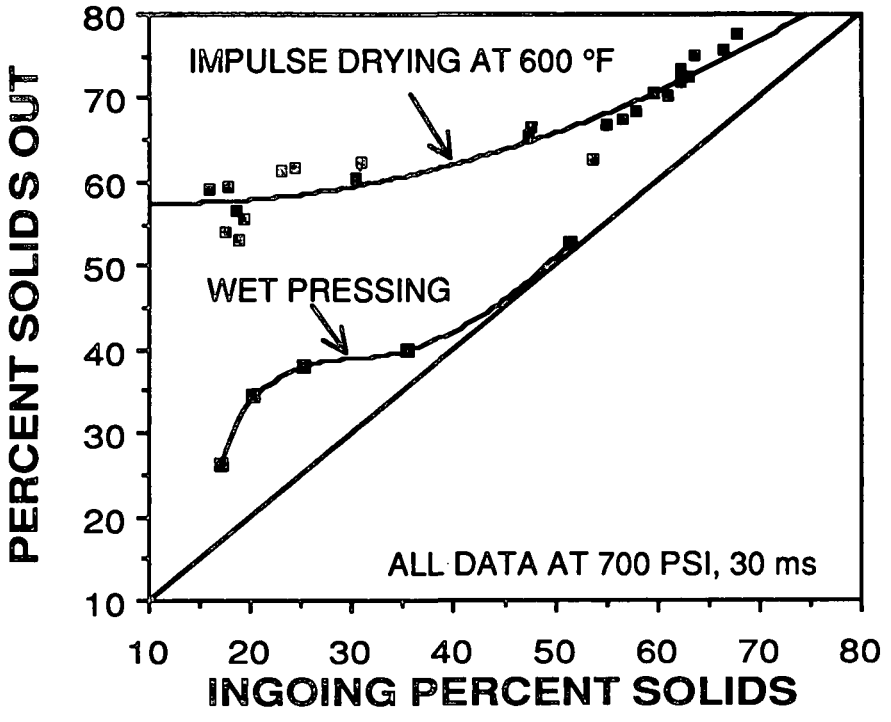


*Figure 17. Water removal performance of impulse drying very wet sheets. Wet pressing at 700 psi peak pressure for 30 milliseconds, compared with impulse drying with the same pressure and time conditions at a hot surface temperature of 600°F. Data for linerboard sheets at 125 grams per square meter basis weight preheated to 180°F. Data at for sheets drier than 58% solids were taken on the reverse side of a previously impulse dried sheet.*

pressing at 80°F with a peak pressure of 700 psi for 30 milliseconds with the results of impulse drying under the same nip conditions but at a hot surface temperature of 600°F. A haversine pressure pulse shape was used in both experiments.

Wet pressing water removal was much less effective than impulse drying under these conditions, and was also much more dependent on sheet moisture content. Impulse drying water removal is only slightly dependent on sheet ingoing percent solids over the range from 15% to 50% solids. The final percent solids level was approximately 58% solids over that range of conditions. In addition the water removal ability of wet pressing was exhausted by about 45% solids, while impulse drying was able to continue to remove water from sheets as dry as 75% solids.

The differences in the behavior of wet pressing and impulse drying shown in Figures 16 and 17 suggest that some mechanism is at work in impulse drying beyond the usual web volume reduction process of wet pressing. The likely mechanism is the displacement of liquid water by steam formed near the interface between the sheet and the hot metal surface. The amount of steam produced during impulse drying can be estimated using the lithium chloride tracer technique outlined above. The tracer technique measures the amount of liquid water received by the felt, while the total amount of water removed from the sheet is measured gravimetrically. The amount of steam formed is calculated from the difference between the total water removed and the liquid phase water removal.

The results of experiments run over a range of initial sheet percent solids between 15% and 65% on 125 grams per square meter linerboard sheets are presented in Figure 18. The results indicate that about 0.25 lb of water per pound of fiber of steam is produced at all sheet moisture contents between 25% and 65% solids. The steam necessary for a vapor displacement mechanism is thus present at some point during the impulse drying event.

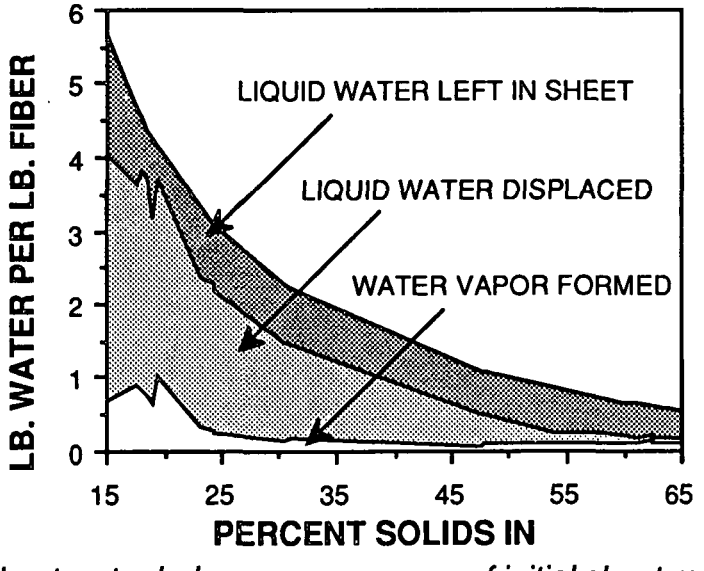


*Figure 18. Sheet water balance over a range of initial sheet moisture contents. Data for linerboard sheets at 125 grams per square meter basis weight preheated to 180°F. Impulse drying performed at 700 psi peak pressure at 600°F surface temperature for 30 milliseconds nip residence time.*

The amount of liquid water displaced by this steam is a strong function of sheet moisture content. At 65% solids, about thirty percent of the mass of water removed is removed in the liquid phase, but at 25% solids over eighty percent of the water is removed as liquid. This response would be expected in a displacement mechanism. Displacement can only be effective as long as there are few paths for vapor to escape from the sheet without displacing water. Drier sheets increase the possibility of local water-depleted regions through which water vapor could escape into the water receiver without also removing water.

The amount of water left behind in the sheet is also approximately constant over the range of ingoing percent solids tested. About 0.6 lb water per lb fiber remains in the sheet. This quantity of water may represent the level at which significant numbers of paths for vapor to flow past the remaining water in the sheet and escape into the felt begin to appear.

However, even relatively dry sheets exhibit excellent water removal performance when compared with conventional papermaking processes. At 42% solids, the water removal indicated in Figure 18 corresponds to a rate of 2500 pounds per water removed per hour per square foot. This is 500 times the rate which conventional cylinder dryers would produce under typical conditions. Eighty-five percent of that water is displaced rather than evaporated, leading to savings in energy relative to conventional drying. These high water removal rates with substantial liquid phase water removal again point toward a vapor displacement mechanism.

Sheets below 25% solids show an increase in steam production, as may be seen in Figure 18. This effect may be due to an increase in water availability at the sheet surface to support boiling. Sheets impulse dried above 25% solids may reach a limit in the water supply near the surface before other process limits take effect.

The vapor production data reviewed above do not provide information on when the steam is formed during the nip. Measurement of the instantaneous heat flux from the hot metal surface in to the sheet shows that the peak heat flux occurs early in the nip, well before peak pressure is attained (Figure 19). The peak heat fluxes observed are in the 4 megaWatts per square meter (1.2 million BTUs per hour per square foot) range, which are of the same magnitude as those reported for pool boiling heat transfer (11). It thus seems probable that the peak heat flux occurs in conjunction with the production of steam and so with the major portion of the liquid displacement event. The decline in heat flux , which generally begins before the peak pressure is reached, probably reflects a limitation in the amount of water available near the surface.

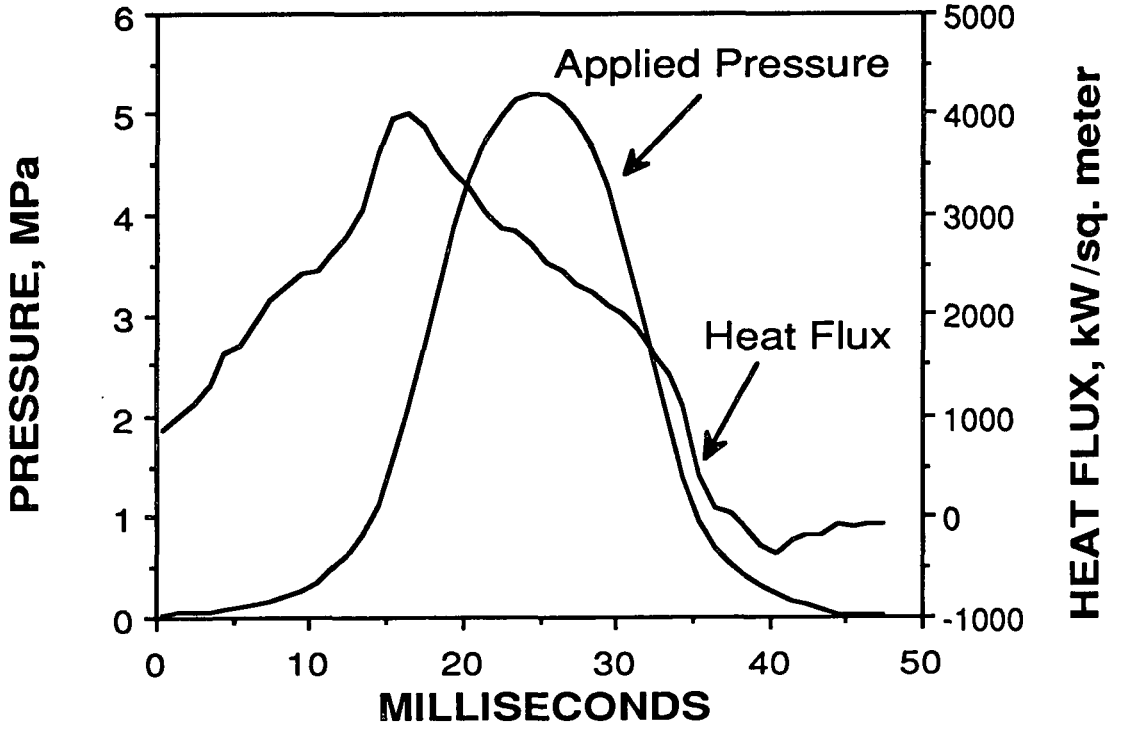


*Figure 19. Instantaneous heat flux observed during impulse drying of a 125 grams per square meter kraft linerboard sheet initially at 35% solids and 180°F using a hot surface temperature of 600°F and 600 psi peak pressure for 30 milliseconds.*

The temperature history through the sheet thickness, shown in Figure 20, also supports the concept of a steam layer near the hot surface of the sheet. The temperature at the one-eighth basis weight point measured from the hot surface rapidly reaches temperatures above 212°F, which persist until the end of the nip. Peak temperatures in this region reach 340°F about two-thirds of the way through the nip residence time. However, temperatures at the middle and the cool side of the sheet rise more slowly and do not reach the levels observed on the hot side of the sheet. The back one-eighth of the sheet reaches 212°F only at the end of the nip. Therefore, it is not likely that steam is present throughout the sheet until late in the nip.

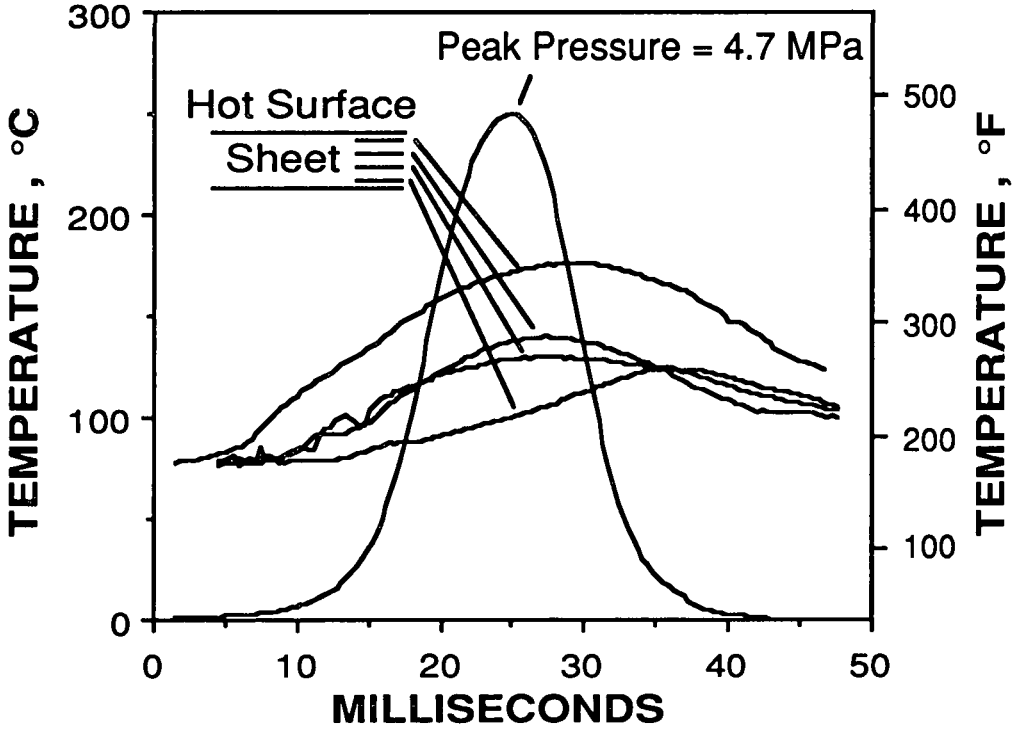


*Figure 20. Sheet internal temperature histories observed during impulse drying of a 125 grams per square meter kraft linerboard sheet initially at 35% solids and 180°F using a hot surface temperature of 600°F and 600 psi peak pressure for 30 milliseconds.*

The decline in temperature as pressure decreases after mid-nip is probably due to water flashing from fine pores in the sheet structure and condensing in the cooler regions of the sheet. In Figure 20, the three thermocouples closest to the hot side of the sheet all register declines in temperature after mid-nip, even though the sheet is still under pressure and receiving heat from the metal surface, as may be seen by comparing the heat flux data in Figure 19. This rapid exchange of heat between the hot side of the sheet and the cooler back side again indicate a vapor-filled region to support intense evaporation/condensation heat transfer across the sheet thickness.

The differences in water removal mechanisms between wet pressing and impulse drying are also apparent in the internal deformations of the sheet. Wet pressing removes water by web compression, which causes a reduction in the void fraction of the sheet and expulsion of the water and air which may be occupying the voids. A typical plot of the void fraction history during a wet pressing event as calculated from internal sheet caliper data is shown in Figure 21. For this 35% solids sheet, the web will reach saturation at a void fraction of 0.74; the void fraction at the end of the nip agrees with the gravimetrically measured 40% solids. The void fraction profile through the sheet reflects sheet stratification due to shear forces compacting the fibers on the water-receiver side of the sheet, a phenomenon which has been described in detail by MacGregor (12).

In contrast, the impulse dried sheet shows a rapid decrease in void fraction in the 25% of the sheet thickness nearest to the hot surface early in the nip (Figure 22). This decease in void fraction occurs at the same time the peak heat flux and surface layer temperatures are increasing. The lower three-quarters of the sheet thickness is much less compacted than during the corresponding wet pressing event (Figure 21) and is compressed to void fractions which are only slightly lower than saturation. These data suggest

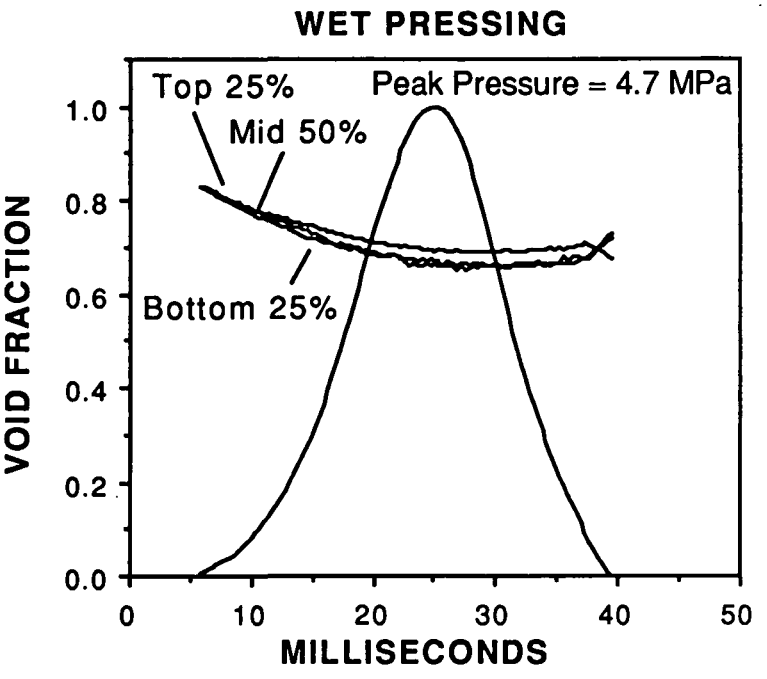


*Figure 21. Void fraction changes during wet pressing calculated from caliper data measured by the eddy current transducer/ copper mesh target technique (5). Wet pressing at 85°F using a haversine pressure pulse with a peak pressure of 600 psi for 30 milliseconds. Sheet was 125 grams per square meter kraft linerboard initially at 35% solids.*

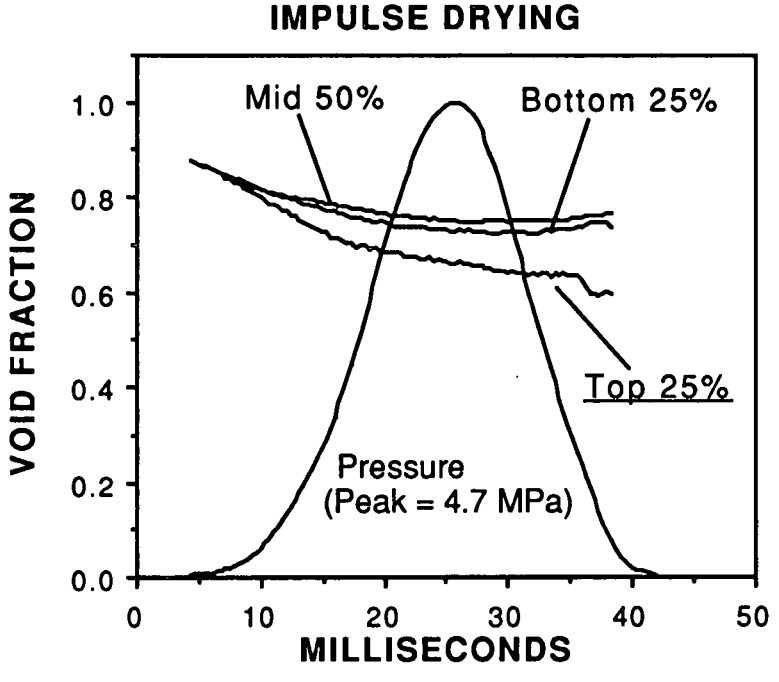


*Figure 22. Void fraction changes observed during impulse drying of a 125 grams per square meter kraft linerboard sheet initially at 35% solids and 180°F using a hot surface temperature of 600°F and 600 psi peak pressure for 30 milliseconds.*

that liquid water is evaporating from the large voids in the region of the sheet near the hot surface, accompanied by the compression of the sheet structure as steam leaves the region. The cooler portion of the sheet experiences liquid water flow in response to the vapor generation, with only a small reduction in void fraction.

The upper one-quarter of the sheet experiences a final reduction in void fraction at the end of the nip, probably due to flashing of superheated water from very small pores in the sheet. The flashing produces the collapse of the fine structure of fibers near the hot surface of the sheet, and contributes to the decline in temperature seen in Figure 20. At the end of the nip, the sheet has been stratified with a dense layer near the hot surface and relatively bulky material in the middle and the cold side of the sheet. This density profile can have important consequences in the development of sheet properties, as was reviewed above, in addition to providing evidence for the presence of new dewatering and densification mechanisms during impulse drying.

These data provide evidence for an overall mechanistic picture of impulse drying, represented in Figure 23. High pressure steam is produced in the web near the hot surface and displaces liquid water from the sheet. Meanwhile, high temperatures near the sheet surface promote densification, with particularly emphatic effects on high yield furnishes. The cooler portions of the sheet regain bulk as hot water flashes to steam as pressure is released at the end of the nip.

## Practical consequences of impulse drying mechanisms

The measurements of water removal in the liquid and vapor phase in Figure 18 may be converted into energy demand by calculating a simple energy balance around the sheet. In this study, the assumption has been made that all the water in the sheet is heated to 212°F and that all vapor is formed at one atmosphere pressure. These assumed sheet

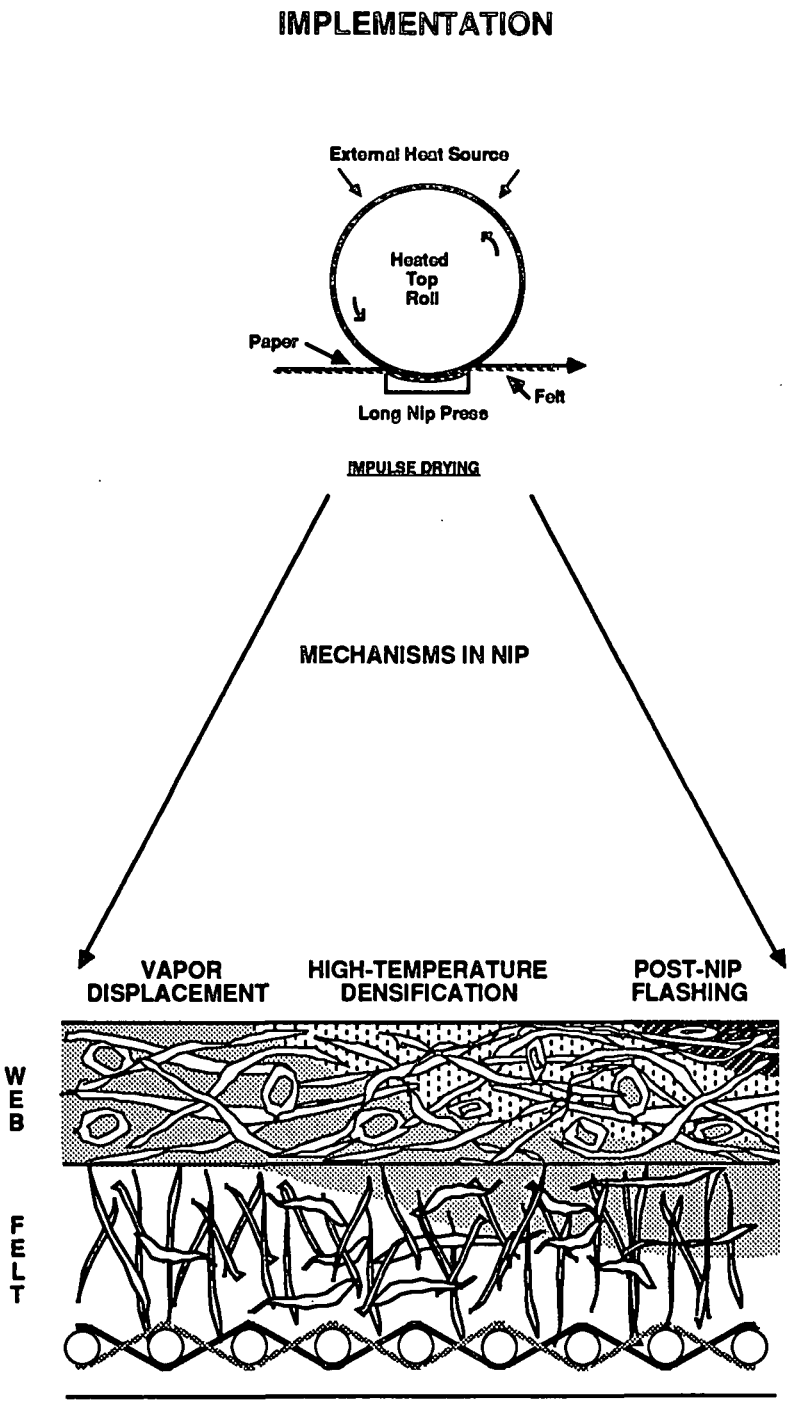


*Figure 23. Water removal and densification mechanisms during impulse drying. High pressure steam produced in the web near the hot surface displaces liquid water from the sheet. Meanwhile, high temperatures near the sheet surface promote densification. The cooler portions of the sheet regain bulk as hot water flashes as pressure is released at the end of the nip.*

conditions lead to a calculation of energy use which is known to be conservative (higher than would be observed on an actual machine), as much of the water is displaced before it is heated to a high temperature (2).

The energy use data show that between 200 and 1000 BTUs are required to remove each pound of water from linerboard (Figure 24). This may be compared with conventional cylinder drying, which requires 1600 to 1800 BTUs per pound on modern machines. The decline in energy requirement as wetter sheets are impulse dried which was reported previously (Figures 11 and 12), continue to decline to a minimum of 200 BTUs per pound at about 25% solids.

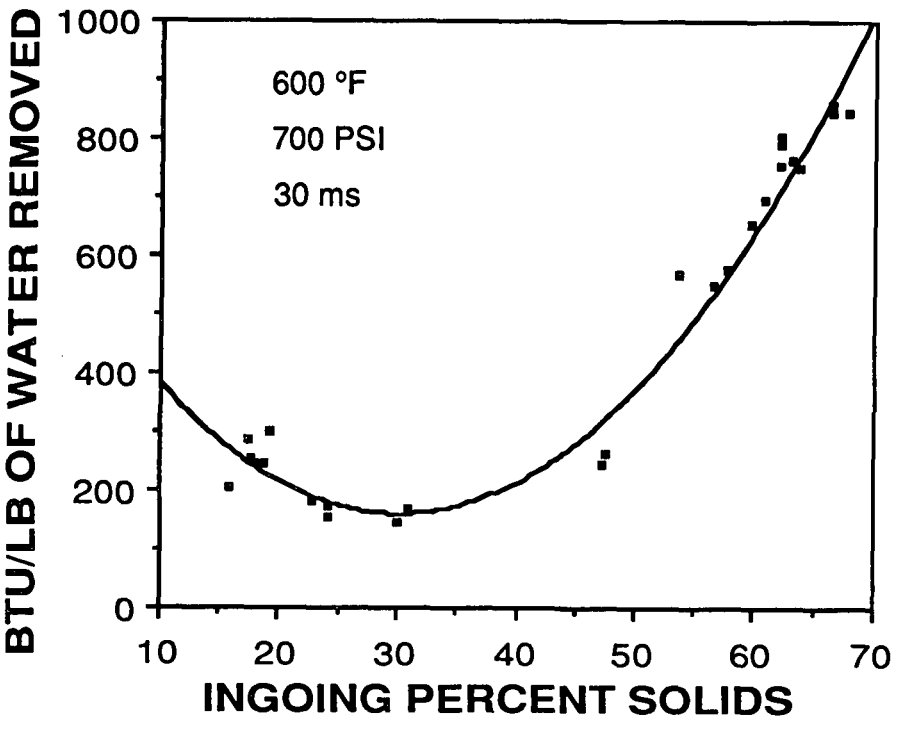


*Figure 24. Specific energy use for linerboard. Specific energy as BTUs per pound of total water removed during impulse drying, as calculated using the lithium chloride tracer method. All data for 127 grams per square meter sheets preheated to 180°F before impulse drying. Impulse drying performed at 600°F at a peak pressure of 700 psi for a nip residence time of 30 milliseconds. Data at for sheets drier than 58% solids were taken on the reverse side of a previously impulse dried sheet.*

A single impulse drying event will leave some water in the sheet; about 0.55 pounds of water per pound fiber remains in the case of 35% solids linerboard. This remaining water would probably be evaporated using conventional cylinder dryers. The energy efficiency of the combined system of impulse drying and conventional drying can be calculated if some assumptions are made about the papermachine system . Figure 25 shows the total energy requirement for a impulse drying plus cylinder drying system on a hypothetical linerboard machine. Conventional drying requirements were assumed to be 1600 BTUs per pound of water removed, with impulse drying energy requirements taken from Figure 24, increased by a factor of 1.4 in an attempt to account for machine efficiency.

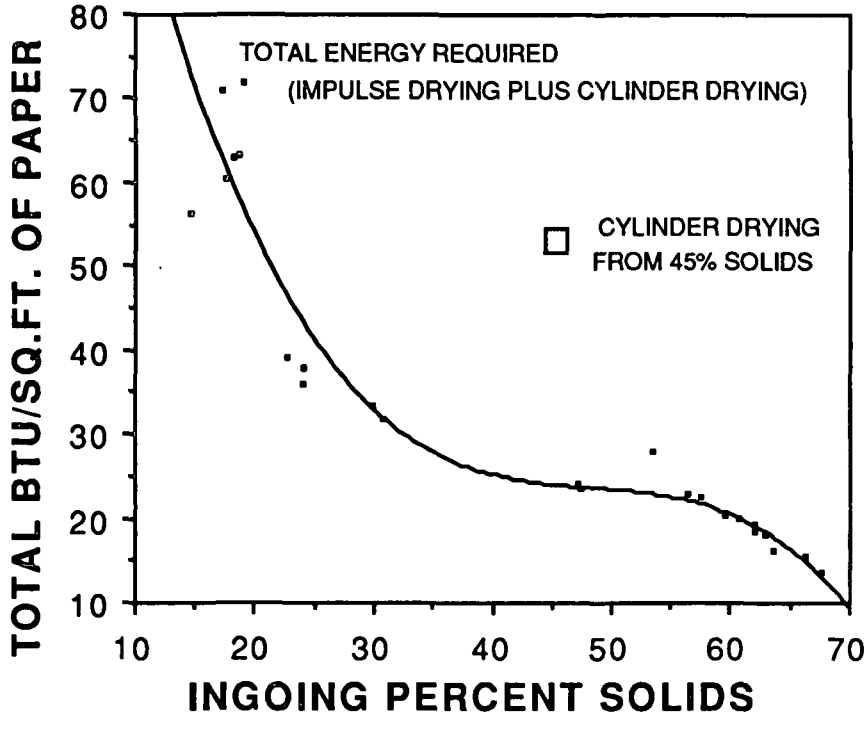


*Figure 25. Total energy use for impulse drying plus final cylinder drying for linerboard. Energy use as BTUs per square foot of linerboard dried to 94% final sheet solids at the reel. Impulse drying energy use estimated as 1.4 times the specific energy use (BTU/lb) shown in the previous Figure. Conventional drying energy costs were assumed to be 1600 BTUs per pound of water removed. All data for 127 grams per square meter sheets preheated to 180°F before impulse drying. Impulse drying performed at 600°F at a peak pressure of 700 psi for a nip residence time of 30 milliseconds.*

For this possible linerboard machine, impulse drying is found to require half the energy per square foot of paper dried as conventional drying for sheets entering the impulse dryer at 35% solids. Impulse drying could begin using sheets as wet as 20% solids before energy use equals conventional levels. These results are important because the lowest capital cost configuration for impulse drying may be in the third press (35% solids) position, where most wide nip presses have been installed to date.

The effects of impulse drying on the configuration of a hypothetical linerboard machine before and after a third-press rebuild to implement impulse drying are shown in Figure 26. These calculations were based on 125 grams per square meter linerboard being produced at 2000 feet per minute on a machine with five-foot diameter cylinder dryers. A cylinder drying rate of 5 pounds of water evaporated per hour per square foot of heat transfer surface was assumed in the calculations. The energy use conditions are those used to construct Figure 25, as described in the previous paragraph. Calculations indicate that if the third press of this machine were rebuilt as an impulse dryer, the machine would require half the cylinder dryers of the original machine, and would consume about two-thirds as much energy. A fifty percent increase in sheet density would be expected, which would potentially allow increases in pulp yield and decreases in refining intensity.

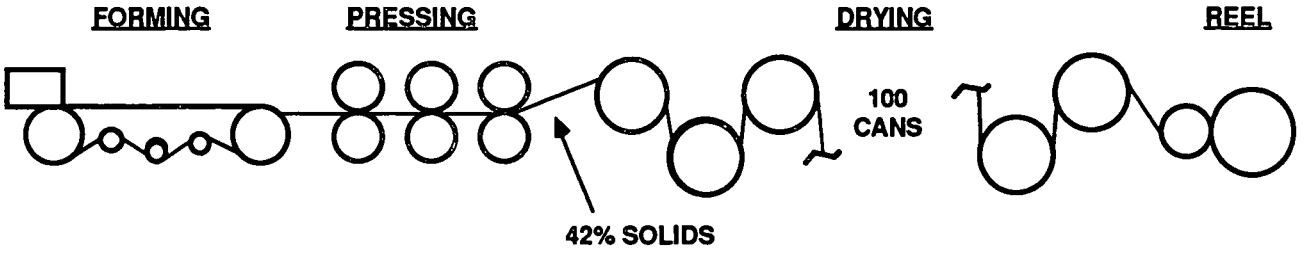


**DRYING ENERGY = 3.8 MILLION BTU/TON**

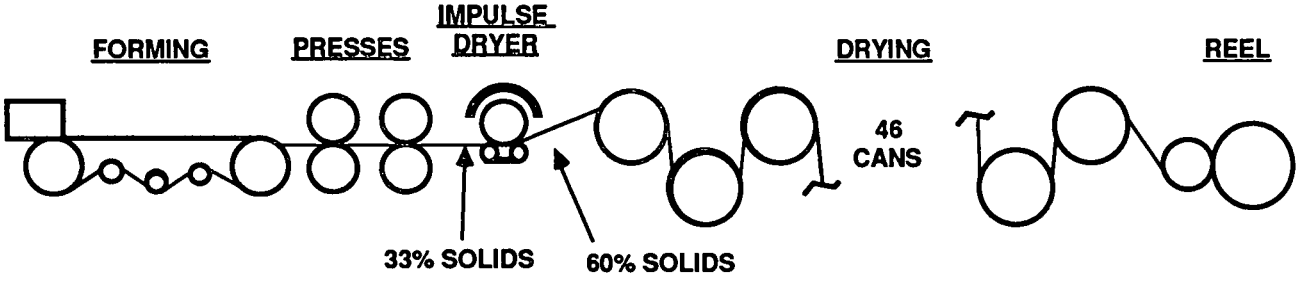


**DRYING ENERGY = 2.3 MILLION BTU/TON**

*Figure 26. Overall machine configuration changes possible with impulse drying. Calculations based on 125 grams per square meter linerboard produced at 2000 ft/minute, with conventional 5 foot diameter cylinder dryers. A cylinder drying rate of 5 pounds of water evaporated per hour per square foot of heat transfer surface was assumed in the calculations. Conventional drying energy costs were assumed to be 1600 BTUs per pound of water removed. All data for 127 grams per square meter sheets preheated to 180°F before impulse drying. Impulse drying performed at 600°F at a peak pressure of 700 psi for a nip residence time of 30 milliseconds.*

## PILOT ROLL IMPULSE DRYER CONSTRUCTION

### Goals of roll impulse dryer construction work

Construction of a pilot roll impulse dryer was essential in the development of impulse drying, as there are a number of important process and product performance questions which cannot be addressed with the bench-scale geometry and sample size limits. These questions include:

1. Will the water removal and densification performance be the same in the roll geometry as in a flat press?

2. What will the energy efficiency of the process be in the roll geometry?

3. Will there be process problems such as sticking or delamination that will develop in a roll geometry?

4. How will the heated roll perform metallurgically under these difficult cyclical conditions? How will felts perform?

5. How will impulse dried sheets perform when they are converted? Large samples are essential to do meaningful evaluations of printing, coating, and the conversion of medium and linerboard to combined board.

To address these questions, the Institute of Paper Chemistry is building a pilot roll impulse dryer with the assistance of a four-year 1.5 million dollar grant from the Department of Energy.

## Construction of the first nip

The pilot roll impulse dryer in its current form is sketched in Figure 27. The ultimate design of the dryer includes two nips; the design of the second nip is now underway with construction scheduled for the first quarter of 1988. A simple press design with two hard rolls has been used, eliminating the mechanical complexity of a wide nip press at the cost of a slow machine speed. Current speed is limited to 350 feet per minute, which can be increased to 700 fpm with a simple belt ratio change if needed in later work. The rolls are plain carbon steel with bolted end plates, two foot in diameter and two foot wide, and generally are used to impulse dry one foot wide web samples made on the Institute webformer. A hydraulic system can load the rolls up to 1500 pli over the 24 inch face width.

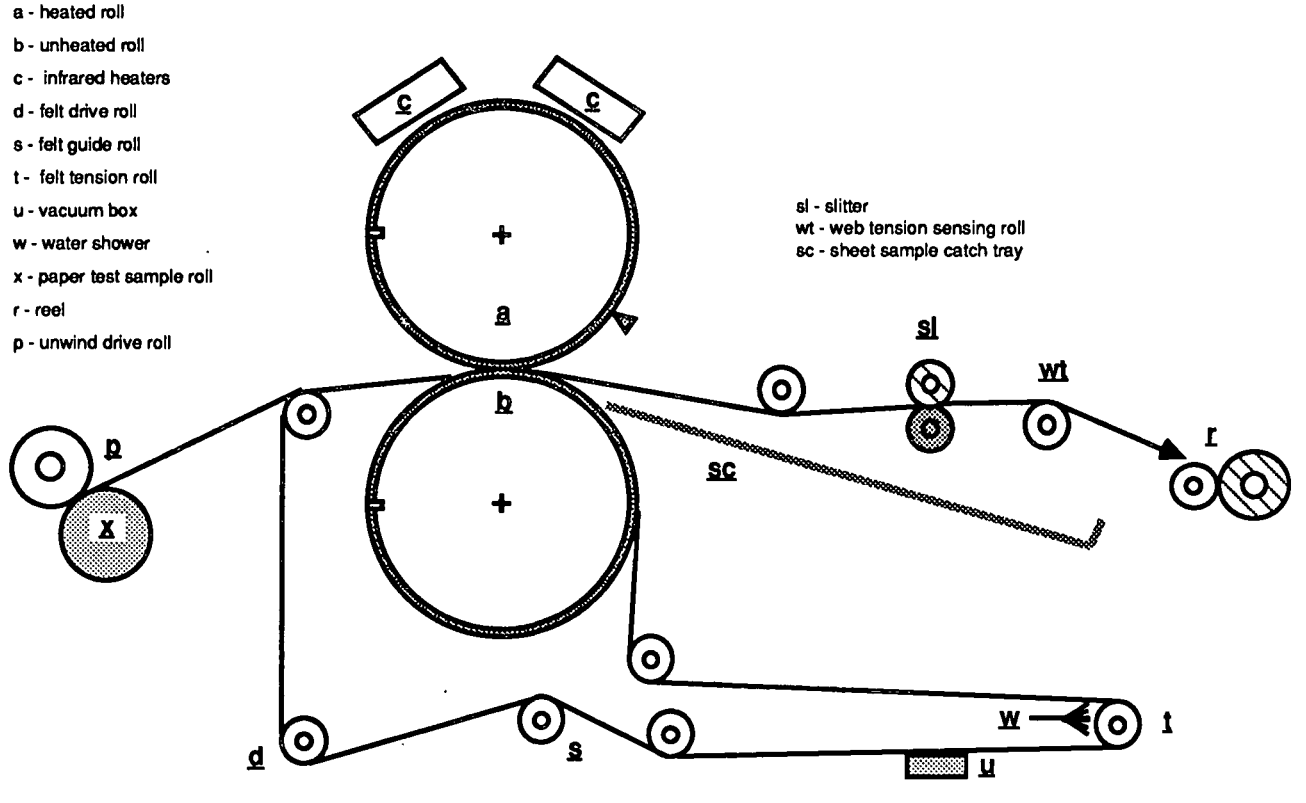


*Figure 27. The pilot web former at the Institute of Paper Chemistry in its September, 1987 configuration.*

Electrical infrared heaters provide thermal energy to the upper roll. The heaters have been able to sustain 700°F roll temperatures against wet felts and paper. Heater control in two zones across the roll face is based on signals from surface junction thermocouples in the roll. Heater response time is fast enough that roll surface temperature can be regained within one roll revolution after initial contact with a wet sheet.

Individual rolls are driven from the line-shaft through clutch/brake systems for independent control. Variation in roll surface speeds due to thermal expansion can be compensated for by slippage in the roll clutch as the nip is closed. A surface-driven unwind stand was added during August, 1987 to simplify handling weak wet webs.

The water receiver is a commercial Nomex fiber wet press felt. The felt has an automatic tracking system, automatic tensioning, a lubricating shower, and a vacuum box to remove excess water from the felt. The felt can be conditioned by running the press nip at ambient temperature. Although the machine was designed to run with the sheet overlapping the edge of the felt for protection, the wet felt has tolerated the temperature conditions well without such precautions. The slitters which were included in the design to cut the wet edges from the web before rewinding have not been needed for that purpose.

Instrumentation includes surface junction thermocouples mounted through the hot roll shell which are used for heater control and, eventually, for energy use measurements. Other control instruments are a tachometer on each roll, load cells on each nip loading cylinder, a transducer for roll rotational position. Machine control is accomplished through a programmable controller donated to the project by Westinghouse. Pressure sensors mounted in the lower roll are used to confirm nip widths and nip residence times. A high-speed data acquisition system records process data so that detailed temperature and pressure histories can be obtained for each test.

Most pilot impulse dryer work before August was done with handsheets or three to five foot long pieces cut from webformer sheets. The sheets were placed on 6 foot long pieces of felt, and the sheet and carrier felt sent through the nip supported by the machine felt. A sample slide was added as shown in Figure 27 to recover the sheet-fed samples.

## PILOT ROLL IMPULSE DRYER EXPERIMENTAL WORK

### Initial operation

The initial physical property data from the new equipment was collected late in April, 1987. Table 3 presents the test values observed from the initial run on 42 lb linerboard, which was impulse dried at 600°F, 400 psi pressure and 100 milliseconds nip residence time. All initial work has been done using a never-dried southern pine kraft linerboard furnish taken from a commercial linerboard mill. This furnish is refined to 650 ml Canadian Standard Freeness before sheet making. Most of the impulse dried test values for this 42 lb product approach the commercial test expectations for 69 lb liner. The magnitude of the strength increases were similar to those observed on early bench-scale work.

| TEST | COMMERCIAL BOARD | IMPULSE DRIED |
|---|---|---|
| Burst, psi | 105 | 137 |
| STFI, lb/in | 21 | 32 |
| Ring Crush, lb/6 in | 75 | 125 |
| ZDT, psi | 50 | 99 |
| Density, g/cc | 0.69 | 0.84 |
| lb/point | 3.6 | 4.4 |

*Table 3. Initial performance data from the pilot roll impulse drier. 42 pound per 1000 square foot southern pine linerboard impulse dried at 600°F, 400 psi peak pressure and 100 milliseconds nip residence time on each side of the sheet.*

The pilot roll impulse dryer has performed with few problems, and has required only a few minor adjustments. The linerboard grade runs well on the roll press. Sheet release from the hot roll has not been a problem, as long as the roll temperature is maintained above 380°F.

The most serious delay-producing problems have resulted from webformer operation, not from the roll press. The webformer press design (Figure 28) made it extremely difficult to produce 42 lb sheets at solids levels above 25% solids; such wet sheets are very weak and difficult to handle. Numerous web breaks made continuous operation of the roll impulse dryer impossible. A rebuild of the webformer press section was completed during August, 1987. We can now produce sheets at 35% solids, which are much easier to handle in roll form without excessive breaks.

## Comparison of roll press and platen press performance

The next step in the experimental program was a direct comparison between the roll press and the bench platen press to confirm the validity of the performance results reported in the earlier work. For 42 pound southern pine linerboard, the water removal response of the platen press (MTS) and the roll press are very similar, as shown in Figures 29 and 30. The slightly lower final percent solids occasionally observed on the roll press are probably the result of rewetting, since the sheet can be separated from the felt more rapidly in the platen press geometry than in the sheet-fed roll press. As would be expected with rewetting, the final percent solids differences are exaggerated in lighter weight sheets (Figures 31 and 32). Variation in water removal due to differences between handsheets and webformer sheets were greater than the variations due to the geometry of impulse drying.

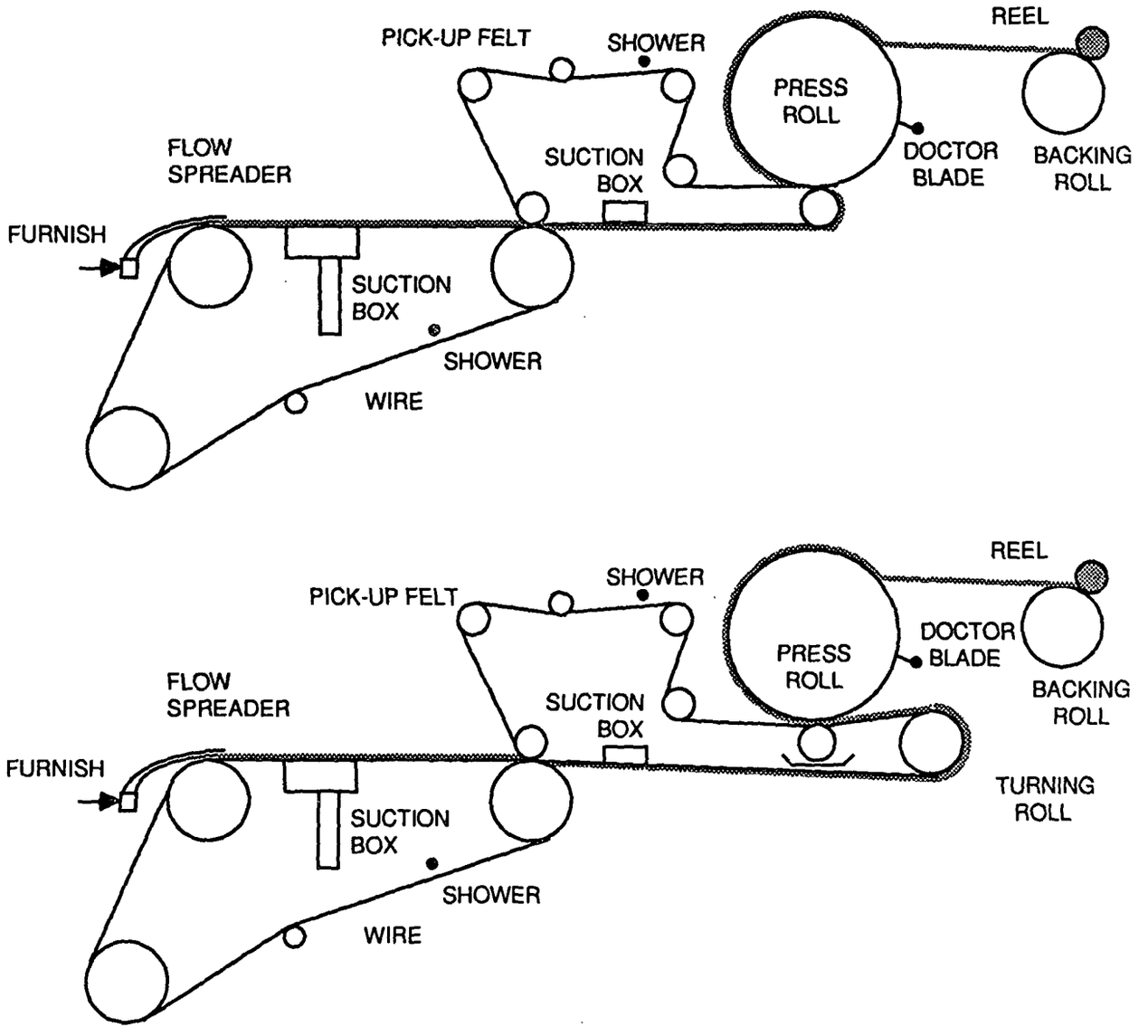


*Figure 28 The Institute of Paper Chemistry webformer before and after the August 1987 press rebuild.*

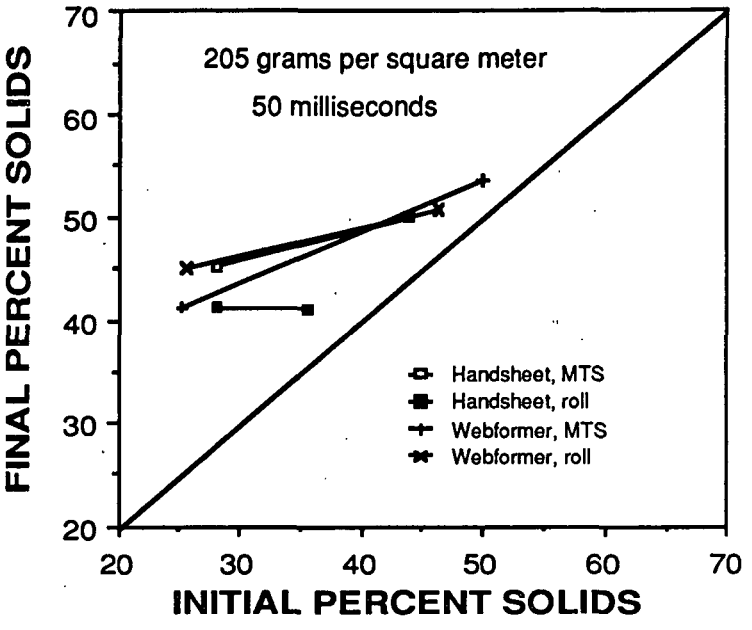


*Figure 29. Comparison between the water removal performance of the pilot roll impulse dryer and the electrohydraulic press, and of handsheets and webformer sheets. All tests run at 400 psi peak pressure and 500°F. Linerboard sheets initially at room temperature (80°F). 205 gram per square meter sheets impulse dried for 50 milliseconds.*

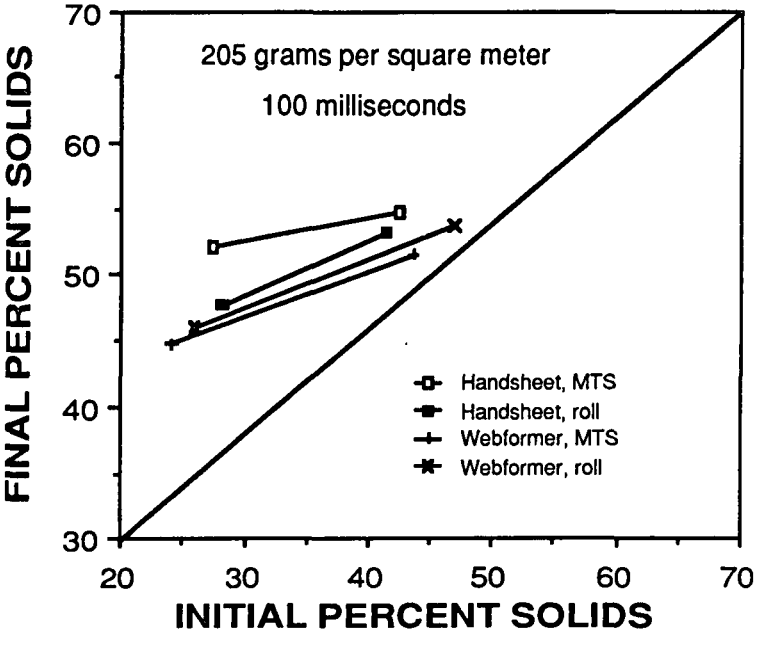


*Figure 30. Comparison between the water removal performance of the pilot roll impulse dryer and the electrohydraulic press, and of handsheets and webformer sheets. All tests run at 400 psi peak pressure and 500°F. Linerboard sheets initially at room temperature (80°F). 205 gram per square meter sheets impulse dried for 100 milliseconds.*

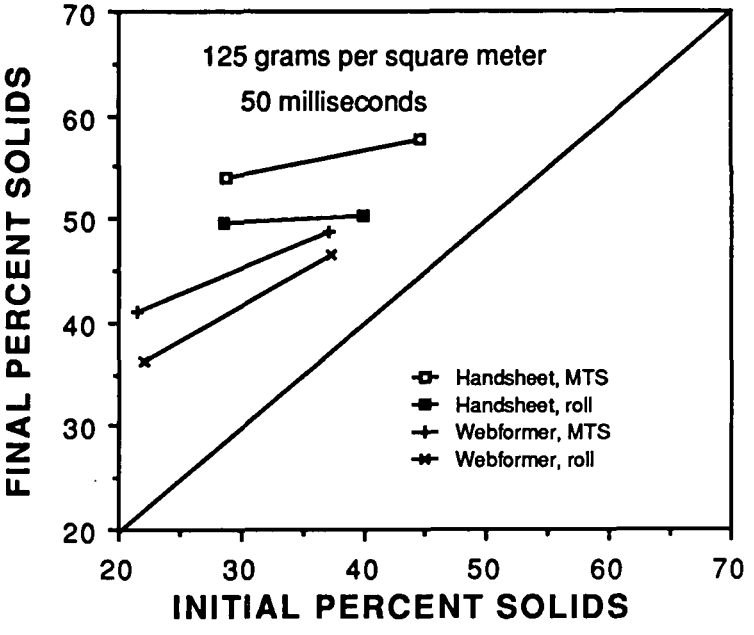


*Figure 31. Comparison between the water removal performance of the pilot roll impulse dryer and the electrohydraulic press, and of handsheets and webformer sheets. All tests run at 400 psi peak pressure and 500°F. Linerboard sheets initially at room temperature (80°F). 125 gram per square meter sheets impulse dried for 50 milliseconds.*

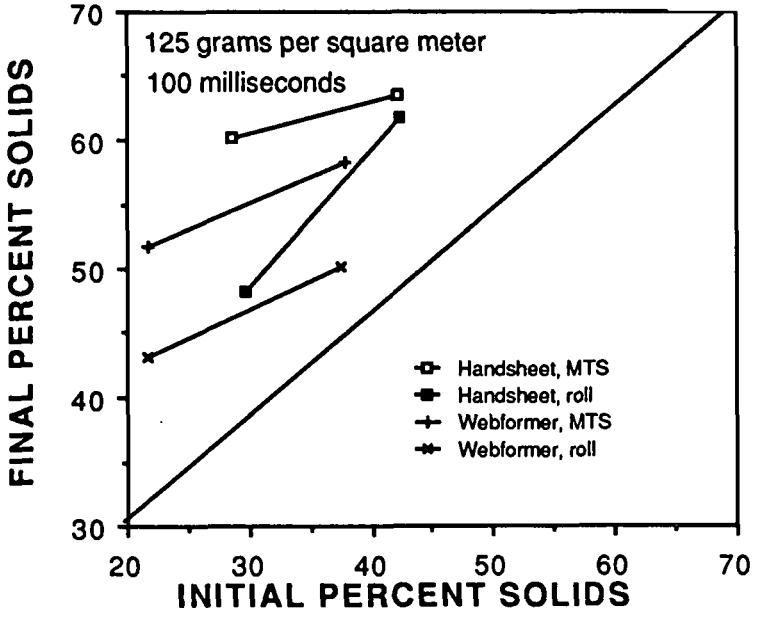


*Figure 32. Comparison between the water removal performance of the pilot roll impulse dryer and the electrohydraulic press, and of handsheets and webformer sheets. All tests run at 400 psi peak pressure and 500°F. Linerboard sheets initially at room temperature (80°F). 125 gram per square meter sheets impulse dried for 100 milliseconds.*

Density variations due to impulse drying geometry were minor. Previous work has shown that impulse drying gives a straight line relationship between density and the percent solids achieved after the nip, with little dependence on the choice of temperature, pressure and nip residence time used to achieve a given solids level. Density development is similarly insensitive to geometry and handsheet/webformer sheet variations, as may be seen in Figures 33 and 34.

The samples from this experiment to compare the effects of roll press geometry are also being evaluated for tensile strength, STFI compressive strength, and Z-direction tensile strength. These results are not yet available but are expected by the October meeting. All previous work showed a linear relationship between density and these variables, however.

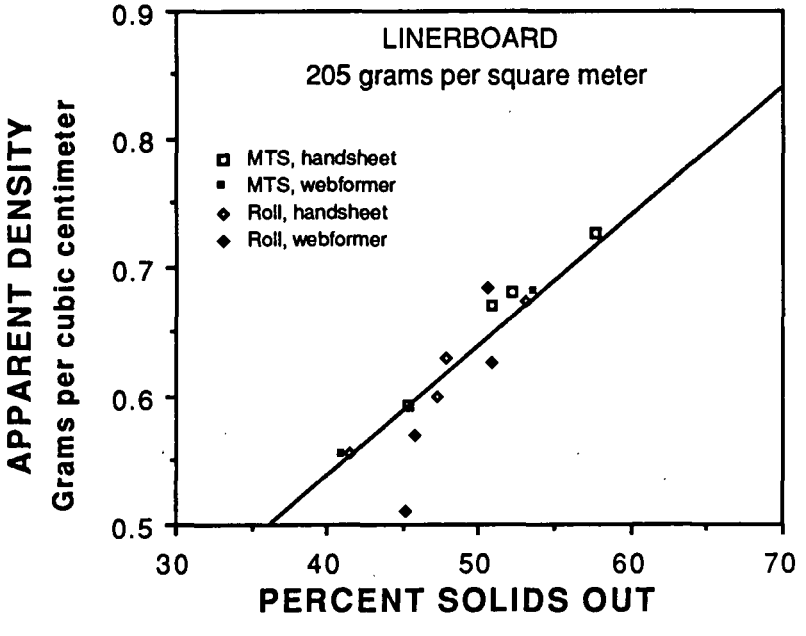


*Figure 33. The density - percent solids relationship effects of impulse drying geometry and sheet type. All tests run at 400 psi peak pressure and 500°F for 50 or 100 milliseconds using 125 gram per square meter linerboard sheets initially at room temperature.*

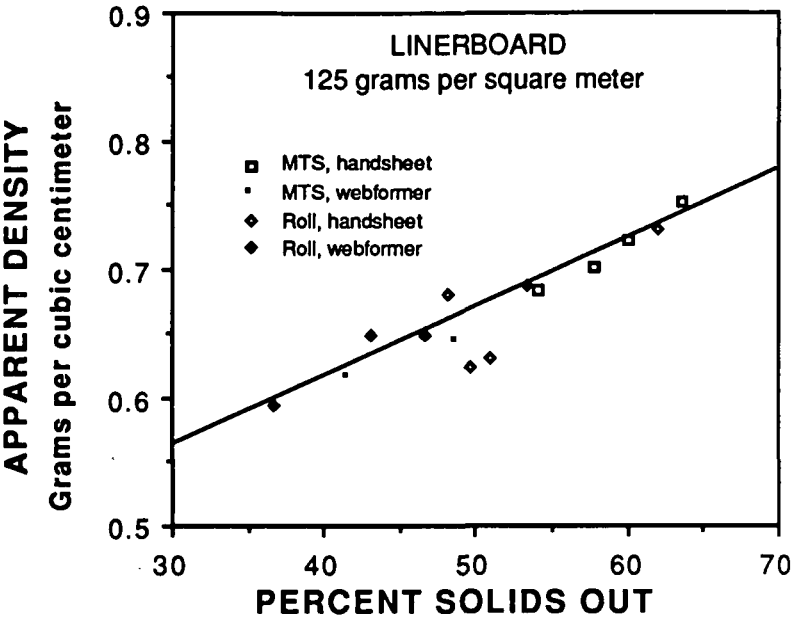


*Figure 34. The density - percent solids relationship effects of impulse drying geometry and sheet type. All tests run at 400 psi peak pressure and 500°F for 50 or 100 milliseconds using 205 gram per square meter linerboard sheets initially at room temperature.*

## Sheet surface quality issues

The next series of experiments was designed to characterize the surface quality of linerboard, principally through the Bristow test and evaluation of double-backer bonding simulator (DBBS) results. Five foot long webformer samples of 42 lb linerboard were impulse dried for these experiments. The samples were impulse dried on one side at 500°F, 400 psi and 50 or 100 milliseconds. Relatively long times were used to emphasize any heat-related changes in surface quality.

The DBBS design is sketched in Figure 35. In the DBBS, glue is applied to a short section of corrugating medium (a commercial medium sample in these tests). The glued flutes are then pressed against a strip of linerboard. The combined medium and liner are then peeled apart, while the force required to bread the glue bond at each flute tip is monitored. The test provides three pieces of information. First, the time required for any measurable bond strength is recorded. Next, the rate at which bond strength develops over time after the initial induction period is completed is observed. Finally, the time required to

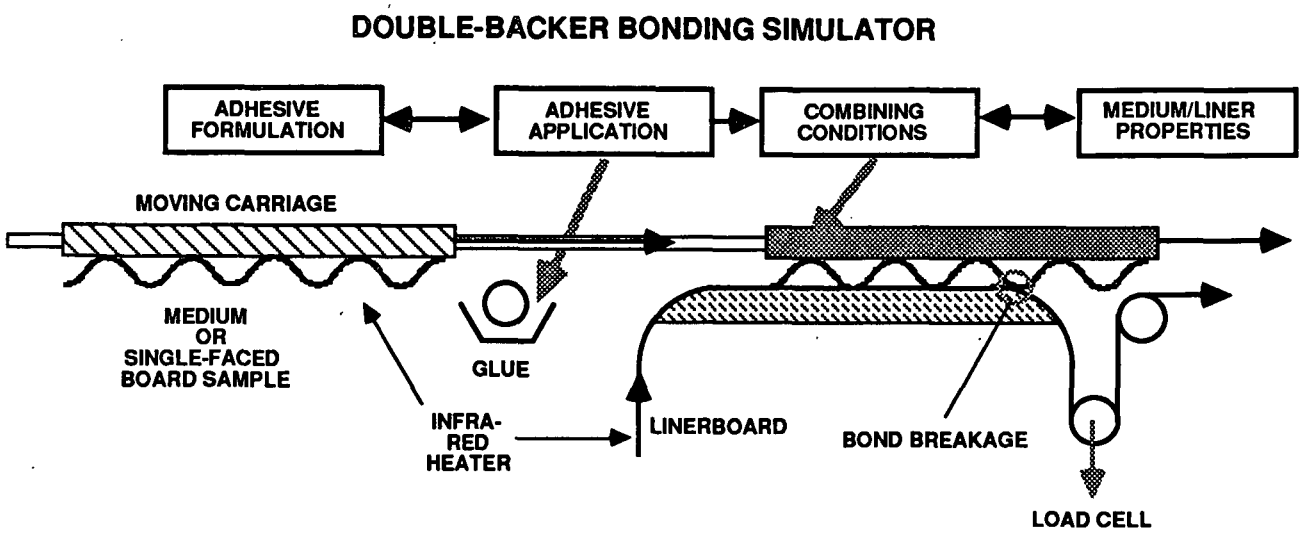


*Figure 35. The Institute of Paper Chemistry double-backer bonding simulator (DBBS).*

develop five psi of bond strength is noted. Improved conversion performance is indicated by reduced induction time, faster bond strength development, and shorter times to 5 psi bond strength.

The DBBS evaluations were performed on both the side of the board which faced the hot roll during impulse drying and on its unheated side, although gluing on the "cold" side would be more likely to take full advantage of the surface appearance of the impulse dried board. A control sample which was conventionally pressed and dried but not impulse dried was also evaluated for comparison.

The results show that all the DBBS parameters are either unchanged or are improved by impulse drying. Glueability improves on both hot and cold sides of the sheet. Figure 36 shows that the induction time before the glue sets remains constant when the glue joints are made on the hot side of the impulse dried sheet and actually improves by about 20% when made on the cold side of the sheet. The rate of development of bond strength is unchanged on the cold side of the sheet (Figure 37). The control board was initially very different on the two sides of the sheet in terms of the rate of bond strength

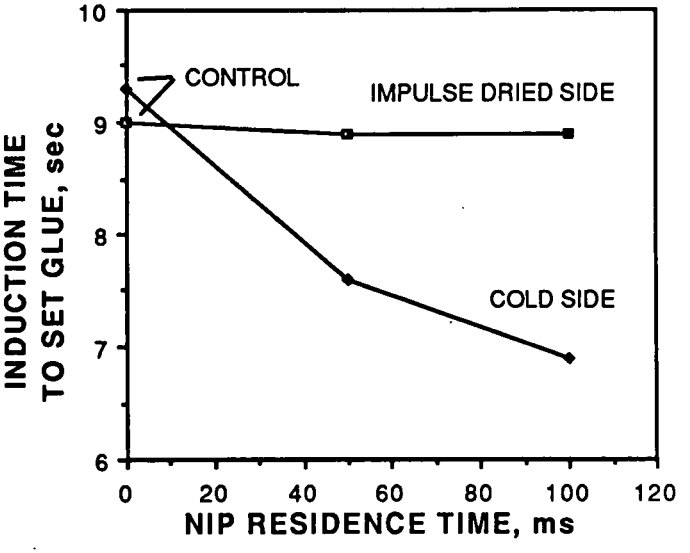


*Figure 36. Induction time before glue bond strength develops as a function of impulse drying nip residence time; 400 psi peak pressure and 500°F surface temperature.*

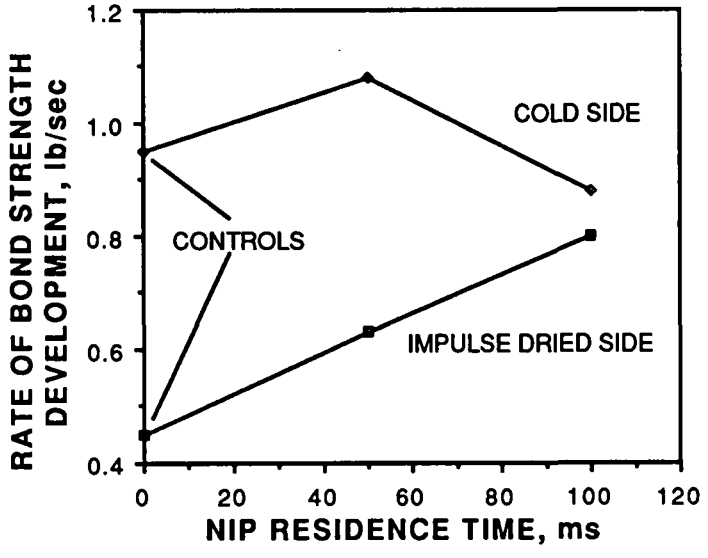


*Figure 37. Rate of glue bond strength development as a function of impulse drying nip residence time; 400 psi peak pressure and 500°F surface temperature.*

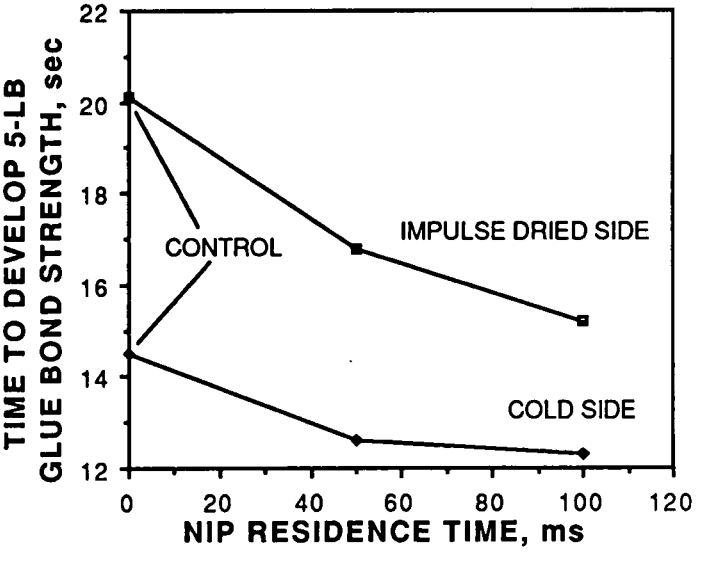


*Figure 38. Time to develop 5 lb of glue bond strength as a function of impulse drying nip residence time; 400 psi peak pressure and 500°F surface temperature.*

development; improvements on the impulse dried side almost removed the difference. The time needed to develop 5 psi of glue bond strength, Figure 38, also improved significantly when the sheet was impulse dried. Both sides of the sheet improved, with the cold side giving the best overall performance.

These results are encouraging, as the water resistant impulse dried surface might have interfered with bond formation. A duplicate run of this experiment has been completed to confirm these important observations. Bristow test results and physical property tests from these experiments are still underway.

## PLANS FOR THE COMING YEAR

During the period from October 1987 through October 1988, we expect to expand both the performance attribute evaluation of impulse drying and improve our fundamental understanding of the process. The major single activity will be the construction of a second nip for the pilot roll impulse dryer which will allow us to develop methods to produce newsprint and fine paper products while minimizing the differences in sheet surface quality between the two sides of the sheet. We will also complete the single-nip evaluation of the surface quality and conversion performance of impulse dried sheets. Studies to better understand sheet delamination under intense impulse drying conditions will continue. Fundamental understanding of the process will be enhanced through Gary Rudemiller's thesis work, plus additional project work on the effects of temperature and pressure on the heat transfer processes during impulse drying which will be performed as time permits. A timeline including the major goals for the project is presented in Figure 39.

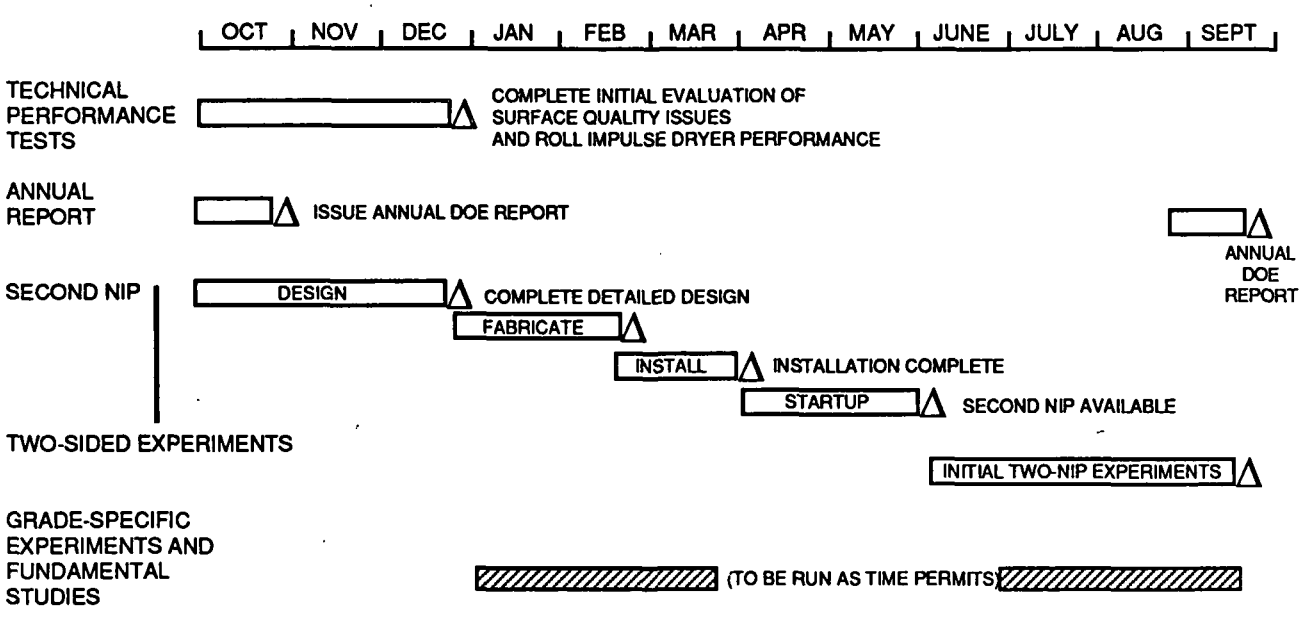


*Figure 39. Timeline including major impulse drying project goals for 1988.*

## COMPLETION OF SHEET SURFACE QUALITY STUDIES

The work remaining on the sheet surface quality issues includes the following grades and issues:

1. Corrugating medium: Physical properties, including CONCORA test, Bristow test of surface water receptivity, and double-backer bonding simulator effects in combination with conventional and impulse dried linerboard,

2. Newsprint: Physical properties, printing performance,

3. Writing papers (freesheet): Physical properties, offset printing performance,

4. Lightweight coating rawstock: pilot scale coating performance, printing evaluations.

The webforming and impulse drying work on these samples will be performed at the rate of one grade per month through December, 1988. Pilot conversion and laboratory evaluation of the product should be essentially complete before April, 1988. Further two-sided sheet quality work on newsprint, writing papers and coating rawstock will be performed during the summer of 1988, after the second nip is completed.

## CONSTRUCTION OF SECOND NIP OF THE ROLL IMPULSE DRYER

The construction of a second nip for the pilot impulse dryer is needed to permit rapid evaluation of combinations of nip conditions. A large number of combinations of temperature and pressure are possible in a two-nip system. A choice of variables which minimizes two-sidedness in the final product must be identified for newsprint and fine paper grades.

The second nip will be a duplicate of the first nip, but with the lower roll heated. The design concept is shown in Figure 40. Detailed design is now in progress, with the goal of a final design by the end of December, 1987. Construction will be complete by the end of April, 1988 with the machine available for the initial two-sided experiments by the end of June, 1988. The matrix of conditions to be tested during these experiments will be determined in part after reviewing the results of the one-sided experiments now in progress.

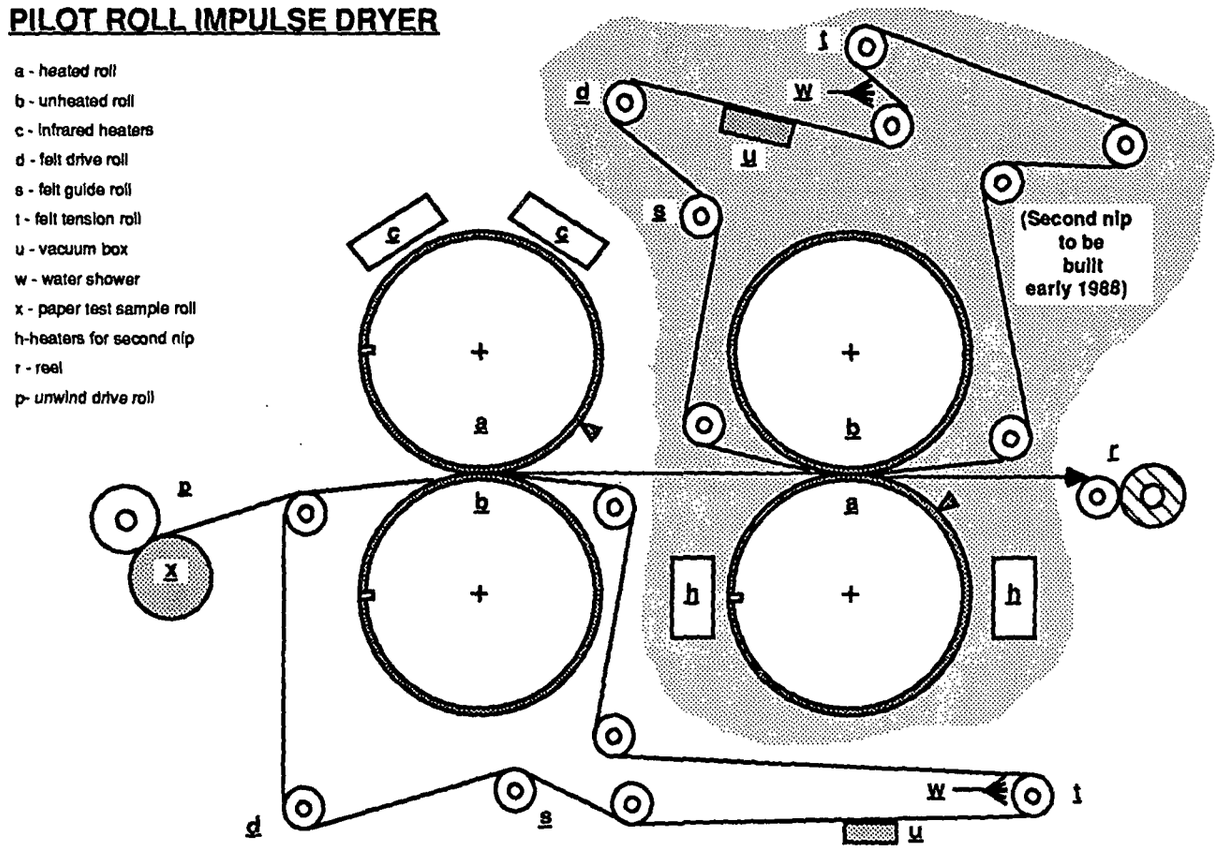


*Figure 40. Final design of the pilot roll impulse dryer, showing the configuration of the second nip which will be built during 1988.*

# REFERENCES

1. Sprague, C. High-Intensity Drying Processes, Report 1 for Department of Energy Contract FG02-85CE40738, DOE/CE/40738-T1, August, 1985

2. Lavery, H.P., High-Intensity Drying Processes-Impulse Drying, Report 2 for Department of Energy Contract FG02-85CE40738, DOE/CE/40738-T2, February 1987

3. Wahren, D., U.S. Patent No. 4,324,613 (April 13, 1982)

4. Gottwald, B.C., Halsey, B.S., Williams, R.C., U.S. Patent No. 3,354,035 (November 21, 1967)

5. Burton, S., Ph.D. Thesis, "An Investigation of z-direction Density Profile Development during Impulse Drying", The Institute of Paper Chemistry, (June 1986).

6. Devlin, C., Ph.D thesis, The Institute of Paper Chemistry, (June 1986)

7. Geidt, W.H., The determination of transient temperatures and heat transfer at a gas-metal interface applied to at 40mm gun barrel, Jet Propulsion, vol. 25, April, 1955, pp. 158-162.

8. Cowan, W.F., An investigation of the hot surface drying of glass fiber beds, Ph.D. thesis, The Institute of Paper Chemistry, Appleton, WI, (June 1961)

9. Wahlstrom, P.B., A long-term study of water removal and moisture distribution on a newsprint machine press section, Pulp and Paper Canada, 61:T379-T401 (August, 1960)

10. DeCrosta, E.F., Toward a unified theory of pressing, CPPA Annual Meeting Preprints, p. B105-B109 (1981)

11. Hsu, Y.Y., Graham, R.W., Transport Processes in Boiling and Two-phase Systems. Hemisphere Publishing Corp., Washington, 1976.

12. MacGregor, M.A., A description of sheet stratification caused by wet pressing, Tappi J., 66(6):53-57(June 1983)

THE INSTITUTE OF PAPER CHEMISTRY

Appleton, Wisconsin

Status Report

to the

ENGINEERING PROJECT ADVISORY COMMITTEE

Project 3480

DISPLACEMENT DEWATERING

October 22, 1987

# PROJECT SUMMARY FORM

DATE: Sept. 25, 1987

PROJECT NO.: 3480 – DISPLACEMENT DEWATERING

PROJECT LEADER: Jeff Lindsay

IPC GOAL:

Develop novel processes for efficient water removal with enhanced control over paper properties.

OBJECTIVE:

Develop a pilot-scale displacement device which demonstrates that high water removal rates can be achieved while maintaining control over paper properties such as bulk.

SUMMARY OF RECENT PROGRESS:

Theoretical investigations of displacement stability have been conducted which indicate that superheated steam has promise as a displacing agent. A numerical model, MIPPS (**M**oving **I**nterface **P**roblems in **P**orous **S**ystems), has been developed which can predict the transient physics of impulse drying and direct displacement processes in a rigid porous system. The computational results from MIPPS give insights into impulse drying-like processes. Capillary flow back to the hot surface in impulse drying has been shown to be an important mechanism contributing to the effectiveness of the displacement process.

Experimental apparatus has been designed to investigate displacement processes with steam and air. The apparatus is now nearing completion.

Because anisotropic permeability is an important consideration in the stability of displacement, a technique was developed to measure both the normal and lateral permeabilities of wet paper. Measurements have indicated that the lateral permeability of linerboard handsheets is consistently less (by a factor of 0.1 to 0.5) than the normal (z-direction) permeability. These are the first measurements of anisotropic permeability in a sheet of paper of which we are aware.

DISCUSSION:

I. Introduction to Displacement Dewatering

Displacement dewatering is a novel technology being developed at the IPC. In an ideal displacement process, a gas phase uniformly pushes free water out of the web using only small volumes of gas. Preliminary research has shown that displacement of water by an applied gas phase can lead to high dewatering rates without the degree of densification seen in wet pressing (Sprague, 1985). The main advantage over traditional wet pressing is that dryness can be decoupled from density. Dewatering through displacement processes may also offer energy savings and decrease the amount of capital equipment needed to dry paper. The final objective of this project is to develop a pilot-scale displacement device which demonstrates that high water removal rates can be achieved while maintaining control

over paper properties such as bulk. Achieving that objective will require further development of the science of displacement in porous media.

Both "direct" and "indirect" displacement processes are being studied. Direct displacement is the process of directly applying a gas phase to the wet sheet, which may also be under an applied mechanical load. Direct displacement drying is an undeveloped technology, although it is a cousin to through drying. Through drying, however, relies primarily on evaporation as opposed to true displacement and requires large volumes of air (Walser and Swenson, 1968). Indirect displacement relies on the generation of a vapor phase at or within the upper surface of the sheet itself through heat transfer. Impulse drying is a form of indirect displacement. which is becoming a devloped technology. Synergistic returns are expected from the current projects in impulse drying and displacement dewatering.

Fundamental and bench scale research into displacement processes will continue through 1988. Pilot scale implementation will begin in late 1988 and continue through mid-1990. During this time, furnish-related issues and other process factors will be explored on both the bench and pilot scale. The research will be supported by student work, member dues and government grants.

## II. Displacement Stability

An important lesson can be learned from the oil industry. When a liquid is displaced in porous media by another immiscible fluid of lower viscosity, the interface between the phases is frequently unstable. Any small perturbation on the initially smooth interface will accelerate,

creating fingers of the more mobile phase penetrating into the phase being displaced (see Figure 1). This phenomena is called viscous fingering (Homsy, 1987). For secondary oil recovery, it means that displacement of oil by water of gas will be inherently inefficient, since large portions of the oil may be bypassed by viscous fingers that break through to the production well. In the paper industry, it means that a gas phase will tend to simply blow through certain paths in the paper, leaving much of the water behind and creating nonuniform dryness (see Figure 2).

However, a number of factors have been shown to enhance stability. For example, if transient heat transfer from the vapor to the liquid is occurring, the interface becomes more stabile (Miller, 1973). As a hot viscous finger penetrates into cooler liquid, the gas begins to cool and contract, thus decreasing the growth rate of the viscous finger. Recent student work by Charles Miller (an A390 problem) also examined the way in which temperature-dependent liquid viscosity can affect the interface stability in immiscible displacement with transient heat transfer. He found that the resulting viscosity gradient cannot make the interface stable, but can decrease the degree of instability. It should be noted that graded viscosity profiles created by polymer injection are used in oil recovery to increase the stability of a water-oil interface (Gorell and Homsy, 1985).

When steam displaces water, the condensation of steam can significantly improve the stability of the vapor/liquid interface (Miller, 1973). For instance, as steam breaks through and contacts cooler liquid, it will condense. The viscous fingers become "self-sealing" to some extent, making the interface more stabile. The combined effects of heat transfer

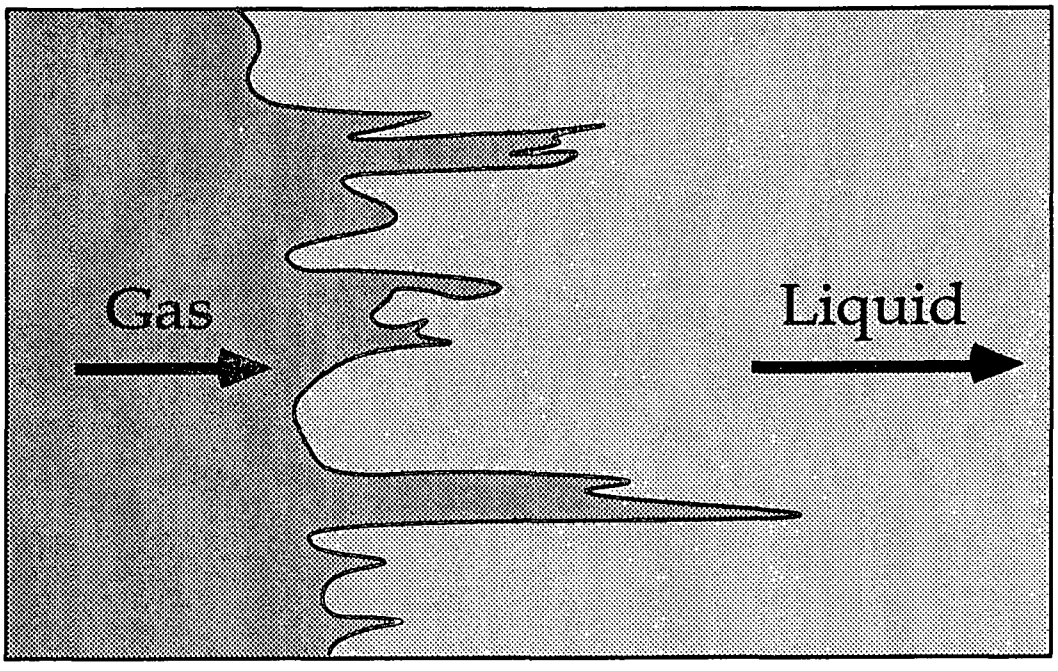


Figure 1. Viscous fingering during displacement in a porous medium.

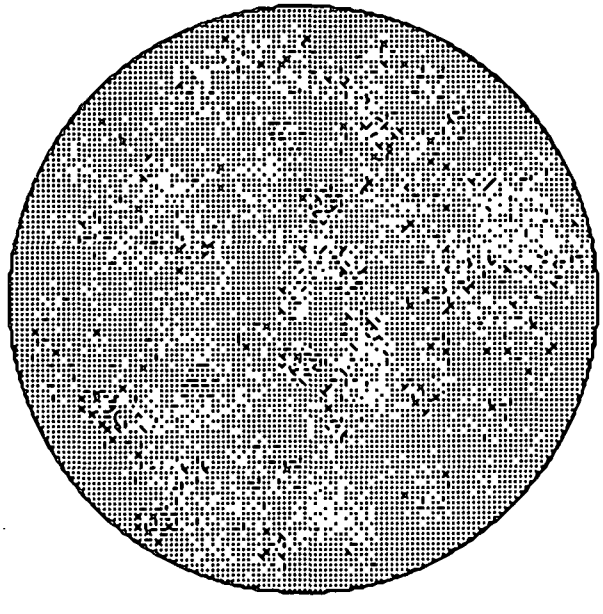

Figure 2. Nonuniform dryness in a handsheet.

and condensation are believed to make the interface in impulse drying stable during most of the impulse event, thus making impulse drying an efficient dewatering process.

In oil recovery, foams have been used to increase the stability of displacement (for example, see Hahn et al., 1985). The structure of foam decreases the mobility of the gas phase, giving it a high effective viscosity. The inherent instability of displacement is therefore decreased. In the paper industry, Skelton (1987) has reported that application of foam to paper increases water removal by suction. Skelton writes that the reasons for this effect are unknown. The analogy to oil recovery, however, would appear to provide at least part of the explanation. The stability of the displacement process in suction is increased, and water removal becomes more efficient. The decrease in surface tension caused by surfactants in foams is also likely to increase water removal, as is noted below in the discussion of recent experimental work.

Anisotropic permeability in paper can also enhance displacement stability. If the lateral permeability is greater than the normal permeability, a viscous finger could tend to spread out in the plane of the paper, thus creating a more uniform surface. A review of the literature and a survey of researchers revealed the surprising result that apparently no measurements of radial permeability in paper have ever been reported. Experimental difficulties, primarily with sealing the plane surfaces of paper, seemed to have frustrated earlier attempts. One study was conducted in a model system made of nylon fibers (Peterson, 1970), but its

applicability to paper is uncertain. Work was therefore done to investigate radial permeability in paper, and is reported below.

## III. Recent Experimental Work

Lateral Permeability. The anisotropic permeability of paper became of interest because of its possible influence in the stability of a displacement interface. Because of a serious lack of experimental data, a technique was sought and developed to measure the lateral permeability in paper itself. The result was the simple apparatus shown in Figure 3. Two flat acrylic blocks are used. One surface of each block is given a uniform coating of paraffin wax. A rectangular strip of paper is then placed between the two wax coatings, and the blocks are clamped together.

The wax deforms to seal the surface of the paper, thus preventing flow between the paper and the wax itself, without penetrating more than a few fiber thicknesses into the cross section of the paper. A proper seal between the paper and the wax can usually be detected visually because the wax becomes more transparent when a seal is formed. Three edges of the paper are then sealed with epoxy glue, which does penetrate into the paper. The reduction in effective paper width is easily measured. The unsealed edge of the paper becomes the outlet for flow injected at the inlet port. The thickness of the paper in the assembly can be measured with a hand micrometer by taking the difference between the assembly with and without paper, or by measuring the thickness of the paper itself under a similar compressive load with an IPC micrometer. Thicknesses measured with

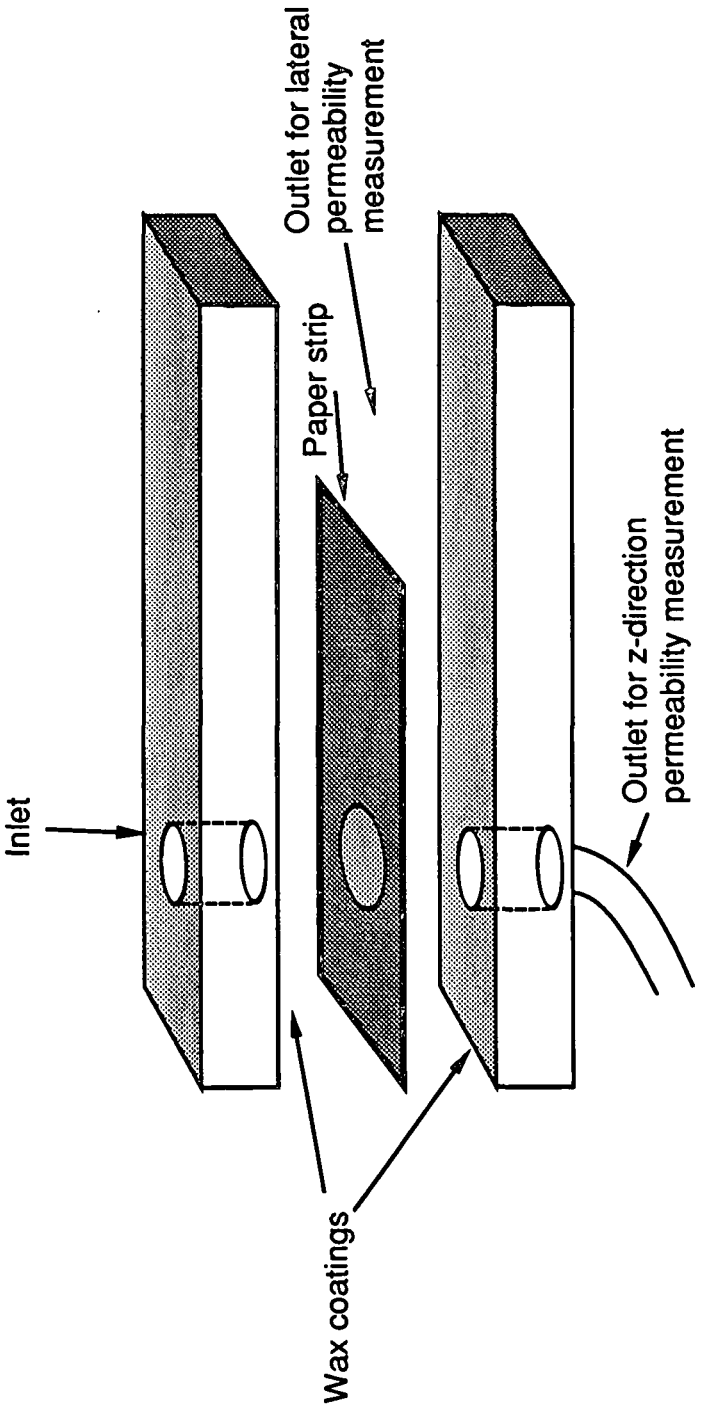


Figure 3. Measurement cell for lateral and normal permeability in paper

both methods agreed within about 5%, and the accuracy of the measured thicknesses is estimated at ±10%.

One source of systematic error comes from the assumption that the flow through the paper follows parallel rectilinear streamlines immediately after leaving the inlet port. Numerical results from FLUENT, a computational fluid dynamics package, showed that the errors due to the assumption of straight streamlines can be ignored.

The lateral permeability is then found using Darcy's law. Water is injected into the inlet port at a known hydraulic pressure which is measured with a commercial displacement cell. The flow rate of liquid through the paper is then measured. Knowledge of the flow rate, the paper thickness and width, the liquid properties, the pressure drop, and the length of the flow path from inlet to outlet is required to determine the lateral permeability. For each paper sample used, typically 20 or more replicate measurements are made.

Measurement of the normal permeability can then be made on the same paper sample without removing it from the clamped blocks. In this case, the flow is allowed to exit through a port underneath the paper which is aligned with the inlet port. Both the inlet and outlet ports are covered with a wire mesh to create an effective surface that is even with the wax coating. Again, the permeability can be measured using known values of pressure drop, flow rate, paper dimensions, and liquid properties. Replicate measurements are made for each sample. Uncertainties in the normal (z-direction) permeabilities made in this way are estimated at 10-15%. It is again assumed that the streamlines follow a straight path from

the inlet to the outlet port. This assumption introduces a systematic error. Conformal mapping was applied to obtain an analytical solution for the flow field, from which the error could be determined. For the sheet thicknesses used in this study, the error due to the assumption of straight streamlines in the z-direction is always less than 5%. This result was confirmed with numerical solutions from FLUENT.

The ratio of lateral to normal permeabilities gives the anisotropy ratio for the paper. This ratio consistently ranged from 0.1 to 0.5 for linerboard handsheets. The errors in the individual measurements cannot account for ratios this small, and thus we conclude that lateral permeability is less than normal permeability in the linerboard handsheets. This work will now be extended types of paper as well. These results for paper conflict with results for a matt of nylon fibers in which the lateral permeability was reported to be 25-30% higher than the z-direction permeability (Peterson, 1970).

A smaller lateral permeability means that anisotropy in the paper will not contribute to stability in displacement, and as such is a negative result. However, knowledge of lateral permeability itself is important to other issues in papermaking such as crushing and the fluid mechanics of pressing, and thus deserves to be pursued further.

Variations on Impulse Drying. Experimental work has also been conducted to see if methods for indirect displacement other than normal impulse drying offer any advantages. In particular, methods to increase control over bulk were sought. Regular impulse drying gives a character-

istic dryness-versus-density curve. Can variations on impulse drying give less density for a given dryness? A series of exploratory tests were conducted with the MTS system under impulse-drying conditions, but with special treatments applied to the upper side of the paper. For instance, a variety of fabrics or meshes with varying degrees of moisture were also placed over the paper and then pressed with a hot (400-600°F) MTS platten. The idea was to generate vapor in a porous layer outside of the paper itself, and see if the external vapor could then displace water efficiently. The results indicated that no detectable advantage over impulse drying could be obtained.

In other tests, surfactants were applied to the surface of the paper. Increased bulk could be obtained in some cases, but the result appears to be due primarily to the decreased surface tension of the water which lessens the bonding forces between fibers (and thus weakens the paper). More extreme results (extreme in both bulk and weakness) were obtained when volatile fluids such as methyl alcohol or acetone were applied to the paper before pressing in the hot MTS system. Evaluation of the results of this exploratory research does not justify further work at the time.

New Displacement Apparatus. The experimental investigation of direct displacement processes in paper began several years ago with the work of Sprague and Ahrens at the IPC. Some experimental work with air displacement suggested that promising dryness results could be achieved. Displacement with steam was not examined. Difficulties in obtaining reproducible results led to the temporary abandonment of the project. Part of the problem was nonuniform delivery of the air pulse to the paper sheet.

An improved system for direct displacement has been designed for studies of steam and air displacement processes. The apparatus is shown in Figure 4. An upper and lower head mount on the MTS apparatus. Paper is placed between the two heads. A compressive load can be applied by the MTS system, and steam or air can then be discharged into the upper head at a selected instant. The upper head can be heated to control temperature and prevent condensation. the vapor passes through the upper drilled plate through the sheet, a felt, and the lower drilled plate. Vapor exits out the lower head. A wide variety of mechanical pressure pulses, vapor pressure pulses, and vapor temperatures will be studied to examine the possibilities of displacement processes. The apparatus is currently being constructed and installed.

## IV. Numerical Modeling

Both impulse drying and direct displacement processes involve complex physical processes, especially when heat transfer is involved. Before a displacement process can be properly designed and optimized, the physics need to be better understood. Numerical modeling was selected as a tool which could provide fundamental insight into displacement and impulse drying physics.

The most noteworthy physical characteristic of a displacement system is the moving boundary between the gas and the liquid phase. The class of heat transfer problem in which boundaries move because of phase change are called Stefan problems. Stefan problems have been studied in connection with the solidification of molten metal, the melting of ice and

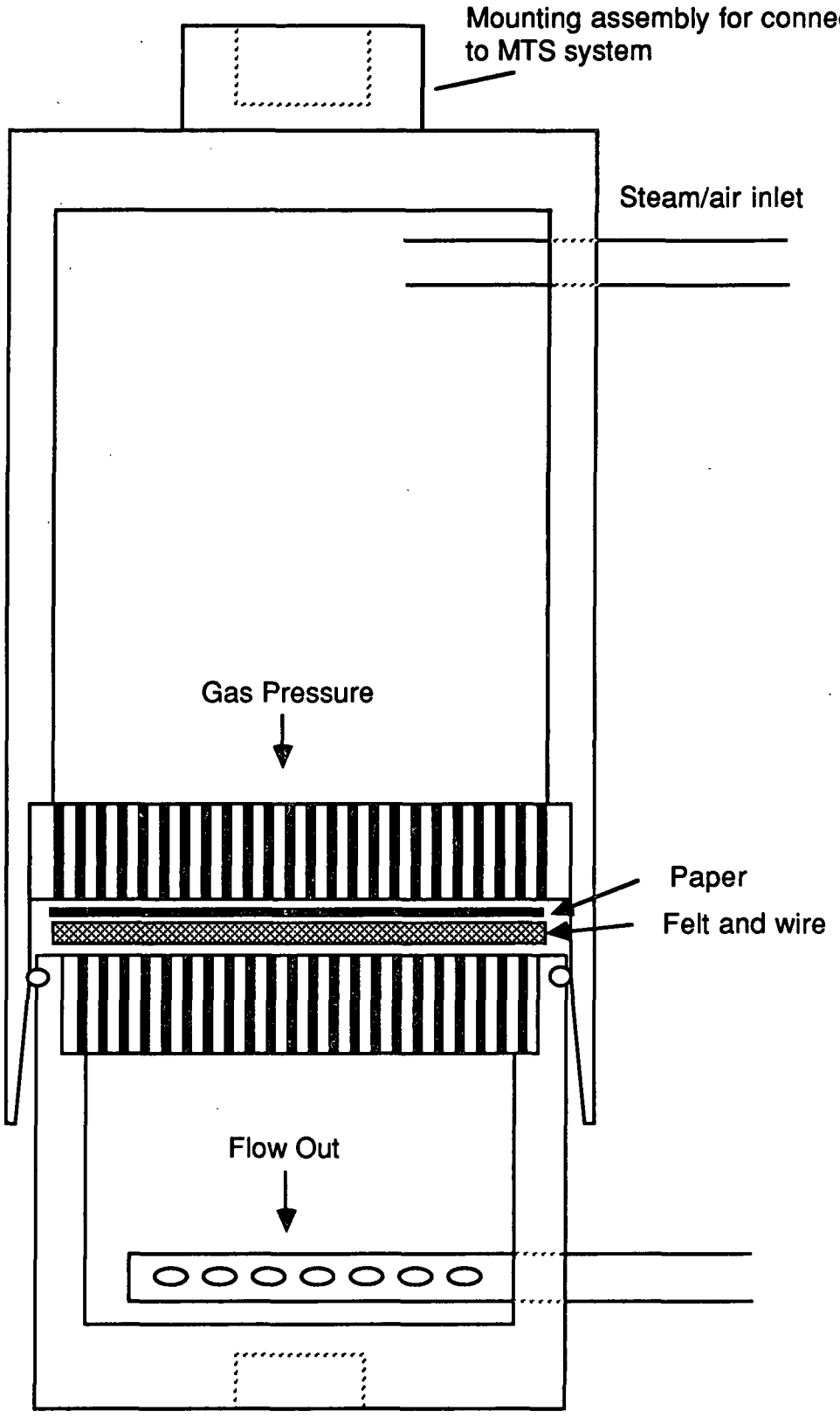


Figure 4. Schematic of new displacement apparatus.

other simple solids, the vaporization of containing walls in a nuclear reactor and the formation of fog from moist air. The variation of the Stefan problem related to impulse drying or steam displacement has not been studied before. It is a particularly challenging variation, in which the gas-phase pressure and the interface temperature are not constant, and in which fluid is being expelled at a varying rate from the system by hydraulic pressure.

A numerical model has now been developed which can deal with the major heat transfer and fluid flow mechanisms in impulse drying and related moving boundary processes. The model, MIPPS (**M**oving **I**nterface **P**roblems in **P**orous **S**ystems), describes transient heat and fluid flow in vapor and liquid phases coupled with a moving boundary in a one-dimensional rigid porous system. An example of such a system with impulse drying-like boundary conditions is shown in Figure 5. MIPPS uses finite difference equations. Physical properties are treated as functions of temperature, not as constants. The temperature range in impulse drying, for example, is great enough that the common assumption of constant properties could lead to gross errors.

The governing equations are solved separately for each phase. The governing equation for heat transfer in the gas phase is written in a form suitable for the compressible nature of the flow:

$$\rho C_v\left(\frac{\partial T}{\partial t} + u\frac{\partial T}{\partial x}\right) = \frac{-\partial}{\partial x}\left(k\frac{\partial T}{\partial x}\right) - P\frac{\partial u}{\partial x} \qquad (1)$$

where $\rho$ is the density, $C_v$ is the constant volume heat capacity, T is temperature, u is velocity, k is the conductivity, and P is the pressure. The

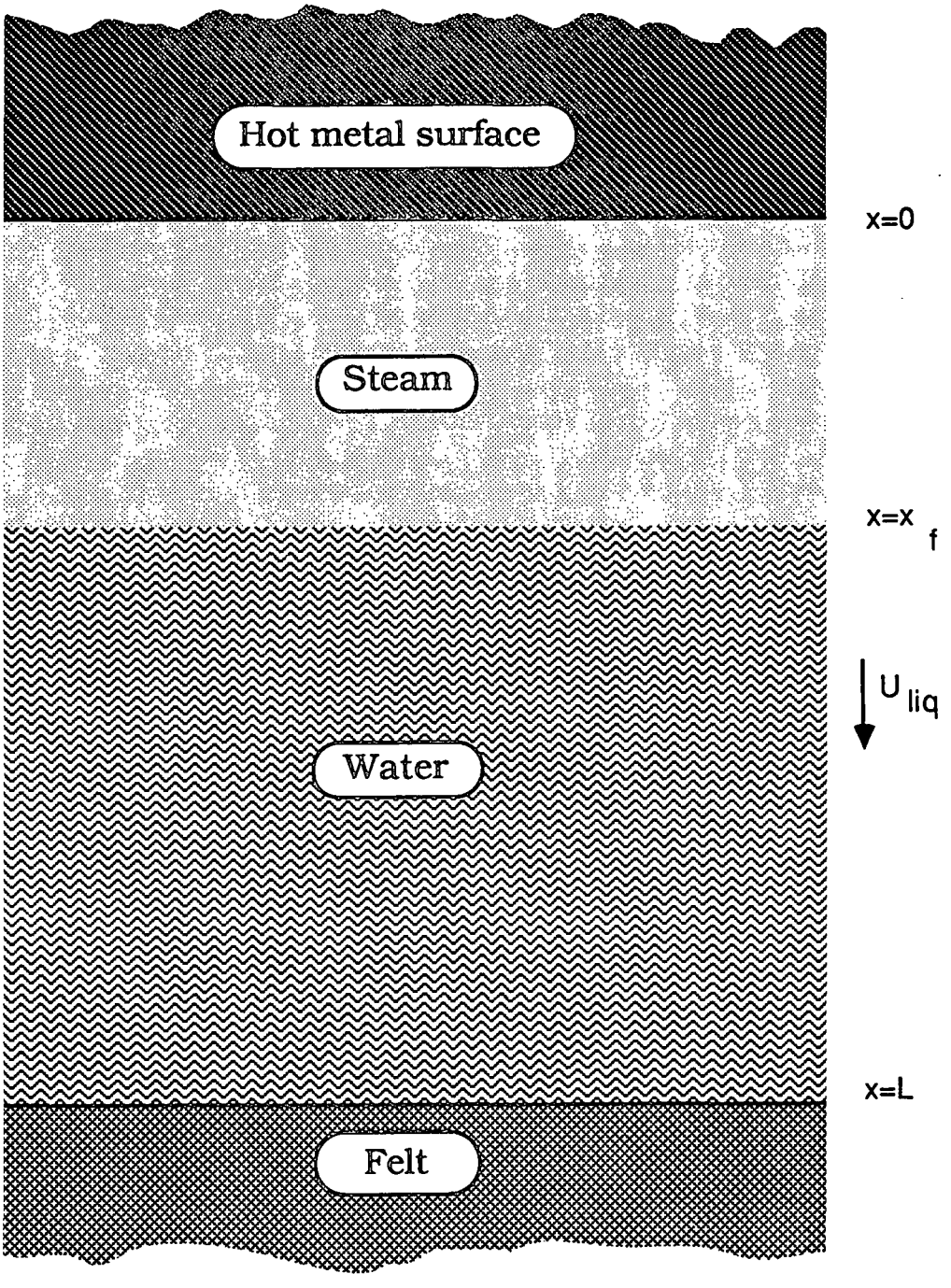


Figure 5. Displacement in a porous medium during impulse drying.

temperature at the surface is specified. It may be constant or a function of time. The gas velocity is given by

$$\frac{\rho}{\varepsilon}\left(\frac{\partial u}{\partial t}+u\frac{\partial u}{\partial x}\right) = -\frac{\partial P}{\partial x}+\frac{1}{\varepsilon}\frac{\partial}{\partial x}\left(\mu\frac{\partial u}{\partial x}\right)-\left(\frac{\mu_f}{K}+\frac{\rho C|u|}{\sqrt{K}}\right)u \qquad (2)$$

where $\varepsilon$ is the porosity, $\mu$ is the viscosity, $\mu_f$ is an effective viscosity, K is the permeability, and C is a constant which accounts for inertial effects. In the cases run so far, inertial effects been neglected and $\mu_f$ has been assumed equal to $\mu$. For impulse drying, the upper boundary (x=0) is solid, so the gas velocity there is set to zero. A finite gas velocity would be used in a direct displacement case.

Continuity in the gas phase is given by

$$\varepsilon\frac{\partial \rho}{\partial t}+\frac{\partial(\rho u)}{\partial x}=\dot{m} \qquad (3)$$

where m is a mass source term due to phase change. The gas is assumed to be ideal, so

$$\rho_g=\frac{PM}{RT} \qquad (4)$$

where M is the molecular weight and R is the gas constant.

Heat transfer in the liquid phase is given by

$$\rho C_p\left(\frac{\partial T}{\partial t}+u\frac{\partial T}{\partial x}\right)=\frac{-\partial}{\partial x}\left(k\frac{\partial T}{\partial x}\right) \qquad (5)$$

where $C_p$ is the constant pressure heat capacity. At the outlet boundary, the temperature gradient is set to zero. The Darcian liquid velocity is given by

$$\frac{\rho}{\varepsilon}\frac{\partial u}{\partial t} = \frac{-\partial P}{\partial x} - \frac{\mu u}{K\rho} + \rho g \qquad (6)$$

where g is the gravitational component in the direction of flow. Taking advantage of the continuity equation for an incompressible fluid ($\partial u/\partial x = 0$), a macroscopic equation for the liquid velocity can obtained:

$$\frac{1}{\varepsilon}\frac{du}{dt} = \frac{-1}{\rho}\frac{P_{int}-P_{\infty}}{L-x_f} - \frac{u}{K\rho}\frac{\int_{x_f}^{L}\mu(T(x))dx}{L-x_f} \qquad (7)$$

where L is the thickness of the porous medium (the sheet), $x_f$ is the location of interface, $P_{int}$ is the pressure at the interface, and $P_{\infty}$ is the specified pressure at the exit boundary of the system.

The gas and liquid phases are joined through boundary conditions at the interface. The interface is a common boundary between the two phases with a single temperature, velocity, and pressure. The temperature and pressure are required to be in equilibrium. The velocity is the liquid velocity plus a contribution from evaporation or condensation at the interface:

$$U_{int} = U_L + \frac{\dot{m}}{\rho} \qquad (8)$$

where $U_{int}$ is the interface velocity and $U_L$ is the bulk liquid velocity. The evaporation rate is determine by the difference between the incoming heat flux from the gas phase and the outgoing heat flux into the liquid phase:

$$\left(-k\frac{\partial T_G}{\partial x}\right) - \left(-k\frac{\partial T_L}{\partial x}\right) = \dot{m}\, h_v \qquad (9)$$

where $h_v$ is the heat of vaporization.

Nonuniform, moving grids are used in the fully implicit finite-difference approach. The grid spacing becomes increasingly dense as the interface is approached. Cubic spline interpolation is used to transfer information to new grid structures between and during time steps.

Significant complications in the model stem from the changing gas pressures and interface equilibrium conditions. Under relaxation of interface boundary conditions during the iterative solution procedure for each time step is required. The compressible gas phase also increases the complexity of the code. A compressible form of the popular SIMPLE pressure correction scheme derived using principles outlined in Patankar (1970). Attempts to use the standard SIMPLE procedure consistently resulted in divergence.

Once MIPPS was written, a number of test cases were run to examine the accuracy of the model. For instance, the boundary conditions and initial conditions were altered in the code to create a sealed, insulated porous system with a gas phase and a liquid phase that were not in equilibrium. MIPPS then computed the transient behavior of the system as

the vapor and liquid approached equilibrium. The steady state conditions could be determined *a priori* from thermodynamic considerations. After several hundred time steps, the computed system temperature, pressure, and vapor/liquid distribution were examined. Within the limits of rounding error in the output results, the computed pseudo-equilibrium values agreed with the thermodynamic prediction. This does not prove the code is correct in any sense, but is an encouraging indication. Other simple tests for physical reasonableness were conducted at each stage of model development, and the code appears to be proper. Nevertheless, improvements and additional features are still needed in a variety of areas, and several student projects related to MIPPS are envisioned.

MIPPS is general enough that it can be applied to direct and indirect displacement processes, as well as other drying processes. Boundary conditions need to be altered for each new physical arrangement, and some subroutines may need to be turned off. In addition, subroutines for some special physical processes may need to be added.

One important physical process that has been included in MIPPS is wicking, i.e., the capillary flow of water from the saturated region back to the heat source. Currently the rate of wicking is simply specified, although work is in progress to employ a more sophisticated scheme.

The most serious problem with MIPPS is the lack of adequate computational facilities. The complexity of the transient physical processes being predicted requires substantial computer time for each time step. Acquisition of a medium scale mainframe for scientific use (preferably a VAX computer) is strongly recommended.

Predictions for impulse drying-like situations have been made. Figure 6 shows the motion of the steam/vapor interface as a function of time for several combinations of permeability and wicking rate (M). (Permeability has units of $m^2$, and wicking rate has units of kg/s-$m^2$.) The porous sheet was 1 millimeter thick and initially saturated at 373°K. A hot surface at 600°K was then pressed against the top of the sheet. The hydraulic pressure at the felt side was specified at 1 atm. On Figure 6, an interface location of 0.8 mm means that 80% of the free water has been removed. The predicted rates of dewatering are consistent with the high rates observed in real impulse drying. The curves also show a strong dependence on wicking rate. Wicking greatly increases the rate of dewatering because it contributes to the extra hydraulic generated by the vapor phase.

MIPPS predictions have also been made for transient heat flux rate, and the results show that significant wicking is required to explain the experimentally observed heat fluxes in impulse drying. Conduction heating through the vapor phase plays an important role, but continued boiling at the surface of the resupplied water must also be occurring in impulse drying.

MIPPS predictions also show that the vapor pressures generated in impulse drying-like processes are on the order of 40 -200 psi, depending on the details of the physical system. These values are consistent with measurements made by Steve Burton at the IPC who reported pressures on the order of 60 psi. His values, however, are believed to be systematically low.

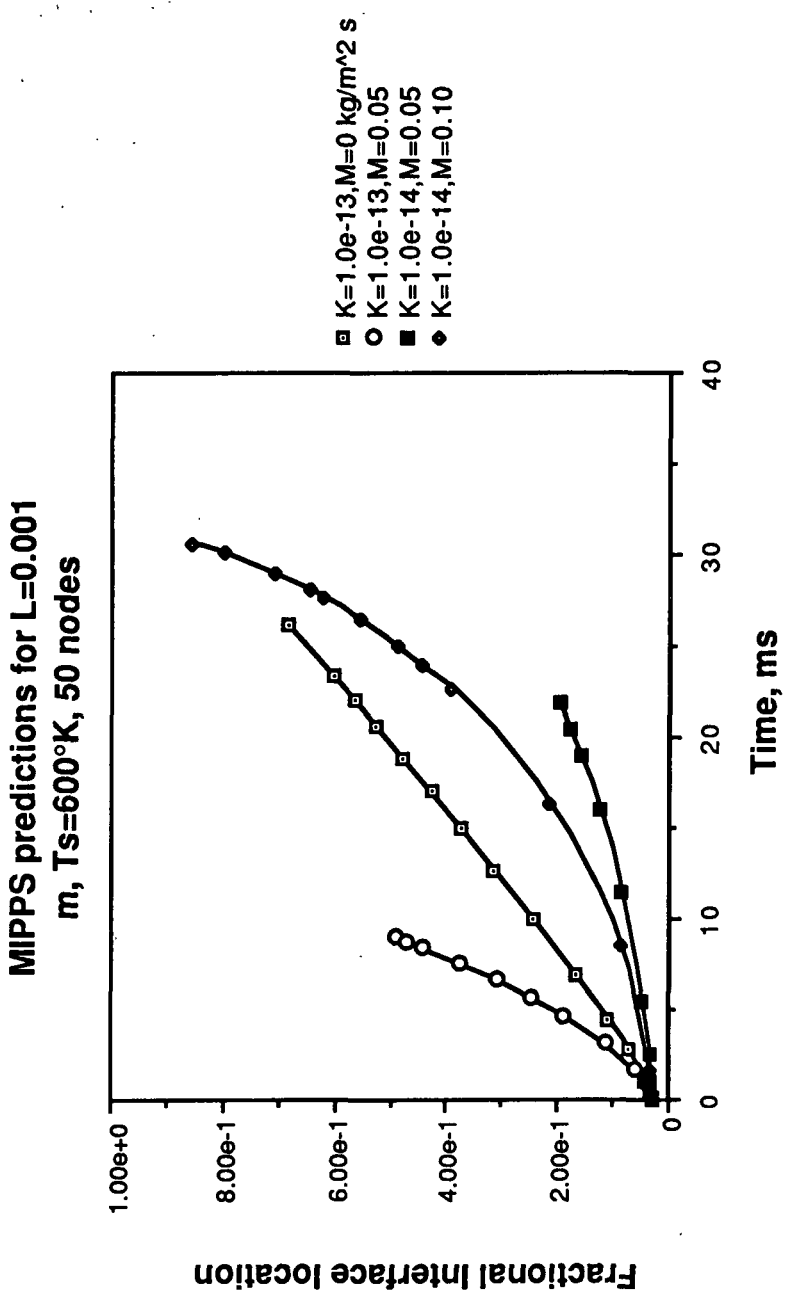


Figure 6. MIPPS predictions of interface position for various combinations of permeability (K) and wicking rate (M).

Several limitations in MIPPS are apparent. The complete impulse drying process can not yet be simulated by MIPPS because a rigid porous media is assumed. Future plans include extending MIPPS to deformable porous media. MIPPS also assumes that the porous media is either saturated with water or saturated with vapor (although the use of wicking in the model implies that that liquid water is present in the vapor portion of the system, but it does not interact with the vapor). Again, a more sophisticated approach may be of value.

While it has limitations, MIPPS should be of use in further understanding the physics of displacement phenomena. Through such understanding, improved processes may be developed.

PLANS FOR NEXT PERIOD:

1. Finish installation of displacement apparatus.

2. Develop experimental design for displacement tests and begin testing with air and steam.

3. Measure lateral permeability in a variety of papers.

4. Continue refinement of MIPPS.

SIGNIFICANCE TO THE INDUSTRY:

Displacement dewatering offers the potential of efficient water removal as well as enhanced control over physical properties such as bulk. Developments in the science of displacement phenomena, especially through numerical modeling, may also lead to improvements in the proven technology of impulse drying.

LITERATURE CITED:

S. B. Gorell and G. M. Homsy, "A Theory for Most Stable Variable Viscosity Profile in Graded Mobility Displacement Processes," *AIChE J.*, **31**, 1498-1503 (1985).

P. S. Hahn, T. R. Ramamohan, and J. C. Slattery, "Mobility Control in the Displacement of Residual Oil by an Unstable Foam," *AIChE J.*, **31**, 1029-1035 (1985).

G. M. Homsy, "Viscous Fingering in Porous Media," *Ann. Rev. Fluid Mechanics*, **19**, 271-311 (1987).

C. A. Miller, "Stability of Moving Surfaces in Fluid Systems with Heat and Mass Transport," *AIChE J.*, **19**, 909-915 (1973).

S. V. Patankar, *Numerical Heat Transfer and Fluid Flow*, Hemisphere Publishing Corp., Washington, D.C., 1980.

R.M. Peterson, "Two-Dimensional Flow of Incompressible Fluids Through Deformable Porous Media," *Tappi J.*, **53**, 71-77 (1970).

P. A. Rice, D. J. Fontugne, R. G. Latini, and A. J. Barduhn, "Anisotropic Permeability in Porous Media," *Flow Through Porous Media*, ed. R. J. Nunge, American Chemical Society Publications, Washington, D.C., 1970.

J. Skelton, "Foam Assisted Dewatering – A New Technology Emerges," *Paper Tech. and Ind.*, **28**, 435-436 (1987).

C. H. Sprague, "Process Fundamentals of Wet Pressing," Project 3480/3584 Status Report to the Engineering Project Advisory Committee, The Institute of Paper Chemistry, Apleton, Wisconsin, Sept. 11, 1985.

R. Walser ad R. S. Swenson, "Air Through-Drying of Paper," *Tappi J.*, **51**,184-190 (1968).

THE INSTITUTE OF PAPER CHEMISTRY

Appleton, Wisconsin

Status Report

to the

ENGINEERING PROJECT ADVISORY COMMITTEE

Project 3479

HIGHER CONSISTENCY PROCESSING

October 22, 1987

PROJECT SUMMARY FORM

DATE: September 23, 1987

PROJECT NO: 3479 - Higher Consistency Processing

PROJECT LEADER: Ted Farrington

IPC GOAL: Reduction in complexity of forming systems

OBJECTIVE:

To develop experimental and computational techniques necessary to better understand the behavior of fiber suspensions over a range of consistencies encompassing both current and potential future operations.

To apply a better knowledge of fiber suspension microrheology to increase paper machine wet-end consistencies from 0.1-1.5% to 2.0-10.0%, depending on grade, without loss of machine speed or paper physical properties.

Ultimately, to apply any new knowledge or techniques developed in this work to other high speed multiphase flow problems of interest to the pulp and paper industry.

CURRENT FISCAL BUDGET: $200,000

BACKGROUND:

High consistency forming has the potential of reducing both capital and energy costs and improving formation and physical properties control. Previous attempts have produced paper which appeared felted, with inferior in-plane properties. This can be traced to lack of control of out-of-plane fiber orientation in the sheet. At high consistencies, this orientation is largely

fixed within the headbox and slice. Without the ability to measure fiber orientation at actual process conditions, process development must proceed by trial and error.

The initial objective of this project has been the development of some means for measuring fiber orientation distribution in concentrated fiber suspensions during high speed flows. Flash x-ray radiography (FXR) will be used to study fiber orientation distribution in both idealized and more practical flow situations. The objective of the idealized flow experiments (currently underway) is to assess to what extent fiber orientation distribution can be controlled under the best of conditions. If significant results cannot be realized here, it will be unlikely that any improvement can be made in practical flows.

While most of our effort is directed at the problem of fiber orientation distribution which must be overcome if one hopes to produce high quality grades at high consistency, it is recognized that many grades do not require (or even desire) coplanar fiber distributions. A MC headbox was obtained from the Thermo Electron Corporation some time ago so we could perform simple MC forming tests and compare results with traditional processes. While this area has not seen much activity thus far, we do see it becoming more important as the benefits of producing even felted structures at higher consistencies become clear.

Although the primary application of the FXR imaging technique is in the fiber suspension area, it has demonstrated potential for providing new knowledge in others areas of importance to the industry. Two of these areas

are black liquor spraying and high solids coatings. Each of these is being pursued as student research at this time. Black liquor sprays and coatings research have each received start-up funding on the order of $20,000 from direct member company contributions.

Several proposals for government funding have been submitted, primarily to the U.S. Department of Energy. Proposals requesting $400,000 and $1,500,000 have been submitted for high consistency forming and black liquor delivery systems respectively. A separate proposal to obtain a much needed image analyzer was submitted to the DOE University Instrumentation Grant Program for $169,000. Of these, the black liquor delivery systems proposal ($1.5M over four years) was recently approved for funding beginning February 15, 1988.

One of the spinoffs of this work has been an investigation of soft x-ray imaging of paper sheets as a means for determining true mass distribution. Handsheets were produced over a broad basis weight range with various levels of uniformity. These were subsequently imaged in a cabinet x-ray system. As of the last review, these were awaiting analysis.

SUMMARY OF RESULTS SINCE LAST REPORT: (March, 1987 October, 1987)

Status of Proposals:

At the time of the last review, two of our proposals (black liquor delivery systems and image analyzer) were receiving serious consideration at the DOE. In July, we were informed that the image analysis proposal had been rejected. This was a major setback for our work as we felt we had an

outstanding chance of winning and had planned several activities on the assumption that an image analyzer would be in place by the fall.

On a more positive note, the $1.5M black liquor delivery systems proposal was recently approved with funding to commence February 15, 1988. Funds are included within this program to purchase essentially the same image analyzer described in the instrumentation grant proposal.

The net result is that we now have a major DOE contact in hand to support our activities, we will have the badly needed image analyzer, but it will arrive 7-8 months later than originally hoped. Unfortunately both of our student projects and the fiber suspension work are producing images for analysis already. We are in the process of contracting for image analysis time at the manufacturer and with member companies to get us through the coming few months.

Higher Consistency Forming:

As discussed at the last review, we are proceeding with the nylon fiber system with nylon-coated silver filaments for tracers. Considerable time was spent (lost?) in search of a method to mass produce tracer fibers of well controlled length. One method which showed promise came from Sylvania. Here an epoxy cylinder is cast around a bundle of filaments. The cylinder is cut to desired length and the epoxy removed with a solvent to yield cut filaments. Unfortunately, the price quoted to produce $10^6$ tracer fibers this way was prohibitive. A local machine shop was then approached to design and build a more brute force device to cut fibers. The system delivered cuts about 10000 fibers per hour, one at a time. The machine is far from main-

tenance free but does get the job done. The high concentration, high velocity experiments are currently in progress. Experimental design parameters are as follow:

| | - | + |
|---|---|---|
| fiber length(mm) | 1.0 | 2.0 |
| exit velocity(m/s) | 5.0 | 10.0 |
| concentration($cl^3$) | 50.0 | 75.0 |

At this time, most of the images have been taken and are awaiting analysis.

Black Liquor Sprays:

In addition to obtaining the DOE contract, significant progress was made in this area through a grant from the Weyerhaeuser Company. A simple spray facility was completed in June. Part of this is a low pressure drop spiral-tube heat exchanger donated by Alpha-Laval. Much higher nozzle pressures and flowrates can now be achieved.

This past summer Weyerhaeuser employed Tom Spielbauer (M.S.) and placed him at IPC to develop the spray imaging techniques and investigate several specific liquor/nozzle combinations. Both B&W and CE nozzles were tested over solids concentrations ranging from 64% to 70+%. This work was quite productive and Tom will report on some of the general results at the fall PAC meeting. As with the fiber suspension work, this is badly in need of some image analysis capability and we are now proceeding to beg, borrow or steal time on other machines.

High Solids Coatings:

The Beloit Corporation has built and donated a coater simulator (backing roll) for this work which will allow tests at speeds up to 5000fpm. This is

currently being installed in the third "Ted's lead shed". Nick Triantafillopoulos (Ph.D.) has spent most of his time evaluating tracers for this work and studying coating flow geometries via computation fluid dynamics. He will report on the work at the fall PAC meeting.

Computational Fluid Dynamics (CFD):

While attempting to design flow devices for the fiber suspension work it became obvious that we had very little (no) capability for carrying out fluid dynamics computations at IPC. With so many pulp and paper processes involving fluid flow phenomena we considered this situation unacceptable and spent some time investigating commercially available CFD codes which could be used not only in the fiber suspension work but in a number of other areas of current research.

Several companies were found which market large scale three-dimensional CFD codes. Persons in the recovery section of Chemical Sciences were already evaluating PHOENICS (Cham Inc.) for use in recovery boiler simulation. It proved too inconvenient and expensive to use via remote timesharing.

A second possible CFD code, FLUENT (Creare, Inc.) was identified. It was found that Creare would donate free copies of this code to any academic institution with a VAX computer, which we do not have. Arrangements were made with Lawrence University to run FLUENT on their VAX 11/780.

FLUENT is a large scale finite volume CFD code for analyzing three dimensional steady problems in fluid mechanics and heat transfer. The version we were given has up to 10,000 nodes and can simulate laminar flows, turbulence

(K-ε and Reynolds stress models), powerlaw fluids, flow through porous media, radiative heat transfer and combustion.

Acquisition of this code has moved us forward several years in terms of our ability to quantitatively investigate fluid flow phenomena of interest to the pulp and paper industry. It is currently being used to simulate kraft recovery boilers (Andy Jones, Allen Walsh) where 11/780 execution times are measured in days, to study coater flow patterns (Triantafillopoulos, Rudemiller), and to investigate headbox flows (Ginnow). Several other less intensive applications also exist.

We are now far and away the heaviest users of the LU VAX and steps are being taken to run FLUENT at IPC. All recovery boiler modeling is being transferred to a VAX Station II purchased specifically for this work. One of the secondary requirements of the image analyzer we have been seeking is that it be able to run FLUENT (DEC compatible). The RCI image analyzer comes with a microVAX II, which will give us a second capability at IPC. Both of these systems will allow over 50,000 node simulations which are needed for many three dimensional applications. Creare has agreed to upgrade our version to 50,000 at no cost.

One limitation of FLUENT is that it works only in cartesian or polar coordinates. This poses problems in several areas such as coating and headbox flows. Creare is about to release a body-fitted coordinates program which they have also agreed to give us at no cost. In our view, this is a real success story at IPC. In less than a year, we have gone from not being able to calculate flow down a pipe to performing state-of-the-art large scale simulation of complex flow phenomena. This has tremendously increased our ability

to carry out quantitative research in a number of areas. Nick Triantafillopoulos will share some of his experiences in this area at the fall PAC meeting.

Soft X-ray Imaging of Paper Sheets:

Our activities in this area have come to a close with the results being summarized in a short paper presented at the Fall '87 TAPPI Engineering Conference (IPC TS #240). Handsheets were produced over a range of basis weights with formation controlled by settling time in the handsheet former. Physical properties were measured as listed in Table 1. X-ray images were taken of all samples with Figures 1 and 2 showing 50 gram sheets (0 and 60 s settling time respectively) plus mylar calibration wedges.

TABLE 1. Handsheet Physical Properties

| Sample No. | Basis Weight ($g/m^2$) | Settling Time (s) | Tensile Strength (kN/m) | Opacity (%) | Formation Index |
|---|---|---|---|---|---|
| 60STD | 60 | 0 | 5.13 | 69.1 | 92.1 |
| 60/30 | 60 | 30 | 4.47 | 69.6 | 45.6 |
| 60/60 | 60 | 60 | 4.47 | 70.3 | 29.4 |
| 100STD | 100 | 0 | 8.23 | 82.1 | 79.8 |
| 100/30 | 100 | 30 | 7.71 | 81.0 | 45.9 |
| 100/60 | 100 | 60 | 7.77 | 83.4 | 36.2 |
| 150STD | 150 | 0 | 12.9 | 89.5 | 72.3 |
| 150/30 | 150 | 30 | 10.7 | 89.6 | 44.7 |
| 150/60 | 150 | 60 | 11.2 | 90.3 | 35.9 |
| 200STD | 200 | 0 | 15.8 | 93.9 | 69.2 |
| 200/30 | 200 | 30 | 12.7 | 93.7 | 42.2 |
| 200/60 | 200 | 60 | 12.5 | 94.1 | 36.1 |

A Tracor-Northern image analyzer was used to digitize and process the radiographs. Several practical problems were observed which could be traced to nonuniform x-ray field intensity and to manual processing. Even with these problems, soft x-ray imaging was shown to give quantitative information on true mass distribution. Figure 3 compares the mass distributions of the 150/standard and 150/60 sheets. While the imaging technique could resolve single fiber dimensions easily, overall resolution was set by the image analyzer setup. In this case, final resolution was approximately 50 μ.

Two dimensional FFT's were also performed for two reasons. First, one should be able to remove the long wavelength variations caused by the nonuniform x-ray field by digitizing a blank and subtracting its image in Fourier space from that of the sample. Also, the 2-D power spectrum should give quantitative information on floc size distribution. 2-D power spectra of samples 150/standard and 150/60 are shown in Figures 4 and 5. Figure 4 shows much fine structure (high frequency) in the standard sheet while the poorly formed sheet is dominated by lower frequency variations (large flocs).

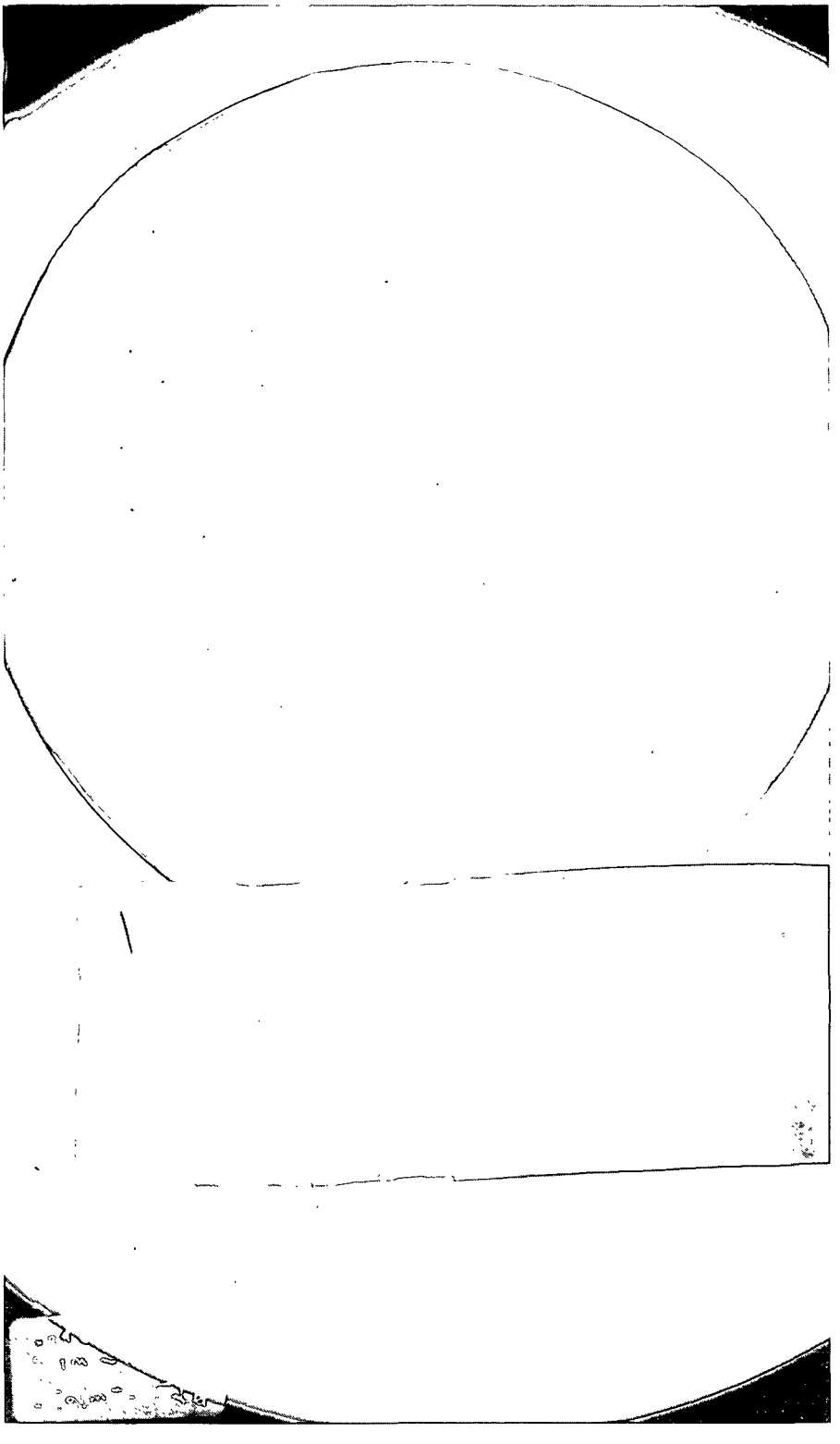

Figure 1. Soft x-ray image of sample 150/STD

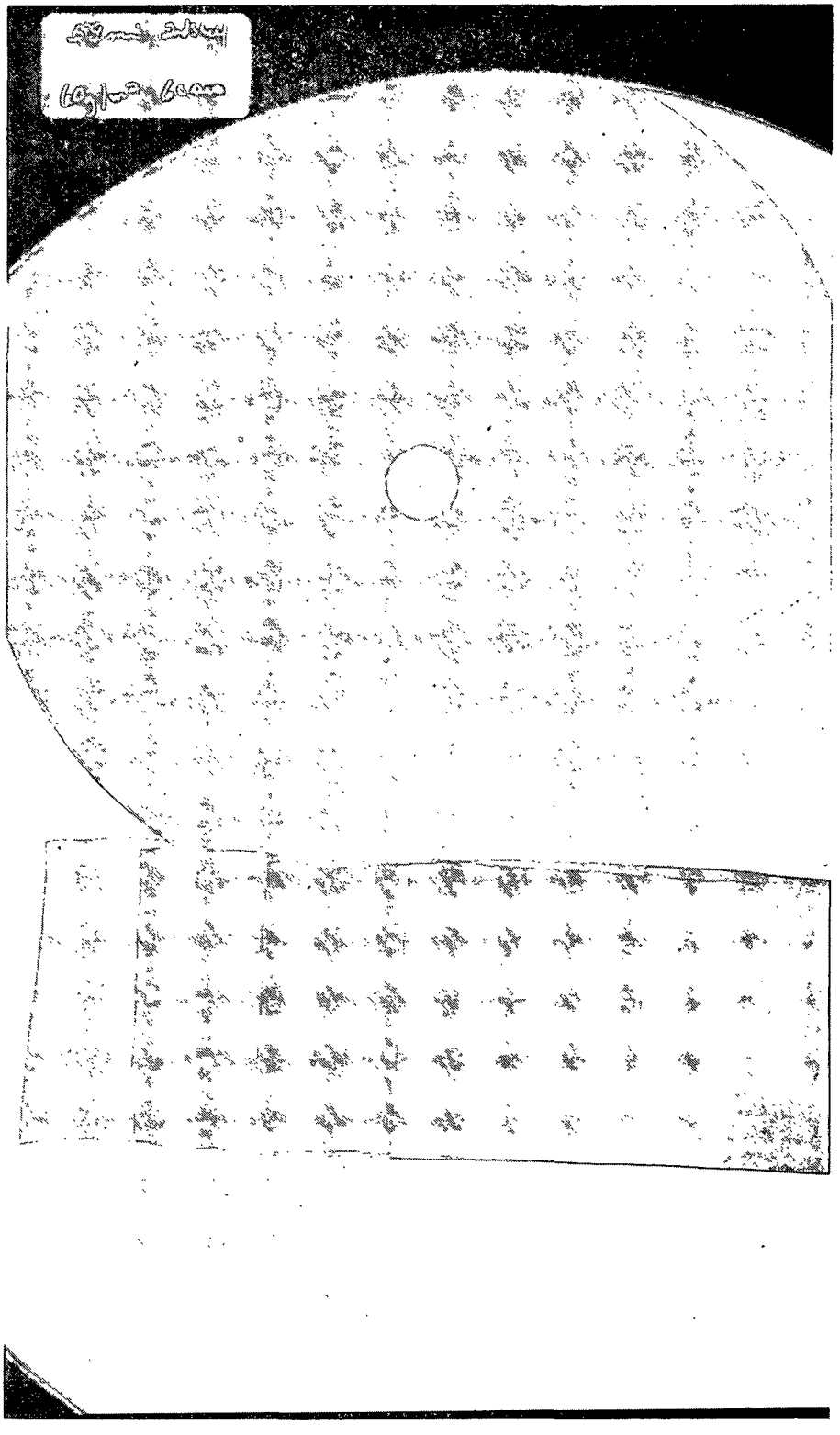

Figure 2. Soft x-ray images of sample 150/60

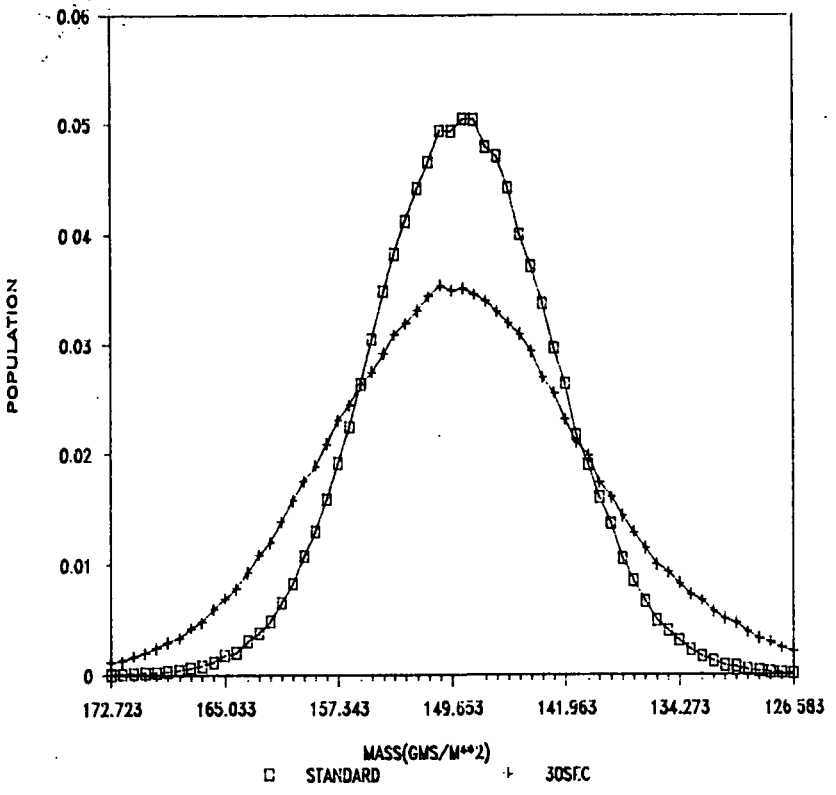


Figure 3. Mass distribution of samples 150/STD and 150/60 (50u)

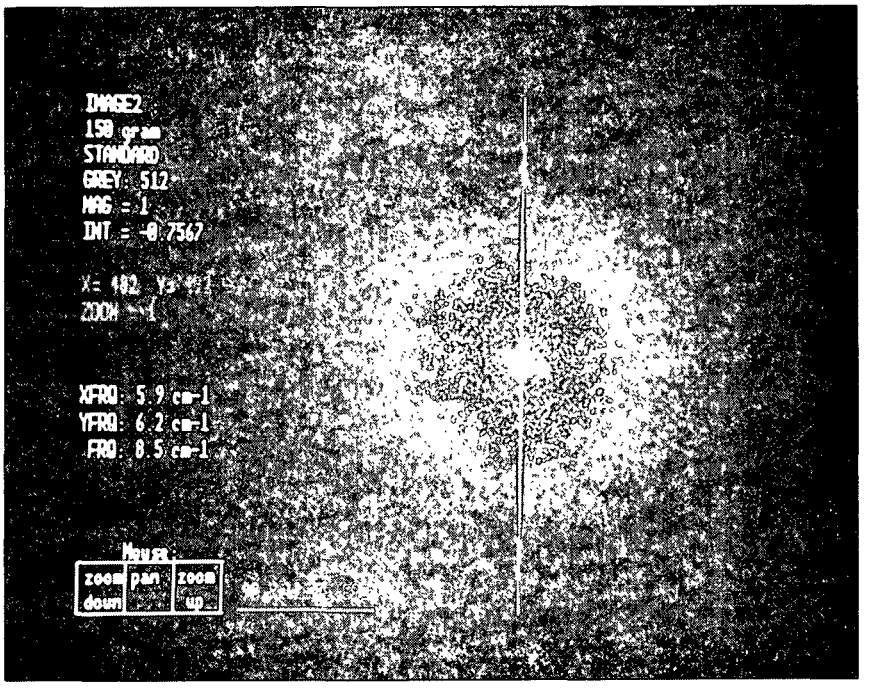


Figure 4. 2-D power spectrum of sample 150/STD

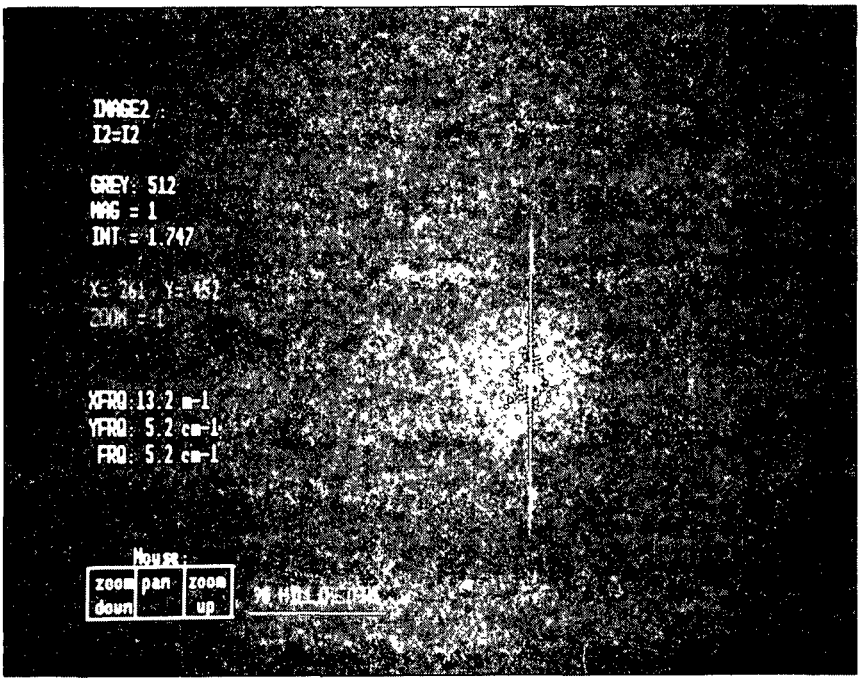


Figure 5. 2-D power spectrum of sample 150/60

CURRENT ACTIVITIES:

Fiber suspension tests are now in progress. With the installation of the new narrow channel converflow headbox nearly complete, we are investigating the possibility of some experiments to directly compare low and medium consistency (TE headbox) sheets.

Black liquor spray work is continuing as student research at this time. We are trying to better define the techniques and experiments to be pursued when DOE funding begins in February. Necessary equipment for the coating work is now being installed.

PLANS FOR NEXT PERIOD:

Complete at least three of the four combinations of high/low concentration and high/low velocity included in the overall plan for fiber suspension tests. Be in the process of analyzing these on some image analyzer prior to next PAC meeting. Compare sheets made at low and medium consistencies using new Beloit headbox and Thermo-Electron headbox respectively.

Place orders for all long lead items required for black liquor delivery systems contract.

SIGNIFICANCE TO THE INDUSTRY:

Higher consistency forming has the potential to reduce both capital and energy costs. Perhaps more important is the potential to obtain novel three dimensional sheet properties.

Flash x-ray radiography has demonstrated the ability to provide very unique information regarding several multiphase flow problems of interest to the pulp and paper industry. These include black liquor delivery systems and coating flows.

Potential energy and productivity benefits from improved firing of kraft black liquor have been estimated to be 2.2 x 1013 Btu/yr ($110,000,000/yr) and 0.44 x 106 ADTP/yr ($100,000,000/yr), respectively.